2020

Delta/theta-rhythmically interleaved gamma and beta oscillations in striatum: modeling and data analysis

BOSTON UNIVERSITY

SCHOOL OF MEDICINE

Dissertation

DELTA/THETA-RHYTHMICALLY INTERLEAVED GAMMA AND BETA OSCILLATIONS IN STRIATUM: MODELING AND DATA ANALYSIS

by

JULIA CHARTOVE

B.A., Swarthmore College, 2014

Submitted in partial fulfillment of the

requirements for the degree of

Doctor of Philosophy

2020

Approved by

First Reader

Nancy Kopell, Ph.D.
William Fairfield Warren Distinguished Professor,
Professor of Mathematics and Statistics,
Professor of Pharmacology and Experimental Therapeutics,
Professor of Biomedical Engineering

Second Reader

Daniel Bullock, Ph.D.
Professor Emeritus of Psychological and Brain Sciences

You can get a certain vision of life where everything is seen to be a complex pattern of rhythm. Dances. The human dance, the flower dance, the bee dance, the giraffe dance. [...] And that's what all this is: it's jazz, you see? This is a big jazz, this world. And what it's trying to do is to see how jazzed up it can get, how far out this play of rhythm can go.
Alan Watts, from *The World as Self*

ACKNOWLEDGMENTS

My greatest thanks go to my mentor, Dr. Nancy Kopell. It was such an honor to be able to work with one of the greatest mathematical minds in the entire field of neuroscience. I never would have been able to come this far without her guidance through incredibly difficult concepts and her endless patience with me when I became overwhelmed. I owe her my deepest gratitude to her for her faith in my potential and for believing that I could do great work, even when I didn't believe in myself. I feel that I have had an incredible privilege to have her mentor me through this intellectual journey.

I also want to thank my coauthors, Ben Pittman-Polletta and Michelle McCarthy, for providing mentorship on an individual level that was equally as important to my education as Nancy's guidance. I've learned a huge amount about programming, mathematics, and writing from both of them, and I'm eternally grateful for their willingness to take me under their wing when I was floundering in the initial shallowness of my knowledge. In addition, I want to thank the people who made the data analysis chapter of this thesis possible both by generously sharing their data, educating me in an area of analysis I knew very little about, and writing much more code than I did in support of my research goals: Robert Reinhart, John Nguyen, and Frederik Baumgardt.

This work wouldn't have been possible without the members of our working group who took on the monumental task of developing the Dynasim toolbox in order to meet the computational requirements of this kind of research. In particular, I'd like to thank Jason Sherfey for captaining the team and working tirelessly to turn Dynasim into a reality, and Erik Roberts for taking the time out of his extremely busy schedule to work with me to adapt Dynasim and the GIMBL-Vis

package to my specific parameter exploration whims.

The list of members of my community I'd like to thank in this section is very long, and in the interest of actually submitting this dissertation manuscript and graduating, I don't think I can list them all. Briefly: I want to thank the administrators and fellow students of the Graduate Program for Neuroscience, as well as my other friends in the Boston area research community, for providing a social and intellectual environment where I could flourish. I can't count the number of people who have supported me by helping me with homework, letting me practice my presentations with them, letting me vent when I was frustrated with the state of my work and the world, and just having fun with me when I needed a break (which was always).

Obviously I'd be remiss not to mention the importance of the unconditional love of my parents (Lauren Randel and Alex Chartove) and sisters (Natalie and Sofia Chartove) in supporting me and believing in me; their continued insistence that I was smart and capable of great things was vital to my self esteem, and kept me going through the many ups and downs of my graduate experience. I also want to extend a final shout-out to the many kind people, and tolerant animals, who have shared living spaces with me in the six years I've been in Boston. You all are saints for sticking with me through all of my nonsense, and I appreciate you.

DELTA/THETA-RHYTHMICALLY INTERLEAVED GAMMA AND BETA OSCILLATIONS IN STRIATUM: MODELING AND DATA ANALYSIS

JULIA CHARTOVE

Boston University, School of Medicine, 2020

Major Professor: Nancy Kopell, Ph.D.
William Fairfield Warren Distinguished Professor,
Professor of Mathematics and Statistics, Professor
of Pharmacology and Experimental Therapeutics,
Professor of Biomedical Engineering

ABSTRACT

Striatal oscillatory activity associated with movement, reward, and decision-making is observed in several interacting frequency bands. Rodent striatal local field potential recordings show dopamine- and reward-dependent transitions between a 'spontaneous' state involving β (15-30 Hz) and low γ (40-60 Hz) and a 'dopaminergic' state involving θ (4-8 Hz) and high γ (60-100 Hz) activity. The mechanisms underlying these rhythmic dynamics and their functional consequences are not well understood. In this thesis, I construct a biophysical model of striatal microcircuits that comprehensively describes the generation and interaction of these rhythms as well as their modulation by dopamine and rhythmic inputs, and test its predictions using human electroencephalography (EEG) data.

Chapter 1 describes the striatal model and its dopaminergic modulation. Building on previous work suggesting striatal projection neuron (SPN) networks can generate β oscillations, I construct a model network of striatal fast-spiking in-

terneurons (FSIs) capable of generating δ/θ (2-6 Hz) and γ rhythms. This FSI network produces low γ oscillations under low (simulated) dopaminergic tone, and high γ activity nested within a δ/θ oscillation under high dopaminergic tone. In a combined model under high dopaminergic tone SPN network β oscillations are interrupted by δ/θ-periodic bursts of γ-frequency FSI inhibition. This high dopamine-induced periodic inhibition may enable switching between β-rhythmic SPN cell assemblies representing motor programs, suggesting that dopamine facilitates movement in part by allowing for rapid, periodic changes in motor program execution.

Chapter 2 describes the model's response to square-wave periodic cortical inputs. Comparing models with and without FSIs reveals that the FSI network: (i) prevents the SPN network's generation of phase-locked beta oscillations in response to beta's harmonic frequencies, ensuring fidelity of transmission of cortical beta rhythms; and (ii) limits or entrains SPN activity in response to certain gamma frequency inputs.

Chapter 3 describes an analysis of phase-amplitude coupling at cortical electrodes in human EEG data during a reward task. The alternating rhythms predicted by the model appear in response to positive feedback. While the origins of these rhythms remain unclear, if they represent striatal signals, they provide a direct link between human behavior and striatal cellular function.

CONTENTS

LIST OF FIGURES

LIST OF SYMBOLS AND ABBREVIATIONS

α	.....	alpha
β	.....	beta
BG	.....	Basal ganglia
c	.....	Capacitance
cm	.....	Centimeters
DA	.....	Dopamine
DAergic	.....	Dopaminergic
δ	.....	delta
E	.....	Reversal potential
EEG	.....	Electroencephalography
FSI	.....	Fast spiking interneuron
g	.....	Conductance
GABA	.....	Gamma-aminobutyric acid
γ	.....	gamma
GJ	.....	Gap junction
H	.....	Entropy
HD	.....	Huntington's Disease
Hz	.....	Hertz
I	.....	Current
ING	.....	Interneuronal network gamma
K	.....	Potassium

KL distance	.....	Kullback-Liebler distance
L	.....	Leak current
L-Dopa	.....	Levodopa
LFP	.....	Local field potential
μ_A	.....	Microamperes
mF	.....	Millifarads
MI	.....	Mutual information
ms	.....	Milliseconds
mS	.....	Millisiemens
mV	.....	Millivolts
Na	.....	Sodium
PAC	.....	Phase amplitude coupling
PLV	.....	Phase locking value
PSD	.....	Power spectral density
Q_{10}	.....	Temperature coefficient
s	.....	Seconds
SEM	.....	Standard error of the mean
SPN	.....	Striatal projection neuron
τ	.....	tau
θ	.....	theta
V	.....	Voltage

CHAPTER 1

Introduction

Oscillations in the striatum are correlated with voluntary movement, reward, and decision-making in healthy individuals, while disruptions of these rhythms are biomarkers of mental and neurological disorders (Jenkinson et al. (2013); DeCoteau et al. (2007); Tort et al. (2008)). In particular, beta band oscillations (8-30 Hz) are correlated with bradykinesia in Parkinsons disease, and accordingly, treatment with dopaminergic (DAergic) drugs or deep brain stimulation decreases beta power (Brown (2007)). Gamma band oscillations (40-80 Hz) have the inverse association with movement: they are diminished in Parkinsons disease, while their power increases during motor initiation and during hyperkinesia due to an overabundance of DA (Jenkinson et al. (2013)). Though oscillations in the striatum have been studied for decades, little is known about the mechanisms of their generation, which leads to confusion about the role they play in normal function, and the role disrupted rhythmicity plays in striatal dysfunction. Understanding the generative mechanisms of individual oscillations and their interactions will lend critical insight into their functional roles in striatal circuits, and may provide avenues for restoring striatal function in pathology via the modulation of rhythmic dynamics.

In this thesis, I aim to detail the network mechanisms underlying the generation and functional interaction of striatal rhythms. A critical barrier to understanding the mechanisms and functional significance of striatal oscillations is the complexity of the underlying neuronal networks, whose dynamics cannot be fully understood through the exclusive use of experimental techniques. Striatal networks are composed of thousands of neurons having dozens of neuronal subtypes, the understanding of which necessitates more than a purely experimen-

tal approach. Experimental studies of biological networks are greatly aided by computational modeling. Therefore, I use a biophysical model of striatal neurons with Hodgkin-Huxley-type conductances to explore the origins and interactions of rhythms. The advantage of these models is that each parameter in the model corresponds to a physical property of cells, allowing findings to be translated directly between experiments and simulations. Additionally, biophysical models ensure that the timescales underlying oscillatory cellular behavior are accurately represented, while at the same time maintaining computational tractability for simulations on the order of hundreds of cells.

The striatum is the primary target of cortical input in the basal ganglia and is responsible for using cortical input to inform the selection of motor plans downstream. 95 percent of striatal neurons are striatal projection neurons (SPNs), which receive input from sensorimotor cortex as well as DA from both the substantia nigra and the ventral tegmental area. Half of these SPNs express D1 DA receptors and project to substantia nigra via the motor-facilitating 'direct pathway', while the other half express D2 DA receptors and project to globus pallidus via the motor-inhibiting 'indirect pathway' (Wall et al. (2013)). The striatum has no obvious laminar structural organization, leading many to hypothesize that the SPNs are functionally organized by interneurons (Tepper et al. (2004)).

I chose to focus on parvalbumin-positive, fast-spiking interneurons (FSIs). FSIs are GABAergic, comprise 1 percent of striatal neurons, and fire at 10-20 Hz in the awake brain (Koós & Tepper (1999)). They receive a wide range of cortical input, suggesting a role in information integration. The FSI population forms a subnetwork connected with both gap junctions and GABAergic synapses (Berke (2011)), with unidirectional feedforward projections to the network of SPNs (Tep-

per et al. (2008)). While SPNs form weak GABAergic connections with each other, the strength of FSI inhibitory synapses onto SPNs is around six times stronger (Tepper et al. (2010)), giving FSIs powerful modulatory control over SPNs. Inhibition of FSIs causes dyskinesias, while deficits in the FSI network are associated with Tourettes syndrome in humans, suggesting that FSIs play an important role in motor control (Gittis et al. (2011); Kalanithi et al. (2005)).

The beta rhythm (8-30 Hz) may be the best studied striatal oscillation; it is most commonly known for being abnormally powerful in Parkinsons, but is also associated with healthy movement cessation (Feingold et al. (2015)). However, the striatum shows a wide variety of oscillatory behavior in intracellular and local field potential (LFP) recordings. Striatal gamma oscillations (40-80 Hz) have been associated with arousal and voluntary movement across species (Jenkinson et al. (2013)). Specifically, a 50 Hz ('low') gamma and an 80 Hz ('high') gamma have been shown to have different temporal patterns during goal-oriented behavior and reward (van der Meer & Redish (2009)). Striatal theta oscillations are observed during salient task points such as initiation, completion, and decision-making (DeCoteau et al. (2007); Tort et al. (2008)) as well as during attentive wakefulness (Lepski et al. (2012). Local field potential recordings in striatum suggest that these rhythms are related; LFPs show frequent spontaneous transitions between one state involving beta (20 Hz) and low-gamma (50 Hz), and another state involving theta (8 Hz) and high-gamma (80 Hz). This latter state is also associated with increased DAergic tone (Berke (2009)). Beta has been observed in 100 millisecond packets in healthy striatum, suggesting that epochs of beta rhythmic activity are confined to time windows contained within a single theta cycle (Feingold et al. (2015)).

I simulated FSIs using a cortical FSI model from (Golomb et al. (2007)), which was successfully adapted to striatal electrophysiological data by Sciamanna and Wilson (Sciamanna & Wilson (2011)). This model utilizes the typical Hodgkin-Huxley (spiking) currents as well as a fast-activating slowly-inactivating (D-type) potassium current. This D-type current gives the cell a region of bistability between a quiescent steady state and a periodic high-frequency (>40 Hz) spiking state. The slow inactivation timescale of the D-type current (on the order of 200 ms) causes the cell to move between these states at a theta frequency (5-10 Hz). This causes the cells to exhibit intermittent spiking, known as bursting or stuttering. The intraburst spiking frequency is in the gamma range (due to the timescale imposed by the spiking potassium current). Thus, a model FSI receiving tonic input exhibits theta-modulated gamma rhythmic spiking. This dual rhythmicity underlies the theta and gamma oscillations observed in the FSI network model.

I simulated 50 FSIs connected stochastically by both electrical and chemical (GABAergic) synapses, and found that this network produces either a theta-modulated high gamma rhythm or a persistent low gamma rhythm, depending on the level of (simulated) DAergic drive. The theta rhythm is generated in individual model FSIs by the mechanism explained in the previous section. The gamma rhythm is an interneuronal network gamma (ING) rhythm: in a purely inhibitory network, mutual inhibition synchronizes cell spiking (Whittington et al. (2000)), while gap junction connectivity increases the robustness of ING rhythms (Kopell & Ermentrout (2004)). I modeled the striatal DA level by simulating the known impacts of DA on striatal fast-spiking interneurons: increased excitation, decreased synaptic inhibition, and increased gap junction conductance (Bracci et al. (2002); Onn & Grace (1999)). DA increased the power, frequency, and robustness of the

FSI network gamma. I also found that simulated high DAergic tone was necessary for the FSI network to produce a theta-modulated gamma; under low DA conditions, it produced a persistent gamma.

In order to understand the impact of the oscillations generated by my model on the output of striatum to the rest of basal ganglia, it was necessary to model striatal projection neurons (SPNs), as they are the only output neurons of the striatum. SPNs are connected in a mutually inhibitory GABAergic network and receive input from but do not project to FSIs (Tepper et al. (2004)). Our group has previously modeled the D2 SPN network using Hodgkin-Huxley-type neurons expressing a non-inactivating slow M-type potassium current (McCarthy et al. (2011)). Interaction between the membrane M-current and the synaptic GABAa current promotes post-inhibitory rebound spiking of SPNs at beta frequency. Expanding the FSI network model by connecting it to a previously established SPN network model (McCarthy et al. (2011)) showed that FSI gamma activity can interrupt ongoing SPN beta oscillations in simulated high DA conditions, so that theta modulation of FSI gamma activity produces alternating epochs of gamma and beta rhythmicity within each theta cycle. Our model provides a theoretical framework for the idea that the striatal LFP state characterized by the theta high gamma state is related to striatal 'go' signals, and that dopamine encourages motor program switching. The results from our model provide insight into how cortical input becomes a motor decision and how FSIs can suppress or enhance motor production. This model allows us to identify which ionic mechanisms and neuromodulators in which cells could be targeted in future studies of motor disorders and generates several testable predictions about striatal function.

Striatal networks are comprised of thousands of neurons having dozens of neu-

ronal subtypes, the understanding of which necessities more than a purely experimental approach. Experimental studies of biological networks are greatly aided by computational modeling. Neural circuits can exhibit a broad range of behaviors depending on their location in the space of possible parameters; only computational modeling can describe the volumes of behaviorally delimited parameter spaces and thereby characterize the full capabilities of a neural system. Furthermore, a model network allows more direct observation of the cellular mechanisms generating this behavior more directly than is possible in vivo. Therefore, biophysical modeling is essential for constraining hypothesis space and generating predictions that can be verified experimentally.

All simulations were run on the MATLAB-based programming platform DynaSim, a framework specifically designed by the Kopell group for efficiently developing, running and analyzing large systems of coupled ordinary differential equations, and evaluating their dynamics over large regions of parameter space (Sherfey et al. (2018)). This allows direct assessment of the robustness of the model and its sensitivity to background noise, which is key to determining whether such oscillations could be maintained in a biological system, and whether multiple variable ranges could lead to the same set of behaviors observed in vivo. The advantage of biophysical models is that each parameter in the model corresponds to a physical property of cells, allowing findings to be translated directly between experiments and simulations. Additionally, biophysical models ensure that the timescales underlying oscillatory cellular behavior are accurately represented, while at the same time maintaining computationally tractability for simulations on the order of hundreds of cells. Through our models, we can discover whether modification of several different parameters could lead to a similar outcome in network activity, illu-

minating alternative avenues both for disease genesis and for treatment.

Our model of theta and gamma production by FSIs suggests important functional implications, especially regarding switching from one motor program to another. The model in Chapter 2 can be considered as a model of a striatal population to which cortex is not providing informative input: a population that is not 'selected' by cortex to take part in motor activity, a population that is in a 'listening' state awaiting cortical input, or a population taking part in a learned behavior that can be executed without cortical input. However, cortical input is probably essential in determining which SPNs and FSIs take part in network oscillatory activity. This study was originally inspired by Hjorth et al. (2009), who found that gap junctions allow fast-spiking striatal interneurons to act as detectors of correlated input. As such, this system is of interest in models of decision making and integration of information from cortex. The output from cortex to striatum has several dimensions along which information can be structurally encoded. The Hjorth et al. (2009) study focuses on synchrony in terms of the network geometry of input, i.e. the correlation between simultaneous input at different synapses onto the same network of cells; however, information structure can also be encoded temporally. If the FSIs play a role in organizing the response of the SPNs to cortical input, changing the properties of the simulated input may prove informative in terms of how this organization might take place.

In Chapter 3, in order to determine how the FSI and SPN network integrates patterns of cortical input, I investigate how the model network responds to different input frequencies. In vivo, cortical input to striatum is often oscillatory. For instance, the motor cortex projecting to striatum produces both theta and gamma oscillations; striatal theta oscillations are phase-coupled to cortical theta, and gamma

oscillation amplitude is coupled to local theta in both areas (von Nicolai et al. (2014)). The FSIs of the striatum preferentially entrain to gamma frequency input from cortex, a property which the other cell types in striatum do not share (Schulz et al. (2011); Beatty et al. (2015)). I hypothesized that incorporating synchronicity in cortical input into this model will allow an understanding of how the striatum transforms different varieties of cortical input into different dynamical states and help inform what role these dynamical states may play in motor decision making. To test this, I added rhythmic input to the striatal model and observed the impact of this input on striatal FSI and SPN activity. Since the SPN and FSI networks receive similar cortical input, I also expected the SPN network to entrain to cortical rhythms in a frequency-dependent manner.

The results of providing rhythmic input to my model suggest that the inhibitory actions of FSIs on SPNs mediate specificity in the striatal response to different frequencies of input. Using square wave inputs of various frequencies, I found that the FSIs prevent the SPNs from generating phase-locked beta oscillations in response to input frequencies outside the beta band, ensuring fidelity of transmission of cortical beta rhythms. Without FSIs, the SPN subnetwork can phase lock to a broad range of frequencies, but also produces beta oscillations in response to input frequencies outside of the beta band. When FSIs are present in either low or high dopamine conditions, the beta power produced by the SPN subnetwork in response to non-beta frequencies is dramatically reduced, while transduction of frequencies in the beta range remains intact. Therefore, suppression of beta resonance to input outside of the beta range could be an essential function of the striatal FSI network; one combined role of striatal FSIs and SPNs may be to act as a band pass filter on cortical input such that only beta oscillations can reliably produce a

beta in response.

The second major result presented in Chapter 3 is that certain gamma input frequencies can cause the FSIs to limit or entrain SPN activity. In the high DA condition, specific frequencies of gamma input can cause the FSI network to fire continuously, causing SPNs to entrain to gamma frequencies to which they would otherwise produce a beta in response. This allows FSI gamma to be induced during an arbitrary phase of the ongoing theta oscillation and to last for an indefinitely long or short amount of time, perhaps constituting an override signal sent during times of highly motivated behavior when rapid changes in strategy are needed. This is especially notable in that the SPN subnetwork will not otherwise produce a high gamma as output, suggesting a specific role for fast-spiking interneurons in the striatal microcircuit in vivo. Therefore, cortical gamma input to both cell types combined with dopaminergic tone constitutes a unique network mechanism by which striatum is able to transmit gamma oscillations to downstream basal ganglia structures, a behavior otherwise not permitted by the model network. Overall, the model network behavior has significant possible functional implications and suggests several hypotheses regarding the role of FSIs in routing cortical input through striatum.

In Chapter 4, I explore whether the network behavior predicted by my model would be detectable in noninvasive electroencephalogram (EEG) recordings. I did not have access to data recorded directly from human striatum, but there is evidence that striatal activity can be detected via EEG during reward learning (Foti et al. (2015); Mas-Herrero et al. (2015); Andreou et al. (2017)). If my model holds true in humans, 3 Hz-nested beta activity might be detectable in human electrophysiological recordings during a probabilistic reward learning task, as peak stri-

atal dopaminergic tone should occur when an unexpected reward is given. Via exploratory data analysis of a human EEG dataset recorded during a reward learning task, I determined that the alternating rhythms predicted by my model can be detected by phase-amplitude coupling at cortical electrodes. Within the first 500 milliseconds after subjects were told their answer was correct, amplitude at all beta and gamma frequencies showed increased modulation by the phase of a 3-5 Hz rhythm. Although these findings are consistent with my striatal modeling prediction, it is unclear whether these signals actually originate in striatum. If dopaminergic activity in striatum does produce a signal that can be detected noninvasively, this would greatly facilitate investigation of the predictions of my model and allow for studies directly linking human behavior with striatal cellular function.

The model described here could lend itself to many possible future studies. In particular, the effect of simulated acetylcholine on this circuit would be of great interest, since the DA depleted Parkinsonian state results in an excess of cholinergic tone (Ikarashi et al. (1997)). It is important to identify the contribution of the cholinergic system to network pathology in order to identify appropriate therapeutic targets. Similarly, future studies could propose an experiment involving adding pharmaceutical manipulations or deep brain stimulation to the proposed model in order to examine potential therapeutic mechanisms. Additionally, the proposed model could be expanded to include other striatal interneuron types, in particular cholinergic cells or somatostatin neurons, in order to examine the impact of these cell types upon oscillatory behavior and motor computation. It would also be feasible to utilize the output of this model in simulating downstream impacts of striatum on basal ganglia or thalamus. Finally, while the proposed model is meant

to simulate an awake state, it could be modified to describe striatal behavior characteristic of sleep, which would be of use in studies of memory consolidation and motor inhibition.

CHAPTER 2

A biophysical model of striatal microcircuits suggests gamma and beta oscillations interleaved at delta/theta frequencies mediate periodicity in motor control

2.1 INTRODUCTION

As the largest structure of the basal ganglia network, the striatum is essential to motor function and decision making. It is the primary target of dopaminergic (DAergic) neurons in the brain, and its activity is strongly modulated by DAergic tone. Disorders of the DA and motor systems, such as Parkinson's, Huntington's, Tourette's, and many others, result in abnormal network activity within striatum (Gittis & Kreitzer (2013); Brown & Williams (2005); Ghiglieri et al. (2012); Rothe et al. (2015); Naze et al. (2018); Miller et al. (2011); Cepeda et al. (2013); Leckman et al. (2010); Vinner et al. (2017)). Rhythmic activity is observed in both striatal spiking and local field potential, and oscillations in the striatum are correlated with voluntary movement, reward, and decision-making in healthy individuals (Berke (2009); Stenner et al. (2016); Doñamayor et al. (2012); Cohen et al. (2009); Kalenscher et al. (2010); van der Meer et al. (2011); Feingold et al. (2015); Khanna & Carmena (2017); Masimore et al. (2005)), while disruptions of these rhythms are biomarkers of mental and neurological disorders (Gittis & Kreitzer (2013); Jenkinson & Brown (2011); Jenkinson et al. (2013); Brown & Williams (2005); Brown (2007); Alberico et al. (2017); Alam et al. (2014); Belić et al. (2016); Little & Brown (2014); Tinkhauser et al. (2017); West et al. (2018)). However, the mechanisms of these oscillations, and their role in motor behavior and its dysfunctions, remain poorly understood.

The current study focuses on the oscillatory bands frequently observed in stri-

atal local field potential: δ (1-3 Hz), θ (4-7 Hz), β (8-30 Hz), low γ (50-60 Hz), and high γ (70-80 Hz) (Berke (2009); López-Azcárate et al. (2013); Feingold et al. (2015)). Power in these bands consistently correlates with responses to task parameters including motor initiation, decision making, and reward (Berke (2009); Jenkinson et al. (2013); Stenner et al. (2016); Doñamayor et al. (2012)). Power in the β band is elevated in Parkinson's disease and correlates with the severity of bradykinesia (Brown & Williams (2005)), while striatal γ is associated with the initiation and vigor of movement(Jenkinson et al. (2013); Masimore et al. (2005)). In the healthy basal ganglia, β and γ activity are inversely correlated and differentially modulated by slower basal ganglia rhythmic activity, suggesting that the balance of these distinct oscillatory dynamics is important to healthy motor function (Feingold et al. (2015)). In rat striatum *in vivo*, spontaneous β and low γ oscillations transition to θ and high γ dynamics upon reward receipt and with administration of DA agonist drugs(Berke (2009)); similarly, in rat caudate and putamen, DAergic agonists produce robust low-frequency modulation of high γ amplitude (López-Azcárate et al. (2013)).

In this paper, we propose a biophysical model of striatal microcircuits that comprehensively describes the generation and interaction of these rhythms, as well as their modulation by DA. Our simulations capture the dynamics of networks of striatal fast-spiking interneurons (FSIs) and striatal projection neurons (SPNs), using biophysical Hodgkin-Huxley type models. Our model consists of three interconnected populations of single or double compartment Hodgkin-Huxley neurons: a feedforward network of FSIs, and two networks of SPNs (the D1 receptor-expressing "direct pathway" subnetwork and the D2 receptor-expressing "indirect pathway" subnetwork). SPNs, responsible for the output of the striatum, make

up 95% of striatal neurons in rodents (Koos et al. (2004)). SPN firing is regulated by relatively small populations of striatal interneurons, including fast spiking interneurons (FSIs), which strongly inhibit SPNs. Our model FSIs exhibit a D-type potassium current (Golomb et al. (2007)), and our model SPNs exhibit an M-type potassium current (Shen (2005)). Both cell types are modulated by DAergic tone: FSIs express the excitatory D1 DA receptor(Bracci et al. (2002)), while two distinct subpopulations of SPNs express exclusively the D1 or the inhibitory D2 receptor subtype. We modeled both SPN subpopulations, with high simulated DAergic tone increasing and decreasing D1 and D2 SPN excitability, respectively. To model DA effects on the FSI network, we simulated three experimentally observed effects: increased excitability due to depolarization (Bracci et al. (2002)), increased gap junction conductance(Onn & Grace (1994), and decreased conductance of inhibitory synapses(Bracci et al. (2002)). Both gap junctions and inhibition are known to play a role in the generation of rhythmic activity (Sherman & Rinzel (1992); Wang & Rinzel (1992); Van Vreeswijk et al. (1994); Whittington et al. (1995); White et al. (1998); Skinner et al. (1999); Whittington et al. (2000); Lewis & Rinzel (2000); Traub et al. (2001); Bem & Rinzel (2004); Mancilla et al. (2007)).

Our previous experimental and modeling work suggests that striatal SPN networks can produce a β (15-25 Hz) oscillation locally (McCarthy et al. (2011)). Our current model demonstrates that FSI networks can produce δ/θ, low γ, and high γ oscillations. A fast-activating, slow-inactivating potassium current (the D-type current) allows FSIs to produce γ and δ/θ rhythms in isolation, and network interactions make these rhythms, otherwise highly susceptible to noise, robust. In our simulations, DA induces a switch between two FSI network states: a low DA state exhibiting persistent low γ rhythmicity, and a high DA state in which a δ/θ

oscillation modulates high γ activity. As a result of FSI inhibition of SPNs, DA induces a switch in striatal dynamics, between a low DA state in which low γ and β rhythms coexist, and a high DA state in which bursts of FSI-mediated high γ and SPN-mediated β rhythms alternate, nested within (and appearing at opposite phases of) an FSI-mediated δ/θ rhythm. Thus, our model generates a hypothesis as to how observed relationships between DA and rhythmicity impact the function of the motor system. Namely, DA appears to encourage or permit periodic motor program switching, allowing the emergence of an FSI-mediated δ/θ-nested γ rhythm, which in turn breaks up the “stay" signal mediated by SPN β rhythms(Engel & Fries (2010)).

2.2 RESULTS

2.2.1 Single model FSIs produce delta/theta-nested gamma rhythms whose power and frequency is modulated by excitation

We modified a previous single-compartment striatal FSI model(Sciamanna & Wilson (2011)) by adding a dendritic compartment (shown to be an important determinant of gap-junction mediated synchrony (Rinzel (2003); Lewis & Rinzel (2004); Zahid & Skinner (2009); Schwemmer & Lewis (2014))) and increasing the conductance of the D-type K current to 6 mS/cm^2. Previous work showed that two characteristic attributes of FSI activity *in vitro*, stuttering and γ resonance (defined as a minimal tonic firing rate in the γ frequency range), are dependent on the D-current(Golomb et al. (2007); Sciamanna & Wilson (2011)). Our modified FSI model successfully reproduced these dynamics as well as revealing other dynamical behaviors (Fig. 2.1).

With increasing levels of tonic applied current (I_{app}), our model FSI transitions

from quiescence to (periodic) bursting to periodic spiking. The bursting regime, of particular interest in this work, is dependent on the level of tonic excitation and, centrally, the D-current conductance (Fig. 2.1). FSI spiking frequency increases with tonic drive (Figure 2.1A). As shown previously(Sciamanna & Wilson (2011)), the FSI model's γ-rhythmic intraburst spiking arises from its minimum firing rate, which is also set by the D-current conductance. When this conductance is zero, the model has no minimum firing rate; firing rate is a continuous function of I_{app} with a minimum firing rate of zero (Fig. 2.1B). As the D-current conductance is increased, the firing rate below which the cell will not fire also increases. Therefore, our choice of D-current (g_d = 6, resulting in a minimum firing rate around 40 Hz) reflects not only our interest in the bursting regime, but also our desire to match experimental observations of striatal γ frequency (Berke (2009); Sciamanna & Wilson (2011)).

The frequency of bursting depends on the decay time constant of the D-type potassium current (τ_D); in the absence of noise, it is in the δ frequency range for physiologically relevant τ_D ($<\sim$200 ms, Figure 2.1C). Note that τ_D changes the inter-burst interval without changing the timing of spikes within a burst. With lower levels of D-current (as used in previous FSI models (Golomb et al. (2007); Sciamanna & Wilson (2011); Corbit et al. (2016)), bursting is aperiodic. For sufficiently large D-current conductance, FSI bursting occurs for a broad range of applied currents (I_{app} over 5 $\mu A/cm^2$, Fig. 2.1D,E). Since simulated DA acts on our FSI model by increasing tonic excitation, DA causes an increase in model FSI spiking from low γ rhythmicity to high γ rhythmicity. Below, we demonstrate that the FSI γ is determined by this single-cell rhythmicity and is mostly independent of the timescale of inhibitory synapses.

In addition to increasing with tonic excitation, burst frequency increases to δ/θ

frequencies when the input includes small amounts of noise (Fig. 2.2A,B), which decrease the interburst interval. However, noise of sufficient amplitude abolishes rhythmic bursting altogether (at least in single cells, Fig. 2.2C).

In summary, a single model FSI displays low-frequency-nested γ oscillations, dependent on the D-type current, under a wide range of tonic excitation levels. Both low frequency power and γ frequency increase with tonic excitation. While noise increases the frequency of the slower rhythm from δ to θ, it also diminishes the power of this rhythm in the single cell. Below we demonstrate that all of these effects are also present in a network of FSIs, with a key difference: the network δ/θ rhythm is robust to noise.

2.2.2 FSI networks produce DA-dependent delta/theta and gamma rhythms

To determine if γ and δ/θ oscillations persist in networks of connected FSIs, and how DA could modulate these network dynamics, we simulated a network of 50 model FSIs connected randomly by both inhibitory synapses (connection probability 0.58 (Gittis et al. (2010))) and gap junctions (connection probability 0.3 (Hjorth et al. (2009))). We also implemented three experimentally observed effects of DA on FSI networks: increased tonic excitation of individual FSIs (Bracci et al. (2002)), increased gap junction conductance between FSIs (Onn & Grace (1994)), and decreased inhibitory conductance between FSIs (Bracci et al. (2002)) (see Methods). We used the sum of all synaptic inputs within the network as a surrogate measure for simulated local field potential (LFP); this measure is hereafter referred to as “surrogate LFP".

Unlike in single cells, FSI network δ/θ rhythmicity is dependent on sufficient levels of tonic excitation: at low levels of tonic input ($I_{\text{app}} <\sim 1\mu A/cm^2$), the FSIs

do not attain enough synchrony for a strong network δ/θ (Fig. 2.3Ai). As in single cells, FSI network δ/θ power increases with tonic input strength (Fig. 2.3Ai). Sufficiently strong gap junction coupling is also a requirement for the FSI network to attain sufficient synchrony to produce δ/θ rhythmicity (Fig. 2.3Bi). Gap junctions function to protect the FSI network δ/θ rhythm from the effects of noise (as in (Skinner et al. (1999); Sherman et al. (1988))); the δ/θ oscillation in the network is far more robust to noise than the same oscillation in a single cell (S1 Fig.). Finally, inhibitory synaptic interactions between FSIs have a desynchronizing effect that interferes with network δ/θ, and increasing inhibitory conductance within the FSI network decreases power in the δ/θ band (Fig. 2.3Ci). FSI network γ power and frequency both increase with tonic input strength (Fig. 2.3Aii), and, like the network δ/θ, the network γ rhythm is dependent on sufficient gap junction conductance and is disrupted by inhibition (Fig. 2.3B & C, ii). Both network rhythms are robust to a wide range of heterogeneity in applied current and conductances (S2 Fig.).

To explore whether the γ rhythms observed in the FSI network are generated by inhibitory interactions, we examined the dependence of γ frequency on the time constant of $GABA_A$ inhibition, as the characteristic frequency of canonical interneuron network γ (ING) has been shown to depend on this time constant(Wang & Buzsáki (1996); White et al. (1998); Chow et al. (1998); Whittington et al. (2000)). The frequency of the γ rhythm produced under low DA conditions decreased with increases in the $GABA_A$ time constant (Fig. 2.3D), suggesting this rhythm is ING-like. However, the γ produced under high DA conditions had a frequency that was not highly dependent on the inhibitory time constant, suggesting that this γ rhythm is mechanistically different from previous ING models, being generated

by synchronous γ frequency bursts in individual cells, as opposed to inhibitory interactions.

In order to explore FSI network dynamics that might be observed during normal fluctuations in DA during goal-directed tasks (Schultz et al. (1997)), we simulated FSI network activity under two conditions, simulated low (or baseline) and high DAergic tone (Fig. 2.4A). Parameter values for low and high DA were chosen so as to best demonstrate qualitative differences in network behaviors while maintaining physiologically realistic behavior on the cellular level (see Methods).

During simulated low DAergic tone, characterized by low levels of FSI tonic excitation and gap junction conductance, and high levels of inhibitory conductance, the network produces a persistent low frequency γ oscillation ($\sim$ 60 Hz) in the surrogate LFP (Fig. 2.4Bi-Di). The raster plot of FSI spike times (Fig. 2.4Eii) shows that individual FSIs exhibit sparse spiking in the low DA state. Although individual FSIs exhibit periodic spike doublets or bursts (γ-paced and entrained to the network γ) that recur at δ/θ frequency, the timing of these bursts is independent (Fig. 2.4Di, Ei). Therefore, while δ/θ power is present at the level of individual FSIs, there is not sufficient synchrony for it to appear in the network; while the voltages of individual cells show power in the δ/θ band, a power spectrum of the surrogate LFP does not (Fig. 2.4Di).

During simulated high DAergic tone, characterized by high levels of tonic excitation and gap junction conductance and low levels of inhibitory conductance, network activity is much more structured: a strong 80 Hz γ rhythm, phase-modulated by a 3 Hz δ/θ rhythm, is evident in both the surrogate LFP and network raster plots (Fig. 2.4Bii-Eii, right). In this state, active FSIs spike at the same phase of both δ/θ and γ, producing dual (and nested) network rhythms.

2.2.3 SPN networks generate DA-dependent beta oscillations

Previous work by our group on the striatal origin of pathological oscillations in Parkinson's disease found that robust β oscillations can emerge from inhibitory interactions in model networks of SPNs (McCarthy et al. (2011)). The interaction of synaptic $GABA_A$ currents and intrinsic M-currents promotes population oscillations in the β frequency range; their β timescale is promoted by the M-current, which allows rebound excitation at $\sim$50 ms in response to synaptic inhibition. Excitation of SPNs increases β power and frequency (see Methods). With this previous striatal SPN network model, we explored the transition from a healthy to a parkinsonian state with pathologically low levels of striatal DA (McCarthy et al. (2011)). Here, to explore the generation of β rhythmicity during normal fluctuations in DAergic tone, we simulated two independent networks of 100 D1 receptor expressing ("direct pathway") SPNs and 100 D2 receptor expressing ("indirect pathway") SPNs. Model SPNs are single compartment neurons expressing the Hodgkin-Huxley spiking currents and the M-type potassium current, interconnected all-to-all by weak inhibitory $GABA_A$ synapses (i.e., connection probability 1). We simulated the effects of DA on model D1 and D2 SPNs by increasing and decreasing their levels of tonic excitation, respectively. (Whether DA generates a positive or negative applied current was the only difference between D1 and D2 expressing SPNs in our model; see Methods and Fig. 2.5A. For further explanations of parameter choices and discussion of simplifications made while modeling the network, see the "Caveats and limitations" section of the Discussion.) In the absence of FSI input, neither population was sufficiently excited to exhibit spontaneous spiking under low DA conditions (Fig. 2.5i). Subthreshold low-β oscillations are present in the mean voltage of the non-firing SPN networks due to the

timescale of the M-type potassium current (McCarthy et al. (2011)). Under high DA conditions, D1 SPNs exhibited persistent high-β rhythmicity at $\sim$20 Hz (Fig. 2.5ii) due to the increase in applied current.

2.2.4 FSI network gamma and delta/theta oscillations rhythmically modulate SPN network beta oscillations only in high DA state

To understand the interactions between FSI and SPN networks, and between β, γ, and δ/θ rhythms, we simulated a combined FSI-SPN striatal microcircuit, in which 50 model FSIs randomly connect to two independent networks of 100 SPNs, one each consisting of D1 and D2 SPNs (connection probability from FSIs to D1 or D2 SPNs of 0.375 (Corbit et al. (2016))). FSIs were interconnected by gap junctions and inhibitory synapses (connection probability 0.3 and 0.58 respectively). D1 and D2 SPNs were connected by all-to-all inhibitory synapses (connection probability 1) within but not across populations. There were no connections from SPNs back to FSIs (Koós & Tepper (1999)).

During simulated baseline DAergic tone, we modeled D1 and D2 SPNs as being equally excitable, with equal firing rates matching *in vivo* observations (Berke et al. (2009)) while under the influence of FSI inhibition. The presence of FSIs is sufficient for the SPNs to fire in the low dopamine state (Fig. 2.6i); this paradoxical excitatory effect of GABAergic input arises because SPNs can be excited via post-inhibitory rebound, as demonstrated in previous work (McCarthy et al. (2011)). Both SPN networks produce a low-β rhythm (15 Hz), while the FSI network produces a low γ (60 Hz, Fig. 2.6i & 2.7i). The SPN subnetwork does not entrain to the FSI γ. The generation of low γ and β rhythms matches observations of striatal rhythmicity in resting healthy animals *in vivo* (Berke (2009)). Our model suggests that these γ and

β rhythms are independently generated by FSI and SPN networks, respectively.

During simulated high DAergic tone, an FSI-mediated high γ ($\sim$80 Hz) and an SPN-mediated β ($\sim$15-20 Hz) are observed during opposite phases of an ongoing FSI network δ/θ rhythm (Fig. 2.6ii & 2.7ii). During the peak of the δ/θ, the incoming γ frequency input from the FSIs silences the SPNs. When the FSIs are silent during the δ/θ trough, both D1 and D2 SPN populations are sufficiently excited to produce a β rhythm. Thus, while the SPNs cannot entrain to the γ frequency of FSI inhibition, they are modulated by the FSI-generated δ/θ rhythm. Due to the differences in excitability under high DAergic tone, the D1 SPN subpopulation produces a higher frequency β ($\sim$20 Hz) than does the less excitable D2 subpopulation, which produces a low β ($\sim$15 Hz). Preliminary data suggest that the SPN network is more sensitive to input in the high DA condition, when the ongoing β rhythm is periodically disrupted by the FSI-induced δ/θ (S3 Fig.).

2.3 DISCUSSION

Our model suggests that DAergic tone can produce a transition between two dynamical states in striatal GABAergic networks. In the baseline DAergic tone state, ongoing low γ (55-60 Hz) and β ($\sim$15 Hz) oscillations are generated by striatal FSI and SPN networks, respectively (Fig. 2.7i). In the high DAergic tone state, packets of FSI-mediated high γ ($\sim$80 Hz) and SPN-mediated β (10-20 Hz) rhythms alternate at δ/θ ($\sim$3 Hz) frequency (Fig. 2.7ii). Our results make predictions about the generation of striatal rhythms, have implications for the role of FSIs in regulating the activity of SPNs, and suggest an underlying mechanism for the temporal dynamics of motor program selection and maintenance (Fig. 2.7D).

2.3.1 Mechanisms of gamma and delta / theta oscillations in single FSIs

Prior work has shown γ oscillations in striatal FSIs arising from an interaction between the spiking currents and the spike frequency adaptation caused by the potassium D-current, which produces a minimum FSI firing rate in the γ range (Sciamanna & Wilson (2011); Bracci et al. (2003)). The frequency of the FSI γ depends on excitatory drive to the FSIs, which in our model leads to the modulation of γ frequency by DA, a phenomenon also observed in striatal γ oscillations *in vivo* (van der Meer et al. (2010); van der Meer & Redish (2009); Catanese et al. (2016); Kalenscher et al. (2010)).

Prior work has also suggested that the D-current is responsible for the bursting or stuttering behavior of FSIs, in which brief periods of high frequency activity are interspersed with periods of quiescence (Golomb et al. (2007)). However, regularity in these periods of quiescence has not been previously observed. Thus, the present study is novel in its prediction of the generation of low-frequency rhythms by FSIs, dependent on high levels of D-current conductance; FSIs have previously been characterized solely as generators of γ oscillations. In our model, the D-current is activated by burst spiking, e.g., at γ frequency, and hyperpolarizes the cell for roughly a δ/θ period due to its long time constant of inactivation. Though the δ rhythm produced by individual cells decreases in frequency in response to excitatory drive (Fig. 2.1D), the frequency of the resulting δ/θ oscillation in the network has a minimum around 3 Hz (Fig. 2.3i). This lower bound on δ/θ frequency in the network is likely a result of gap-junction induced synchrony driving burst frequency higher than in the individual cell while maintaining robustness to noise. Notably, this study is also a novel demonstration of the generation of both δ/θ and γ oscillations by a single membrane current.

2.3.2 Mechanisms of gamma and delta/theta oscillations in FSI networks

Our model FSI network produces qualitatively different dynamics at high and baseline levels of simulated DA. Under high dopaminergic tone, the FSI network produces high γ band (80 Hz) oscillations modulated by a δ/θ ($\sim$ 3 Hz) oscillation, while under low dopaminergic tone the FSI network produces low γ band (60 Hz) oscillations alone (Fig. 2.4). While both δ/θ and γ are present at the level of individual cells under all dopaminergic conditions, only in the high DA condition is bursting sufficiently synchronized that δ/θ power is present in the network. The presence of δ/θ at the network level can be attributed to the higher level of gap junction conductance in the high DA condition (Fig. 2.3Bi).

The ability of gap junctions to generate synchrony is well established in computational and experimental work (Sherman & Rinzel (1992); Lewis & Rinzel (2000); Rinzel (2003); Bem & Rinzel (2004); Sherman et al. (1988); Munro & Börgers (2010); Hjorth et al. (2009); Lau et al. (2010); Mancilla et al. (2007); Traub et al. (2001); Zahid & Skinner (2009)). Previous models from other groups suggest that gap junctions can enable synchronous bursting in interneurons, by aligning the burst envelopes, as in our model (Skinner et al. (1999)). While a shunting effect of low conductance gap junctions can inhibit spiking (Hjorth et al. (2009)), gap junctions with high enough conductances have an excitatory effect, promoting network synchrony (Munro & Börgers (2010); Traub et al. (2001)). Previous work has also shown the importance of gap junction connectivity in stabilizing network γ oscillations *in silico* (Sherman & Rinzel (1992); Lewis & Rinzel (2000); Börgers et al. (2012)), as well as network γ and δ/θ oscillations in inhibitory networks *in vitro* and *in silico* containing noise or heterogeneity (Traub et al. (2001)). Striatal FSIs *in vivo* are highly connected by gap junctions as well as inhibitory synapses(Fukuda (2009)), similar

to the networks of inhibitory interneurons that produce ING rhythms (Whittington et al. (2000)). Unlike ING, however, our FSI network γ is independent of GABAergic synapses: inhibitory conductance has only a small impact on γ frequency, and γ power is highest when inhibitory synapses are removed (Figure 3C). In slice, the γ resonance of striatal FSIs is dependent on gap junctions but not on GABA (Russo et al. (2013)), suggesting that our model is an accurate representation of striatal FSI γ.

It is important to note that, while our model is conceived as a representation of the striatal microcircuit, physiologically similar FSI networks are present in cortex (Golomb et al. (2007)); therefore, the mechanisms described here may contribute to the generation of δ/θ-modulated γ oscillations in cortex as well.

2.3.3 Support for striatal rhythm generation

Our model provides mechanistic explanations for all four oscillatory bands observed in ventral striatum *in vivo* (δ/θ, β, low γ, and high γ) (Berke (2011)). Previous modeling and experiments suggest β can be generated by striatal SPNs (McCarthy et al. (2011); Kondabolu et al. (2016); Pittman-Polletta et al. (2018)). Our results suggest that FSIs generate striatal γ, and that motor- and reward-related increases in γ power reflect increased striatal FSI activity.

There is evidence to support the existence of a locally generated striatal γ oscillation that is not volume conducted and that responds to local DAergic tone (Popescu et al. (2009); West et al. (2018)). The FSIs of the striatum are the most likely candidate generator of this rhythm: they are unique among striatal cell types in preferentially entraining to periodic input (from each other and from cortex) at γ frequencies (Surmeier et al. (2011); Schulz et al. (2011); Belić et al. (2017); Mancilla

et al. (2007); Naze et al. (2018)). Different populations of striatal FSIs *in vivo* entrain to different γ frequencies, and FSIs entrained to higher frequencies are also more entrained to cortical input (Berke (2011); van der Meer et al. (2010); van der Meer & Redish (2009); Catanese et al. (2016); Kalenscher et al. (2010)). It is likely that different subpopulations of FSIs selectively entrain to specific γ frequencies, determined by physiological and contextual, including neuromodulatory (e.g., DAergic), factors.

Experimental evidence also supports striatal FSI involvement in a DA-modulated δ or θ rhythm. FSIs phase lock to spontaneous striatal LFP oscillations at δ (Hernandez (2014); Sharott et al. (2009); Alberico et al. (2017)) and θ (Sharott et al. (2012); Berke et al. (2009); Garas et al. (2016); Lalla et al. (2017)) as well as γ frequencies. *In vivo*, striatal δ and θ power are modulated by task-related phenomena such as choice points and motor execution, as well as by reward and reward expectation, suggesting responsiveness in both frequency bands to DA (known to phasically increase in response to reward cues) (DeCoteau et al. (2007); Gruber et al. (2009); Emmons et al. (2016); Doñamayor et al. (2012); Lepski et al. (2012); Kimchi et al. (2009)). θ has also been shown to modulate the response of SPNs to reward (van der Meer et al. (2011)).

The slow rhythm generated by our model network is on the boundary between the δ and θ frequency bands, and as such it is difficult to determine for which of the two bands our model has more substantial implications. However, many electrophysiological studies of striatum find a low frequency rhythm in this intermediate 3 to 5 Hz range (Dejean et al. (2011); Stenner et al. (2015); López-Azcárate et al. (2013)). While rodent electrophysiology suggests that δ is more prevalent in the striatum of the resting animal and θ is stronger during high DAergic tone

(Leung & Yim (1993); von Nicolai et al. (2014)), human studies suggest that DAergic reward signals are associated with increased power in the δ band in nucleus accumbens and that θ power (which originates in cortex) is associated with the decreased DA signal following an unexpected loss (Foti et al. (2015); Bernat et al. (2015)). The frequency of this slow rhythm may be determined by entrainment to rhythmic cortical input, or by different subpopulations of cells responding to different components of the dopamine signal (e.g. tonic versus phasic, anticipatory vs consummatory, etc.).

The β oscillations produced by our model network vary in frequency. During simulated baseline DAergic tone, the β frequency in both SPN subnetworks is closer to 15 Hz, while during high DAergic tone, the β frequency produced by the D1 SPN subnetwork approaches 20 Hz, without a change in the frequency generated by the D2 SPN subnetwork (Fig 2.5,2.6). This behavior is not unexpected, as our previous modeling work suggested that the frequency of the β generated by SPN networks is sensitive to excitatory drive (McCarthy et al. (2011)), which is the difference between the cell subtypes in this model. Experimental evidence also supports the association of low-β but not high-β frequencies with the indirect (D2-expressing) pathway of the basal ganglia (Oswal et al. (2016)). Corticostriatal models constructed by our group that include connectivity differences between D1 SPNs and D2 SPNs suggest that these differences in β frequency may be an essential component of how cortical input is routed to the direct versus the indirect pathway during decision making (Ardid et al. (2019)).

2.3.4 Rhythmicity in striatal dynamics and movement

In vivo , striatal β power has a well established negative correlation with DA and locomotion in both health and disease, while striatal γ power has a positive correlation with both (Doñamayor et al. (2012); Brown & Williams (2005); Stenner et al. (2016); Tan et al. (2016); Jenkinson & Brown (2011); Jenkinson et al. (2013)). β oscillations in the basal ganglia are thought to provide a “stay" or “status quo" signal that supports maintenance of the currently active motor program (Engel & Fries (2010)), and they are causally implicated in motor slowing and cessation (Brown (2007); Khanna & Carmena (2017); Lemos et al. (2016); Feingold et al. (2015); Tan et al. (2016); Little & Brown (2014)).

In our simulations of high DAergic tone, FSI spiking at high γ frequencies δ/θ-periodically inhibits SPN-generated β oscillations, permitting SPN β only during the 150-200 millisecond δ/θ trough corresponding to the FSIs' interburst interval. We hypothesize that these periodic gaps between SPN β packets are necessary to terminate ongoing motor programs and initiate new motor programs, both represented by active SPN cell assemblies. During the δ/θ trough, all SPN cell assemblies are simultaneously released from inhibition and viable to compete once again to determine the current motor program, with incoming input from cortex influencing this competition. Under this interpretation, our results predict that striatal networks oscillate between a “stay" or “program on" state marked by SPN β oscillations, and a “switch" or “program off" state marked by FSI high γ oscillations, and that the δ/θ period limits the speed of sequential motor program execution (Fig. 2.7D). Accordingly, the SPN network responds more specifically to input when the FSI-induced δ/θ is periodically disrupting the intrinsic SPN β rhythm (S3 Fig.). Associations formed between sets of SPNs receiving similar input persist

during an ongoing β oscillation, but these associations are broken by FSI-mediated rhythmic inhibition. This inhibitory disruption thereby allows SPNs to flexibly respond to new input, which would otherwise be unable to override the coordinated activity of pre-existing cell assemblies.

In support of this hypothesis, striatal representations of behavioral "syllables" combined to create motor programs are active for a maximum of $\sim$200 ms (Markowitz et al. (2018)), and the velocity of continuous motion is modulated intermittently at a θ frequency ($\sim$6-9 Hz) (Gross et al. (2002)). In healthy animals, the duration of β bursts has an upper limit of $\sim$120 ms, about half a θ cycle (Feingold et al. (2015)), in agreement with our prediction that β activity is δ/θ phase-modulated. Striatal γ has also been observed in transient ($\sim$150 ms) bursts that are associated with the initiation and vigor of movement (Masimore et al. (2005)). Additionally, other biophysically constrained computational models have suggested that SPN assemblies fire in sequential coherent episodes for durations of several hundred milliseconds, on the timescale of one or several δ/θ cycles (Humphries et al. (2009)). Overall, evidence supports the hypothesis that β and γ oscillations in striatum *in vivo*, and therefore the motor states they encode, are activated on δ/θ-periodic timescales.

Furthermore, β and γ power are anticorrelated in EEG and corticostriatal LFP (Jenkinson et al. (2013); López-Azcárate et al. (2013); Zhang et al. (2016)), in agreement with our model's prediction that these rhythms are coupled to opposite phases of ongoing δ/θ rhythms. FSI and SPN firing are inversely correlated *in vivo*, entrained to θ, and they are active during opposite phases of θ, as observed in our model (Howe et al. (2011); Thorn & Graybiel (2014); Berke et al. (2004); Sharott et al. (2012); Berke et al. (2009)). δ/θ-γ cross-frequency coupling is observed in

striatum and increases during reward, when DAergic tone is expected to be high (von Nicolai et al. (2014); Dzirasa et al. (2010); Cohen et al. (2009); Tort et al. (2008); López-Azcárate et al. (2013)). Our model suggests that these cross-frequency relationships occur in part due to FSI inhibition of SPNs. Though FSIs are smaller in number, FSI-SPN synapses have a much stronger effect than SPN-SPN connections, with each FSI inhibiting many SPNs (Tepper et al. (2008); Koós & Tepper (1999)).

During baseline DAergic tone in our model, FSIs produce an ongoing low γ that does not effectively suppress SPN β activity (produced sporadically in both D1 and D2 SPN networks), and thus does not facilitate the switching of the active SPN assembly. Thus, our model suggests that at baseline levels of DA, switching between SPN assembles may be more dependent on cortical inputs or downstream basal ganglia circuit computations. Although the function of FSI low γ input in SPN dynamics is unclear, it may facilitate striatal responsivity to cortical low γ input, which occurs in an afferent- and task-specific manner (Berke (2011)). SPNs do not entrain to γ in our model, suggesting that γ oscillations are not transmitted to downstream basal ganglia structures.

In contrast, both the β and δ/θ rhythms in our model entrain SPN networks and may be relayed to other basal ganglia structures. Intriguingly, alternation between β and γ on a δ/θ timescale has been observed in the globus pallidus *in vivo*, and DAergic tone modulates these oscillations and their interactions (Dejean et al. (2011); López-Azcárate et al. (2013)). Thus, the mechanisms proposed in our model may also play a role in the oscillatory dynamics of other basal ganglia structures, through a combination of rhythm propagation and local rhythm generation by similar circuits. Similar pauses in FSI activity, allowing transient SPN disinhi-

bition and production of β oscillations, occur in a recent computational model of the striatal-GPe network (Corbit et al. (2016)), also based on an earlier model of stuttering FSIs (Golomb et al. (2007)). In contrast to this work, we emphasize the mechanisms producing β and the coordination of β and γ by δ/θ, not addressed previously (Corbit et al. (2016)).

2.3.5 Implications for disease

In Parkinson's disease, which is characterized by motor deficits and chronic DA depletion, β power is correlated with the severity of bradykinesia (Brown & Williams (2005)). Parkinsonian β may be generated by striatal D2 SPNs (McCarthy et al. (2011); Kondabolu et al. (2016); Pittman-Polletta et al. (2018)). Parkinsonian conditions also produce high cholinergic tone (Ikarashi et al. (1997)), known to decrease the conductance of GABAergic FSI-SPN synapses (Koós & Tepper (2002)). Thus, the failure of the FSI inhibition-mediated motor program switching described above may play a role in the motor deficits observed in Parkinson's: if DA is low, and FSIs are unable to inhibit either D1 or D2 SPNs, δ/θ modulation of SPN β rhythmicity will be supplanted by ongoing D2 β rhythmicity, impairing motor initiation by reducing the possibility of motor program switching in the Parkinsonian striatum. Supporting this hypothesis, the β frequency generated by D2 SPNs in our model is substantially lower than that generated by the D1 SPN subnetwork in the high DA condition (Fig. 2.6). Experimental work suggests that parkinsonian β is specifically a low ($<$20 Hz) β, and that treatment by L-DOPA or deep brain stimulation specifically reduces power in the low β band without affecting high β power (West et al. (2016); Hohlefeld et al. (2014); Oswal et al. (2016)). Our model suggests that this distinction in β frequency bands is at least in part due to dif-

ferences in excitatory drive between subtypes of SPNs expressing different DA receptors.

In hyperkinetic motor disorders, γ and θ rhythms are potentiated: mouse models of Huntington's disease (HD) displays unusually high δ/θ and γ band striatal LFP power (Naze et al. (2018); Miller et al. (2011); Ghiglieri et al. (2012)); and L-DOPA-induced hyperkinetic dyskinesia is also characterized by increased high γ and δ/θ power and reduced β power in the striatal LFP (Alberico et al. (2017); Alam et al. (2014); Gittis & Kreitzer (2013)). As these rhythms are tied to FSI activation in our model, we suggest that hyperkinetic disorders may result from striatal FSI hyperfunction. Consistent with this hypothesis, in HD model animals, FSI to SPN connectivity is increased, and SPNs respond more strongly to FSI stimulation (Cepeda et al. (2013)). Computational modeling suggests that FSI-generated γ more readily entrains to δ-frequency input during HD (Naze et al. (2018)).

However, hypofunction of striatal FSI networks can also lead to hyperkinetic disorders, including Tourette's syndrome, dystonia, and dyskinesias (Gittis et al. (2011); Reiner et al. (2013); Rothe et al. (2015); Vinner et al. (2017); Gittis & Kreitzer (2013); Leckman et al. (2010); Xu et al. (2016)). Dystonia, which as a disorder of involuntary muscle activation is considered hyperkinetic, can also be characterized by rigidity and freezing due to activation of antagonistic muscles. Indeed, dystonia may be the consequence of an increase in SPN firing rate due to D2 receptor dysfunction (Sciamanna et al. (2009)). Our model suggests that FSI hypofunction may contribute to dystonia by resulting in excessive SPN β rhythmicity and decreased probability of motor program switching. A reduction in θ-γ cross frequency coupling has been reported in L-DOPA-induced dyskinesia, suggesting that a chronic hyperkinetic high-DA state may also abolish the FSI-generated δ/θ-coupled γ pro-

duced here, possibly by pushing the FSI out of its bursting regime and into a tonic spiking mode (Belić et al. (2016)). These findings underscore the importance of balanced FSI inhibition of SPNs, exemplified by the periodic suppression observed in our model, which we suggest enables the flexible striatal network activity that allows for smooth, purposeful movements.

2.3.6 Caveats and limitations

Little experimental evidence on the striatal FSI D-current conductance exists. The level of D-current conductance we've chosen leads to γ frequencies and FSI firing rates that are more in line with experimental observations than with previous models; this level of D-current also produces δ/θ rhythmicity in FSI networks. Our parameter choices result in a model exhibiting a transition between "low DA" and "high DA" dynamic states that matches experimental observations and has powerful functional interpretations. Validating our results will require further experimental investigation of the D-current in striatal FSIs. Interestingly, DA has been shown to downregulate D-current conductance in prefrontal cortical FSIs (Gorelova et al. (2002)). If striatal FSIs exhibited a similar DA-dependent D-current downregulation, our simulations suggest that the transition between high and low DA states could be different from that described in the current study. The existence and functional interpretations of other dynamic transitions are beyond the scope of this paper.

In general, many DA-dependent changes in striatal neurophysiology have been observed. For the sake of simplicity, most of these have been left out of our modeling. For example, D1 and D2 SPNs respond differently to adenosine (Schiffmann et al. (2007)) and peptide release (Buxton et al. (2017)), but we did not consider

these significant factors in the production of striatal β oscillations. While the nature of the changes induced by DA in our network is based on a review of the literature, the actual values chosen are assumptions of the model. Details on the rationale behind each specific value are given in the Methods section.

We also omitted inhibitory connections between D1 and D2 SPN populations. The connectivity from D1 to D2 SPNs is very sparse (6 percent). Connections from D2 to D1 SPNs are more prevalent, but it seems unlikely that these projections would qualitatively alter our results: during the baseline state, the D1 and D2 SPNs are identical; during the high DA state, SPN inhibition tends to increase SPN β rhythmicity and spiking.

In our model the number of FSIs is small, so every FSI participates on every θ cycle; *in vivo*, the participation of multiple FSI populations is likely coordinated by cortex. Coordinated FSI activity has proven hard to observe over long periods *in vivo* (Berke (2008); Kalenscher et al. (2010)). However, FSIs form local functional circuits (Kulik et al. (2018)), and *in vivo*, striatal FSI assemblies exhibit transient gap-junction dependent synchronization (Lau et al. (2010)), possibly resulting from brief bouts of correlated cortical or homogeneous DAergic input. Furthermore, different subpopulations of FSIs have strong preferences for projecting to either D1 or D2 SPNs, as opposed to the overlapping projections modeled in our current study, and these distinct populations respond differently to cortical oscillations (Garas et al. (2016)). Thus, local γ synchrony may exist in small striatal subnetworks and be amplified by DA or cortical input via the differential recruitment of multiple FSI subpopulations.

Compounding the issues of unrealistic population size, the ratio of FSIs to SPNs in our model is much higher than data from rodent striatum suggest. 20 % of the

cells in our model network are FSIs, while FSIs comprise only about 0.7-1% of cells in rodent striatum (Tepper (2008)). Unfortunately, it would be computationally intractable to reproduce the network dynamics of the present model at a ratio of 50 or 100 SPNs per FSI. However, in humans the proportional number of FSIs is much higher; interneurons may account for as many as 25% of human striatal neurons (Graveland et al. (1985)). We have attempted to structure our model such that each SPN receives a realistic number of incoming connections from FSIs (mean 18.75 in our model, based on a range of 4 to 27 (Koos et al. (2004))), and such that these synapses are of realistic strengths. Therefore, it is reasonable to predict that the qualitative dynamics of FSI to SPN inhibition in our model would be similar even if the number of SPNs present were much higher.

Finally, cortical input to both FSIs and SPNs was simulated as Poisson noise. In a sense, we simulated a model of striatum to which cortex is not providing informative input. It could be the case that this is a population that is not “selected" by cortex to take part in motor activity, a population that is in a “listening" state awaiting cortical input, or a population taking part in a learned behavior that can be executed without cortical input. However, cortical input is probably essential in determining which SPNs and FSIs take part in network oscillatory activity. If the FSIs play a role in organizing the response of the SPNs to cortical input, changing the properties of the simulated input may prove informative in terms of how this organization might take place. In particular, cortical inputs may be more correlated within certain FSI subpopulations than others. Previous modeling work has shown that networks of striatal FSIs can detect correlated input (Hjorth et al. (2009)), a property that may play an important computational role in striatal function. Additionally, we can expect that input from cortex has oscillatory proper-

ties of its own. Exploring these complexities is an important direction for future research into the role of striatal GABAergic networks and rhythmic dynamics in motor behavior.

2.4 MATERIALS AND METHODS

All neurons (FSIs and SPNs) are modeled using conductance-based models with Hodgkin-Huxley-type dynamics. SPNs are modeled with a single compartment and FSIs have two compartments to represent the soma and a dendrite. The temporal voltage change of each neuron is described by (Eqn. 2.1):

$$c_m \frac{dV}{dt} = -\sum I_{memb} - \sum I_{syn} + I_{\text{app}} \tag{2.1}$$

Membrane voltage (V) has units of mV. Currents have units of $\mu A/cm^2$. The specific membrane capacitance (c_m) is 1 mF/cm^2 for all FSIs and SPNs. Each model neuron has intrinsic membrane currents (I_{memb}) and networks of neurons include synaptic currents (I_{syn}). The applied current term (I_{app}) represents background excitation to an individual neuron and is the sum of a constant and a noise term.

All membrane currents have Hodgkin-Huxley-type conductances formulated as:

$$I = \bar{g}(m^n h^k)(V - E_{ion}) \tag{2.2}$$

Each current in Eqn.2.2 has a constant maximal conductance ($\bar{g}$) and a constant reversal potential (E_{ion}). The activation (m) and inactivation (h) gating variables have n^{th} and k^{th} order kinetics, where $n, k \geq 0$. The dynamics of each gating variable evolves according to the kinetic equation (written here for the gating variable

m):

$$\frac{dm}{dt} = \frac{m_\infty - m}{\tau_m} \tag{2.3}$$

The steady-state functions (m_∞) and the time constant of decay (τ_m) can be formulated using the rate functions for opening (α_m) and closing (β_m) of the ionic channel by using the equations:

$$m_\infty = \alpha_m/(\alpha_m + \beta_m)$$
$$\tau_m = 1/(\alpha_m + \beta_m).$$

The specific functions and constants for different cell types are given below.

2.4.1 Striatal fast spiking interneurons

Striatal fast spiking interneurons (FSIs) were modeled as in Golomb et al., 2007 (Golomb et al. (2007)), using two compartments. The voltage in the somatic compartment (V) and in the dendrite (V_d) evolve according to:

$$c_m \frac{dV}{dt} = -I_{Na} - I_K - I_L - I_{\mathrm{D}} - I_{syn} + I_{ds} \tag{2.4}$$

$$c_m \frac{dV_d}{dt} = -I_{Na} - I_K - I_L - I_{\mathrm{D}} - I_{syn} + I_{ext} + I_{sd} \tag{2.5}$$

Background excitation is represented by the term I_{ext}, which is formulated as the sum of a tonic, DA dependent current and Poisson input. The units of I_{ext} are in $\mu A/cm^2$. The tonic, DA dependent current is discussed below. Each FSI receives independent, excitatory Poisson input with a rate of 2000 inputs per second.

The synaptic current (I_{syn}) is the sum of $GABA_A$ currents and electrical connections between FSIs (formulated below). The FSI membrane currents (I_{memb}) consisted of a fast sodium current (I_{Na}), a fast potassium current (I_k), a leak current (I_L), and a potassium D-current (I_D). The formulations of these currents were taken from previous models of striatal FSIs. (Sciamanna & Wilson (2011); Golomb et al. (2007)) I_{ds} represents the current from the dendritic compartment to the somatic compartment and I_{sd} represents the current from the somatic compartment to the dendritic compartment.

The maximal sodium conductance is $\bar{g}_{Na}$ = 112 mS/cm^2 and the sodium reversal potential is E_{Na} = 50 mV.The sodium current has three activation gates ($n = 3$) and one inactivation gate ($k = 1$). The steady state functions for the sodium current activation (m) and inactivation (h) variables and their time constants (τ_m and τ_h, respectively) are described by:

$$m_\infty = \frac{1}{1 + \exp\left[-(V + 24)/11.5\right]} \tag{2.6}$$

$$h_\infty = \frac{1}{1 + \exp\left[(V + 58.3)/6.7\right]} \tag{2.7}$$

$$\tau_h = 0.5 + \frac{14}{1 + \exp\left[(V + 60)/12\right]} \tag{2.8}$$

The maximal conductance for the fast potassium channel is $\bar{g}_K$= 225 mS/cm^2 and the reversal potential for potassium is E_K = -90 mV. The fast potassium channel has no inactivation gates but has four activation gates described by its steady state function (n_∞) and time constant (τ_n):

$$n_\infty = \frac{1}{1 + \exp\left[-(V + 12.4)/6.8\right]} \tag{2.9}$$

$$\tau_n = (0.087 + \frac{11.4}{1 + \exp\left[(V + 14.6)/8.6\right]})(0.087 + \frac{11.4}{1 + \exp\left[-(V - 1.3)/18.7\right]}) \quad (2.10)$$

The leak current (I_L) has no gating variables. The maximal leak channel conductance is g_L=0.25 mS/cm^2 and the leak channel reversal potential is E_L = -70 mV.

The fast-activating, slowly inactivating potassium D-current (I_D) is described mathematically as in Golomb et al, 2007 (Golomb et al. (2007)) and has one activation (a) and one inactivation (b) gate. The steady state functions for the activation and inactivation gates are formulated as:

$$a_\infty = \frac{1}{1 + \exp\left[-(V + 50)/20\right]} \quad (2.11)$$

$$b_\infty = \frac{1}{1 + \exp\left[(V + 70)/6\right]} \quad (2.12)$$

The time constant of the decay is 2 ms (τ_a) for the activation gate and 150 ms (τ_b) for the inactivation gate. The maximal conductance of the D-current is 6 mS/cm^2.

All conductances in the dendritic compartment of the FSIs are $1/10$ the strength of those in the somatic compartment. The somatic and dendritic compartment of each cell are connected bidirectionally with a compartmental conductance of 0.5 mS/cm^2. This electrical coupling is formulated as:

$$I_{sd} = 0.5(V_{soma} - Vdend) \quad (2.13)$$

$$I_{ds} = 0.5(V_{dend} - Vsoma) \quad (2.14)$$

where I_{sd} is the current from the somatic compartment to the dendritic com-

partment and I_{ds} is the current from the dendritic compartment to the somatic compartment.

2.4.2 Striatal spiny projection neurons

Spiny projection neurons were modeled with four membrane currents: a fast sodium current (I_{Na}), a fast potassium current (I_k), a leak current (I_L), and an M-current (I_m) (Shen (2005)). We do not model SPN up and down states which are not prevalent in the awake state of striatum (Mahon et al. (2006)), the state being modeled, and therefore we do not include the Kir current in our model, which is active during the SPN down state.

The sum of all excitatory inputs from the cortex and thalamus and inhibitory inputs from striatal interneurons is introduced into the model using a background excitation term (I_{app}). I_{app} is the sum of a constant term and a Gaussian noise term. The Gaussian noise has mean zero, standard deviation one and an amplitude of $4\sqrt{\delta t}$ where δt is the time step of integration. D1 and D2 SPNs were distinguished only by the value of tonic term of I_{app} when DA levels were high. DA is excitatory to D1 receptors and inhibitory to D2 receptors (Taverna et al. (2008)). Thus, we modeled D1 and D2 SPNs as having the same tonic I_{app} at baseline DAergic tone state with I_{app} = 1.19 $\mu A/cm^2$. To model the high DA state, let the tonic term of I_{app} = 1.29 $\mu A/cm^2$ for the D1 SPNs and I_{app}= 1.09 $\mu A/cm^2$ for the D2 SPNs.

The rate functions for the sodium current activation (m) and inactivation (h) variables are formulated as:

$$\alpha_m = \frac{0.32(V+54)}{1-\exp\left[-(V+54)/4\right]} \tag{2.15}$$

$$\beta_m = \frac{0.28(V+27)}{\exp\left[(V+27)/5\right]-1} \tag{2.16}$$

$$\alpha_h = 0.128\exp\left[-(V+50)/18\right] \tag{2.17}$$

$$\beta_h = \frac{4}{1+\exp\left[-(V+27)/5\right]} \tag{2.18}$$

The maximal conductance of the sodium current is $\bar{g}_{Na}$ = 100 mS/cm^2. The sodium reversal potential is E_{Na} = 50 mV. The sodium current has three activation gates ($n = 3$) and only one inactivation gate ($k = 1$).

The fast potassium current (I_K) has four activation gates ($n = 4$) and no inactivation gates ($k = 0$). The rate functions of the activation gate are described by:

$$\alpha_m = \frac{0.032(V+52)}{1-\exp\left[-(V+52)/5\right]} \tag{2.19}$$

$$\beta_m = 0.5\exp\left[-(V+57)/40\right] \tag{2.20}$$

The maximal fast potassium channel conductance is $\bar{g}_K$=80 mS/cm^2. The reversal potential for potassium is E_K= -100 mV.

The leak current (I_L) has no gating variables ($n = 0$, $k = 0$). The maximal conductance of the leak channel is g_L = 0.1 mS/cm^2. The leak channel reversal potential is E_L = -67 mV.

The M-current has one activation gate ($n = 1$) and no inactivation gate ($k = 0$). The rate functions for the M-current activation gate are described by:

$$\alpha_m = \frac{Q_s 10^{-4}(V+30)}{1-\exp\left[-(V+30)/9\right]} \tag{2.21}$$

$$\beta_m = -\frac{Q_s 10^{-4}(V+30)}{1-\exp\left[(V+30)/9\right]} \tag{2.22}$$

We use a Q_{10} factor of 2.3 to scale the rate functions of the M-current since the original formulation of these kinetics described dynamics at $23\,^{\circ}\mathrm{C}$ (Mainen & Sejnowski (1996)). Thus, for a normal body temperature of $37\,^{\circ}\mathrm{C}$, the M-current rate equations are scaled by Q_s, which is formulated as:

$$Q_s = Q_{10}^{(37\,^{\circ}\mathrm{C}-23\,^{\circ}\mathrm{C})/10} = 3.209 \tag{2.23}$$

The maximal M-current conductance is $\bar{g}_m$=1.29 mS/cm^2.

2.4.3 Synaptic connectivity and networks

Networks of FSIs contained 50 neurons. For networks that additionally had SPNs, we modeled 100 D1 SPNs and 100 D2 SPNs. The model synaptic $\mathrm{GABA_A}$ current ($I_{\mathrm{GABA_A}}$) is formulated as in McCarthy et al., 2011 (McCarthy et al. (2011)) and is the only synaptic connection between SPNs and from FSIs to SPNs. The $\mathrm{GABA_A}$ current has a single activation gate dependent on the pre-synaptic voltage.

$$I_{\mathrm{GABA_A}} = \bar{g}_{ii} s_i (V - E_i) \tag{2.24}$$

The maximal $\mathrm{GABA_A}$ conductance between FSIs is $\bar{g}_{ii}$ = 0.1 mS/cm^2. Conductances from FSIs to SPNs and between SPNs (but not between FSIs) were normalized to the number of SPNs in the target network. Therefore, the maximal $\mathrm{GABA_A}$ conductance from FSIs to SPNs is $\bar{g}_{ii}$ = 0.6/100 = 0.006 mS/cm^2 and between SPNs was $\bar{g}_{ii}$ = 0.1/100 = 0.001 mS/cm^2. These values are consistent with FSI to SPN inhibition being approximately six times stronger than inhibition between SPNs (Koos et al. (2004)).

The gating variable for inhibitory $\mathrm{GABA_A}$ synaptic transmission is represented

by s_i. For the j^{th} neuron (FSI or SPN) in the network:

$$s_j = \sum_{k=1}^{N} S_{i_k i_j} \tag{2.25}$$

The variable $S_{i_k i_j}$ describes the kinetics of the gating variable from the k^{th} pre-synaptic neuron to the j^{th} post-synaptic neuron. This variable evolves in time according to:

$$\frac{dS_{i_k i_j}}{dt} = g_{\text{GABA}_\text{A}}(V_k)(1 - S_{i_k i_j}) - \frac{S_{i_k i_j}}{\tau_i} \tag{2.26}$$

The GABA_A time constant of decay (τ_i) is set to 13 ms for SPN to SPN connections (Taverna et al. (2008)) as well as for FSI to FSI connections and FSI to SPN connections (Hjorth et al. (2009)) The GABA_A current reversal potential (E_i) for both FSIs and SPNs is set to -80 mV. The rate functions for the open state of the GABA_A receptor ($g_{\text{GABA}_\text{A}}(V_k)$) for SPN to SPN transmission is described by:

$$g_{\text{GABA}_\text{A}}(V_k) = 2(1 + tanh(\frac{V_k}{4})) \tag{2.27}$$

The rate functions for the open state of the GABA_A receptor ($g_{\text{GABA}_\text{A}}(V_k)$) for FSI to FSI and FSI to SPN transmission is:

$$g_{\text{GABA}_\text{A}}(V_k) = \frac{1}{\tau_r}(1 + tanh(\frac{V_k}{10})) \tag{2.28}$$

The value of τ_r is 0.25 ms. FSIs were additionally connected by dendritic electrical connections. The electrical coupling for dendritic compartment i is denoted as I_{elec}, has units in $\mu A/cm^2$ and is formulated as:

$$I_{elec} = g_{\mathrm{GJ}}(Vd_j - Vd_i) \tag{2.29}$$

The value of the gap junction conductance g_{GJ} depended on DA level (see below). Within the 50-cell FSI network, each pair of FSIs had an independent 30 percent chance of a dendro-dendritic gap junction chosen from a uniform random distribution (Hjorth et al. (2009)), and an independent 58 percent chance of a somato-somatic inhibitory synapse also chosen from a uniform distribution (Gittis et al. (2010)). SPNs are connected with each other in a mutually inhibitory GABAergic network (Tepper et al. (2004)). We modeled all to all connectivity of inhibitory synapses from any SPN to any SPN of the same receptor subtype, as in (McCarthy et al. (2011)). Probability of connection from any given FSI to any given MSN was 37.5 percent, chosen from a uniform random distribution (Corbit et al. (2016); Gittis et al. (2010)).

2.4.4 Dopamine

DA impacts both connectivity and excitability in the model networks. DAergic tone was simulated as having five components: direct excitation of FSIs (Bracci et al. (2002)), increased gap junction conductance between FSIs (Onn & Grace (1994)), decreased inhibitory conductance between FSIs (Bracci et al. (2002)), increased excitation to D1 SPNs, and decreased excitation to D2 SPNs. DA-induced changes to SPN excitation were discussed above. Excitation to FSIs was modeled as the sum of a tonic, DA dependent input current (I_{app}) and a noise term. DA did not change the noise term in either SPNs or FSIs. The baseline DAergic tone state was modeled in FSIs using I_{app} = 7 $\mu A/cm^2$, g_{GJ} = 0.15 mS/cm^2 and the $\mathrm{GABA_A}$

conductance between FSIs was g_{ii} = 0.1 mS/cm^2. The high DA state was modeled in FSIs using I_{app} = 14 $\mu A/cm^2$, g_{GJ} = 0.3 mS/cm^2 and g_{ii} = 0.005 mS/cm^2. The synaptic conductances were chosen so as to be within an order of magnitude of physiological estimates (0.05 mS/cm^2 for g_{GABA_A} (Corbit et al. (2016); Gittis et al. (2010)); 0.2 mS/cm^2 for g_{GJ} (Galarreta & Hestrin (2002))). The inhibitory conductance for the high DAergic tone state was chosen to be the lowest value possible in this range; the inhibitory conductance for the low DAergic tone state was chosen to be the highest value that would still reliably allow oscillatory behavior in the network. The value of g_{GJ} in the low DAergic condition was then chosen to be the lowest value that was permissive of oscillatory behavior, and the value in the high DAergic condition was chosen to be twice that. Finally, the values of I_{app} were chosen in order to correspond to physiologically realistic firing rates (a minimum of 5 and a maximum of 30 Hz; see (Berke et al. (2004); Berke (2008))).

2.4.5 Local field potential

The local field potential (LFP) was calculated as the sum of all synaptic currents in all cells. Stationarity of the network appears in the raster plots after about 500 ms. To eliminate transients due to initial conditions, our LFP is evaluated only after 1,000 ms of simulated time. We estimated the power spectral density of the simulated LFP using the multitaper method. (Bokil et al. (2007)).

2.4.6 Simulations

All simulations were run on the MATLAB-based programming platform DynaSim, a framework for efficiently developing, running and analyzing large systems of

coupled ordinary differential equations, and evaluating their dynamics over large regions of parameter space (Sherfey et al. (2018)). DynaSim is open-source and all models have been made publicly available using this platform. All differential equations were integrated using a fourth-order Runge-Kutta algorithm with time step was .01 ms. Plotting and analysis were performed with inbuilt and custom MATLAB (version 2017b) code.

2.5 FIGURES AND TABLES

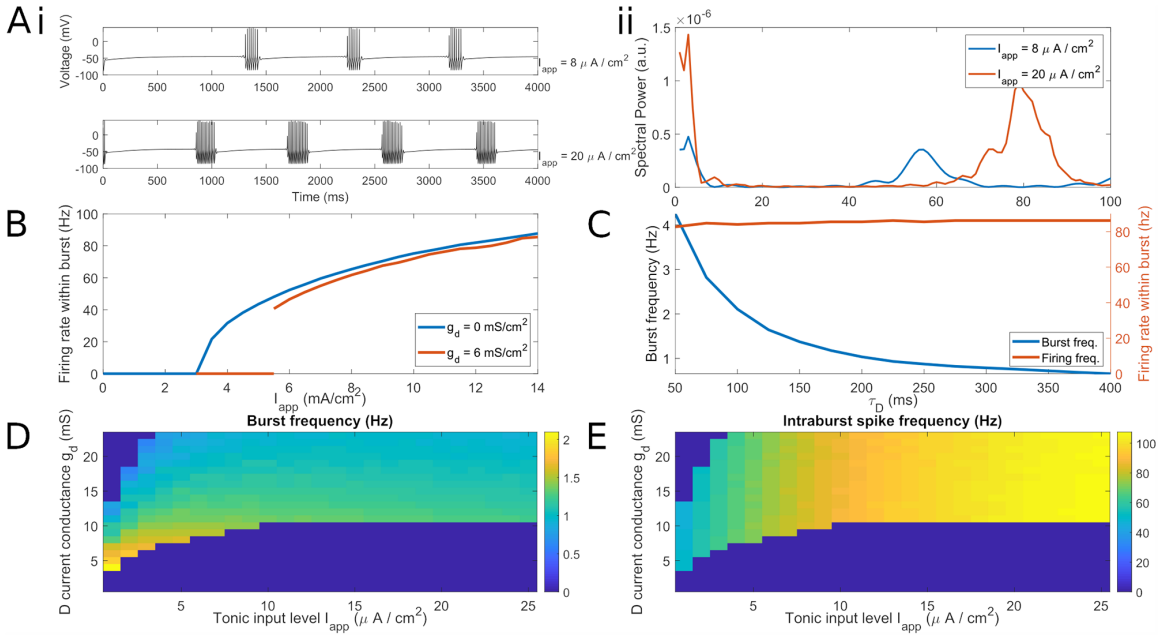

Figure 2.1: Behavior of single model FSI over a range of applied currents and D-current conductances.

(A) i. A single model FSI with low tonic excitation ($I_{app} = 8\mu A/cm^2$) spikes at a low γ frequency nested in slow bursting, while a single model FSI with high tonic excitation ($I_{app} = 20\mu A/cm^2$) spikes at a high γ nested in slow bursting. ii. Power spectral density of voltage traces in (A)i, comparing low and high levels of tonic excitation. Power spectra are derived using Thomsons multitaper power spectral density (PSD) estimate (MATLAB function pmtm). (B) Plot of the minimal firing rate within a burst of a single model FSI with zero and nonzero D current conductance g_D. Note that the cell does not fire below 40 Hz when the D-current is present. (C) Plot of the maximal inter-burst (δ) frequency and intraburst (γ) firing rate of a single model FSI as τ_D, the time constant of inactivation of the D current, is increased. (D) Three-dimensional false-color plot demonstrating the dependence of the bursting regime on g_d and I_{app}. (E) Three-dimensional false-color plot demonstrating the dependence of firing rate on g_d and I_{app}.

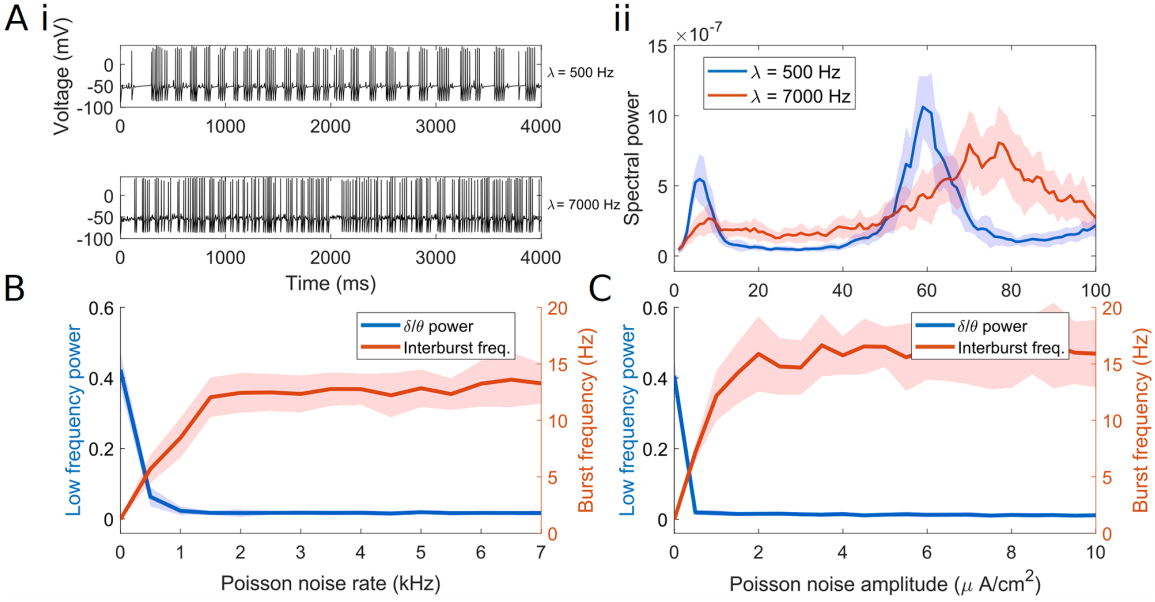

Figure 2.2: Applied noise determines interburst and intraburst frequency of FSI spiking.

(A) i. Single model FSI with tonic excitation (7 $\mu A/cm^2$) and weak Poisson noise ($\lambda = 500$) spikes at γ nested in δ/θ, while a single model FSI with tonic excitation (7 $\mu A/cm^2$) and strong Poisson noise ($\lambda = 7000$) has limited low-frequency content. ii. Power spectral density of voltage traces in (A)i, comparing low and high levels of noise. The solid line represents the mean value over 20 simulations per point. Shading represents standard deviation from these means. Power spectra are derived using Thomsons multitaper power spectral density (PSD) estimate (MATLAB function pmtm). (B) Plot of the inter-burst frequency and power of a single model FSI as Poisson noise of varying rates is applied. (C) Plot of the inter-burst frequency and power of a single model FSI as Poisson noise of varying amplitudes is applied. For B and C I_{app} = 7 $\mu A/cm^2$.

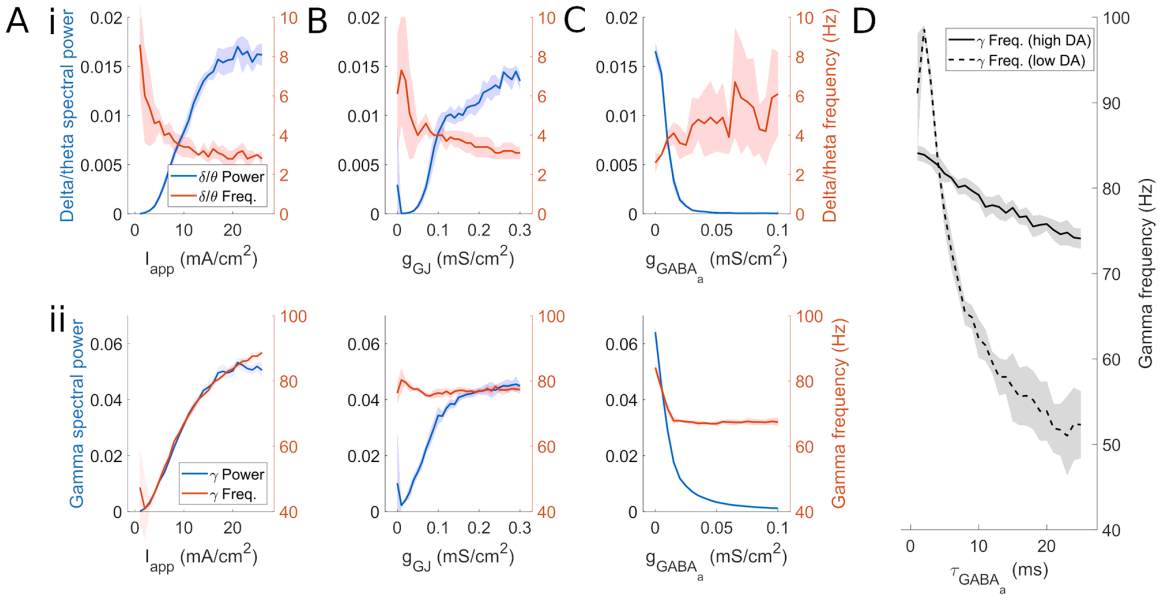

Figure 2.3: FSI network rhythms change with background excitation and synaptic strength.

Power and frequency of δ/θ and γ rhythms in FSI network mean voltage as a function of (A) tonic input current, (B) gap junction conductance, and (C) $GABA_A$ conductance. The parameters not being varied in plots A-C are held at the high DA values (I_{app} = 14 $\mu A/cm^2$, g_{GJ} = 0.3 mS/cm^2, g_{syn} = 0.005 mS/cm^2, τ_{gaba} = 13 ms. The solid line represents the mean value over 10 simulations per point. Shading represents standard deviation from these means. Power spectra are derived using Thomsons multitaper power spectral density (PSD) estimate (MATLAB function pmtm). (D) Gamma frequency as a function of $GABA_a$ synaptic time constant and level of dopamine. High DA values are as previously stated; low DA values are I_{app} = 7 $\mu A/cm^2$, g_{GJ} = 0.15 mS/cm^2, g_{syn} = 0.1 mS/cm^2.

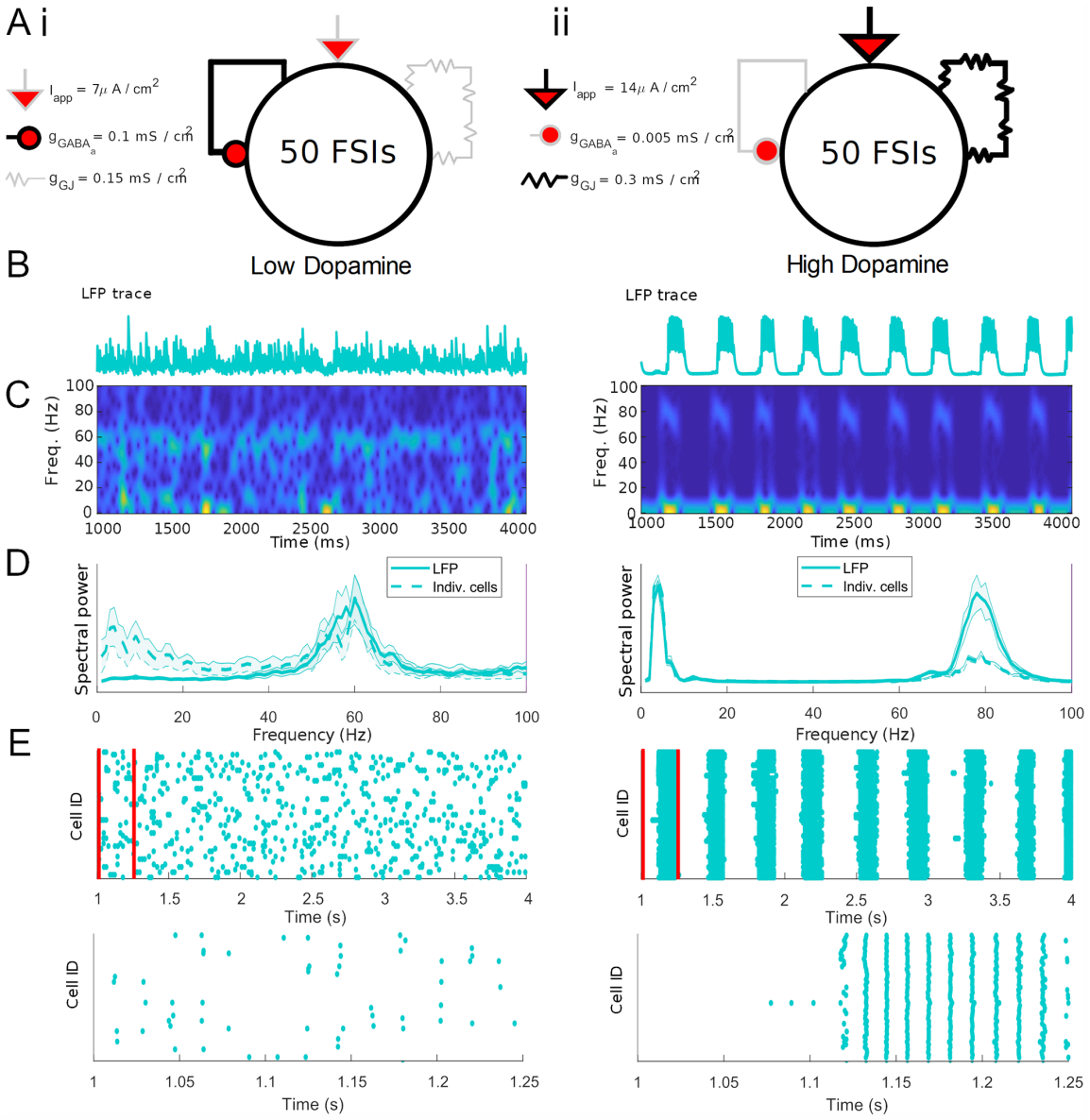

Figure 2.4: FSI network activity and rhythms are altered by DA.
(A) Schematics showing the effects of dopamine on the FSI network during the baseline (i) and high (ii) DAergic tone conditions. (B) Sum of synaptic currents (surrogate LFP) for the FSI network in the two conditions. (C) Spectrograms of (B). (D) Solid line: Power spectral density of summed FSI synaptic currents (surrogate LFP), averaged over 20 simulations. Dashed line: Average power spectral density of each individual FSI voltage trace in the network, averaged over 20 simulations. Shading represents standard deviation from the mean. (E) Raster plots of FSI network activity at multisecond and subsecond timescales (red bars indicate time limits of lower raster plot).

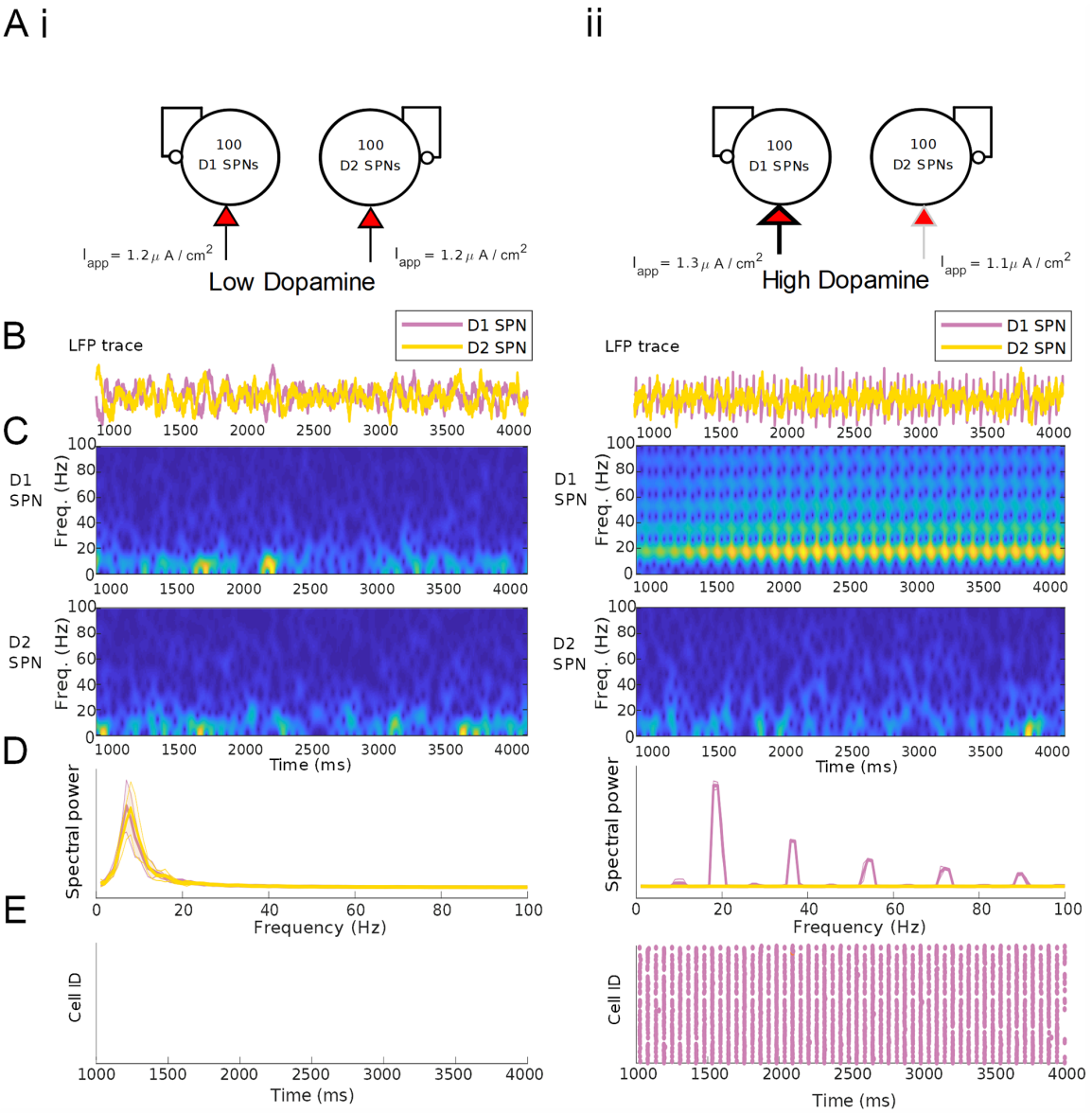

Figure 2.5: Baseline SPN activity is characterized by β oscillations only in the D1 subnetwork under high DA conditions.

(A) Schematics depicting the baseline (i) and high DAergic tone (ii) conditions in an isolated SPN-only network. (B) Mean voltages for the D1 and D2 SPN populations in the two conditions. (C) Spectrograms of mean voltage for the D1 subpopulation (upper) and D2 subpopulation (lower). (D) Power spectral density of D1 and D2 population activity, averaged over 20 simulations. Shading represents standard deviation from the mean. Power spectra are derived using Thomsons multitaper power spectral density (PSD) estimate (MATLAB function pmtm). (E) Raster plots of SPN population activity.

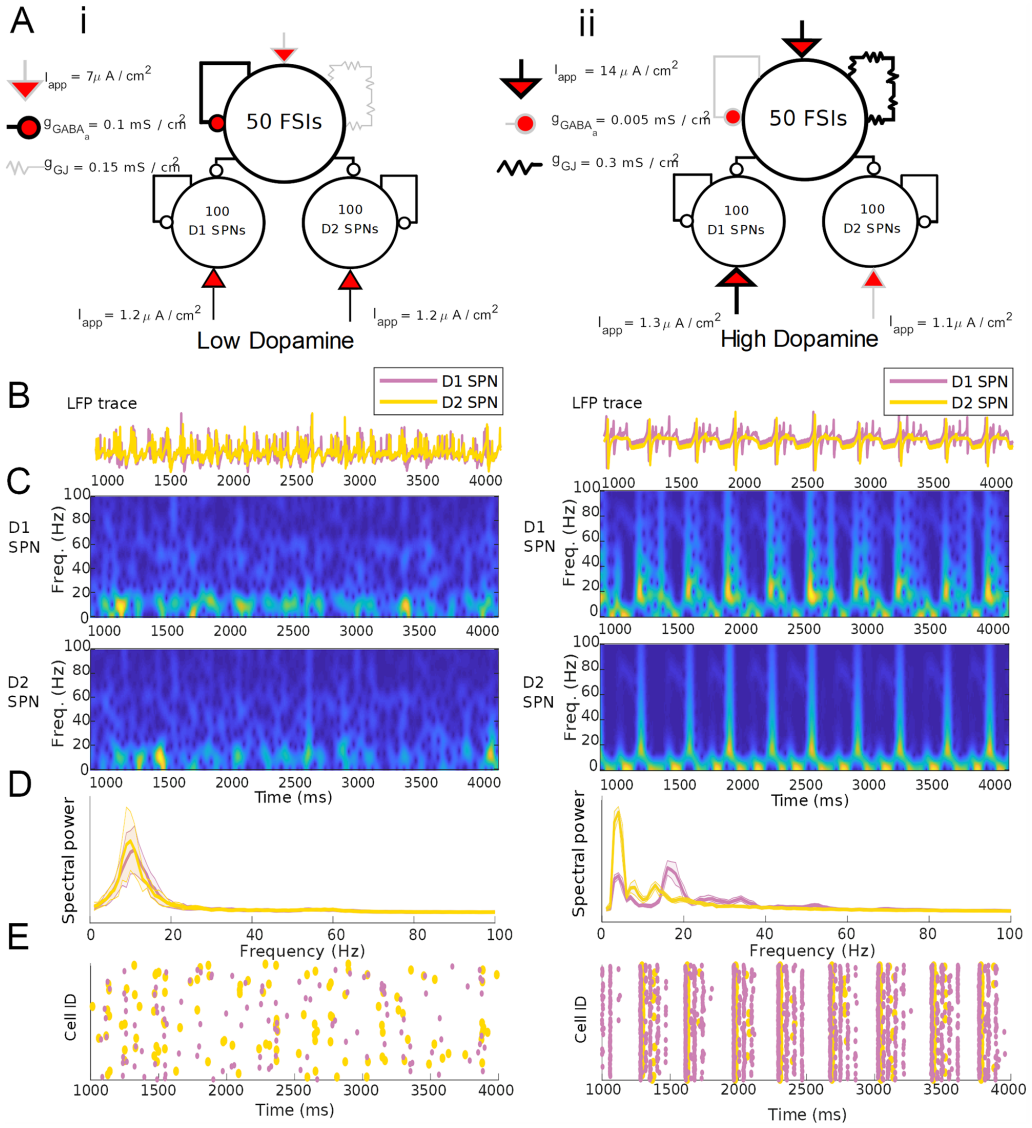

Figure 2.6: FSIs paradoxically excite and pattern SPN network activity.

(A) Schematics showing modulation during the baseline (i) and high (ii) DAergic tone conditions in a combined FSI-SPN network. (B) Mean voltages for the D1 and D2 SPN populations in the two conditions. (C) Spectrograms of mean voltage for the D1 subpopulation (upper) and D2 subpopulation (lower). (D) Power spectral density of D1 and D2 population activity, averaged over 20 simulations. Shading represents standard deviation from the mean. Power spectra are derived using Thomsons multitaper power spectral density (PSD) estimate (MATLAB function pmtm). (E) Raster plots of SPN population activity.

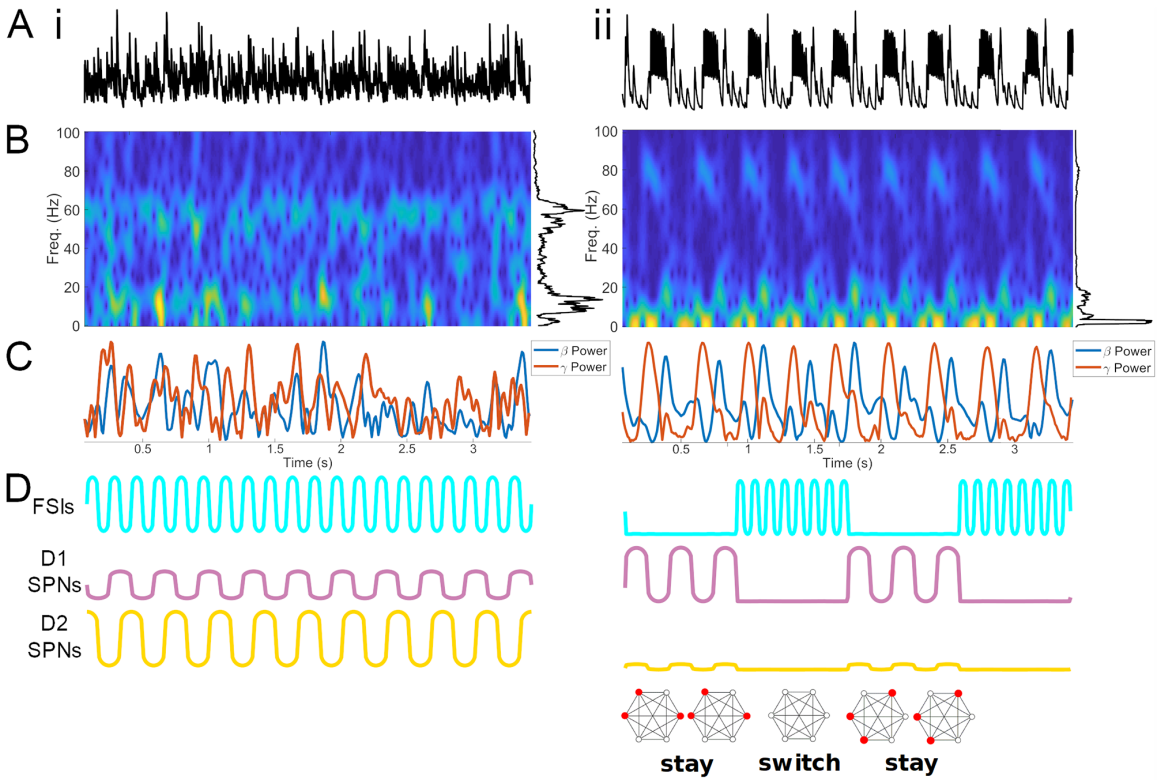

Figure 2.7: In the high DA state, packets of FSI γ and SPN β alternate at a δ/θ timescale.

(A) LFP surrogates (summed synaptic currents) for baseline (i) and high (ii) DAergic tone conditions. (B) Spectrograms of LFP surrogates. (C) Wavelet-filtered β and γ oscillations from the population activity in (A). (D) Schematic of oscillatory activity during baseline and high DAergic tone conditions, with proposed functional impact on ensemble activity.

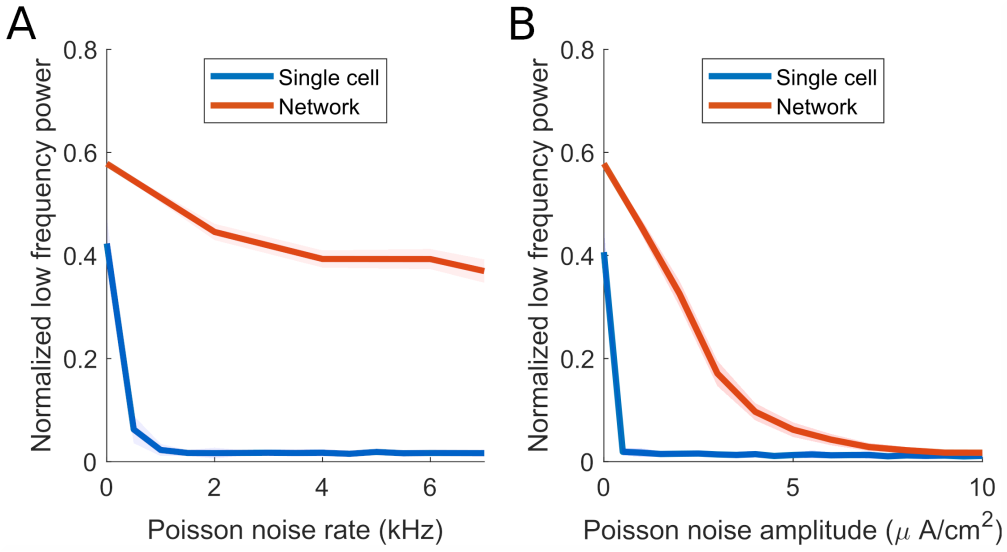

S1 Fig. Low frequency oscillations are more robust to noise in the high dopamine FSI network than in a single FSI.

(A) Plot of normalized low frequency (<10 Hz) power of the voltage of a single model FSI (blue) and the summed voltages of the high DA FSI network (red) as Poisson noise of varying rate is applied. Each cell in the network receives the same amount of noise that the isolated cell receives. I_{app} = 14 $\mu A/cm^2$ for all simulations; in the high DA FSI network, g_{gap} = 0.3 mS/cm^2, g_{syn} = 0.005 mS/cm^2. The solid line represents the mean value over 10 simulations per point. Shading represents standard deviation from these means. Power spectra are derived using Thomsons multitaper power spectral density (PSD) estimate (MATLAB function pmtm). (B) Plot of normalized low frequency (<10 Hz) power of the voltage of a single model FSI and the summed voltages of the high DA FSI network as Poisson noise of varying amplitude is applied.

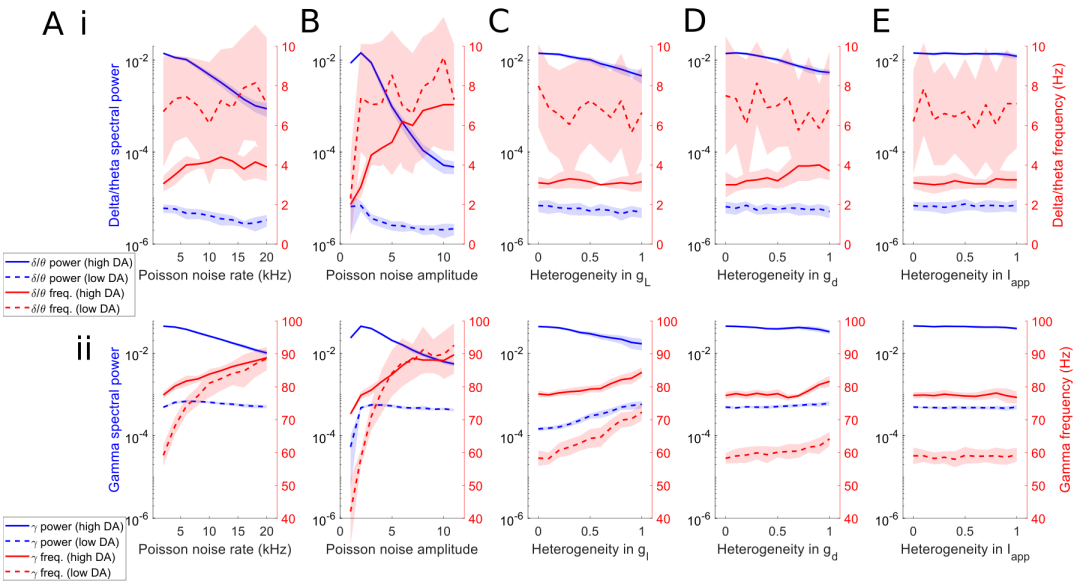

S2 Fig. FSI network rhythms are robust to noise and heterogeneity. Power and frequency of δ/θ and γ rhythms in FSI network mean voltage as a function of (A) noise frequency, (B) noise amplitude, (C) heterogeneity in leak current conductance, (D) heterogeneity in potassium D current conductance, and (E) heterogeneity in applied current. For heterogeneity values, 0 represents completely uniform values and 1 represents a level of heterogeneity where values vary between zero and twice the default value. Default leak current conductance is 0.25 mS/cm^2 and default D current conductance is 6 mS/cm^2; default applied current is 7 mA/cm^2 for low DA and 14 mA/cm^2 for high DA. The parameters not being varied in plots A-C are held at either the high DA values (solid lines, I_{app} = 14 $\mu A/cm^2$, g_{gap} = 0.3 mS/cm^2, g_{syn} = 0.005 mS/cm^2) or the low DA values (dotted lines, I_{app} = 7 $\mu A/cm^2$, g_{gap} = 0.15 mS/cm^2, g_{syn} = 0.1 mS/cm^2), according to the legend. The solid line represents the mean value over 10 simulations per point. Shading represents standard deviation from these means. Power spectra are derived using Thomsons multitaper power spectral density (PSD) estimate (MATLAB function pmtm).

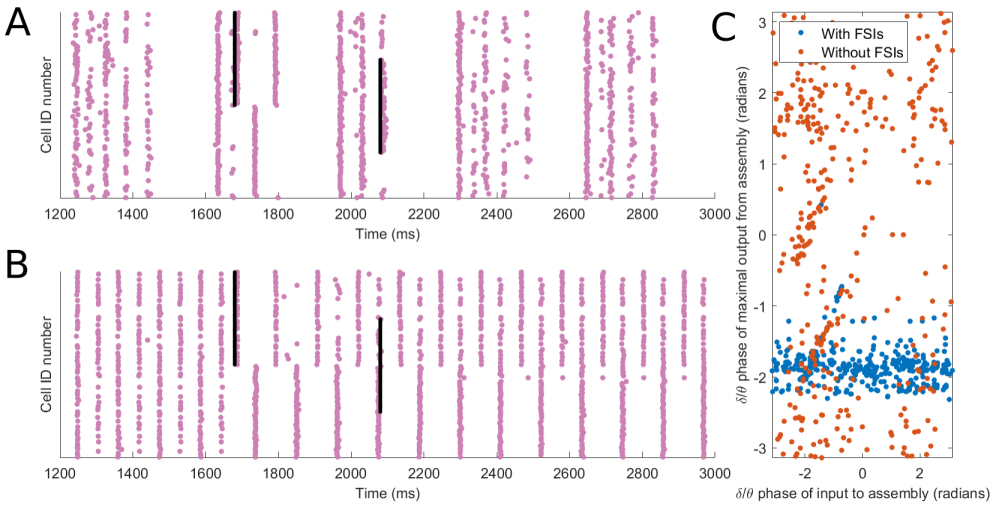

S3 Fig. SPN assemblies are more readily formed in response to new input when FSIs are imposing a δ/θ rhythm that disrupts prior activity.

(A) Example raster plot of the D1 SPN subnetwork receiving δ/θ frequency FSI input while being subjected to input during high DAergic tone: An excitatory 20 millisecond pulse of input is provided to cells 50-100 (assembly 1) at t = 1680 ms and a later excitatory pulse of input is provided to cells 25-75 (assembly 2) at t = 2080 ms. Assembly 1 is active for several β cycles after the first input, causing rebound spiking at antiphase of the cells not in assembly 1 (as in McCarthy 2011 (McCarthy et al. (2011))), but becomes inactive during the δ/θ peak beginning around t = 1800 ms. Assembly 2 can then respond with a high degree of coherence shortly after the second input. (B) Example raster plot of the isolated D1 SPN subnetwork (not receiving any FSI input) being subjected to the input during high DAergic tone. The same two excitatory pulses are provided. Assembly 1 and its antiphase activity begin firing similarly to the example in (A), but since there is no δ/θ input, the β-rhythm firing of assembly 1 persists indefinitely. Input to assembly 2 is thereby unable to generate a specific response, and the coherence of assembly 1 persists even after the second input. (C) Plot showing history-independence of SPN responses when FSIs are present. Regardless of the phase at which input is given, the maximal response of SPNs in any given cell assembly occurs at a preferred δ/θ phase around -2 radians, erasing the information of when the input arrived. When FSIs are not present, there is no theta rhythm in the network, and the response of the cells to input is more random.

CHAPTER 3

Oscillatory input to the model striatal network

3.1 INTRODUCTION

In chapter 1, input to the striatum was modeled as white noise. However, the striatum receives input from diverse regions of cortex, and presumably all of these inputs contain information that may be encoded as frequency content. Electrophysiological recordings of corticostriatal pathways have found coherence between cortex and striatum at frequencies including delta, theta, beta and gamma (Sharott et al. (2012); von Nicolai et al. (2014); Catanese et al. (2016); Naze et al. (2018)). Given the importance of resonance in neural networks (Sherfey et al. (2018); Ardid et al. (2019)), It is likely that inputs to striatum elicit frequency-specific responses depending on the resonance properties of the target cells and networks. These responses in turn may impact the oscillatory output of the striatal network. Much work has been done on the response of striatum to the oscillations, especially beta, that cycle through the cortico-striato-basal-ganglia-thalamic loop (Stein & Bar-Gad (2013); Brittain & Brown (2014); Womelsdorf et al. (2010)). However, because of the cyclical nature of this circuit, it is difficult to tell which rhythms originate in striatum, which are a result of resonance to input, and which are merely volume conducted.

In the previous chapter, I demonstrated that the striatal microcircuit can be a local generator of oscillations at a wide array of frequencies, several of which (namely theta and beta) are presumed to be conducted downstream to the rest of the basal ganglia by striatal projection neurons. However, this does not give us any information as to whether these rhythms can be enhanced or suppressed

by oscillatory input, or even whether the striatal network has a broader range of rhythms it could produce via entrainment to externally imposed oscillations. In order to begin to address these questions, I provided colored input signals to my model network in the form of square waves, and analyzed the responses to this input in terms of firing rate and pattern as well as phase locking. By doing so, I can begin to use my model to make predictions about how the striatal microcircuit processes cortical oscillations. Specifically, I am interested in addressing the role of fast-spiking interneurons in input processing; therefore, the end goal of this chapter is to compare the response to oscillatory input of an SPN network without FSI input to the behavior of the full FSI-SPN model network.

It should be noted that the results presented in this chapter are preliminary, and require substantial further investigation in order to truly make realistic predictions about the behavior of the striatal network in vivo; for instance, multiple iterations of each simulation would need to be performed in order to statistically test the hypotheses presented here. Despite this, the results of the simulations performed in this chapter suggest a number of interesting response properties of the striatal circuit that may shed light on how cortical input can impose different functional states on striatal processing.

The FSI subnetwork has a dopamine-dependent response to input frequencies in the gamma range. Dopamine in the FSI subnetwork is modeled as increasing excitability, decreasing lateral inhibition, and increasing gap junction conductance; the only impact of dopamine on SPNs in the model network is increasing D1 SPN excitability and decreasing D2 SPN excitability. In the low dopamine condition, the FSI network sparsely phase-locks to gamma input but does not increase in firing rate, whereas in the high dopamine condition, input at gamma frequencies

causes both firing rate and bursting rate of the FSIs to increase. These FSI network responses have a downstream impact on the behavior of the SPN subnetwork. Without FSIs, the SPN subnetwork can phase lock to a broad range of frequencies, but also produces beta oscillations in response to input frequencies outside of the beta band. When FSIs are present in either low or high dopamine conditions, the beta power and spiking resonance produced by the SPN subnetwork in response to non-beta frequencies is dramatically reduced, while beta transduction remains intact. In addition, in the high DA condition, specific frequencies of gamma input can cause the FSI network to fire continuously, causing SPNs to entrain to gamma frequencies to which they would otherwise produce a beta in response. These properties have implications for the role of FSIs in routing cortical input through striatum.

3.2 METHODS

The cellular models and network structure are identical to that described in (Chartove et al. (2020)); the only difference in this chapter is that, in addition to the input already present in the model as described, every cell is given an additional input in the form of a square wave. This wave is nonzero and its duty cycle is $1/4$, i.e. $1/4$ of the time, the cell is receiving an additional current, $3/4$ of the time, the cell is receiving no additional current. This square wave is modeled as continuous but its rise time is under 1 ms. The amplitude of the square wave ranges from 0.2 nA to 1 μA. The input to the SPNs is always half as strong as the input to the FSIs in order to account for the fact that cortical synapses are much more dense on FSIs than SPNs (Owen et al. (2018)). Dopamine in the SPN subnetwork is modeled simply as excitation level the same way it was in Chapter 2; in the low/baseline dopamine

condition, all SPNs receive a tonic excitatory current of 1.19 μA, while in the high DA condition, D1 SPNs receive 1.29 μA while D2 SPNs receive 1.09 μA. For an explanation of how dopamine is modeled in the FSI subnetwork, see Chapter 2.

Phase locking value (PLV) was assessed using the method described in (Lachaux et al. (1999)). Briefly, the PLV ranges from 0, indicating random relationships between input phase and spiking, to 1, indicating spiking only at a specific phase of input. In order to assess this value, the square wave input is first converted to an equivalent sinusoid using a wavelet filter. For each spike occurring in the network, we take the angle of the Hilbert transform of this wavelet at the spike time (defined as when the voltage of the cell crosses 0) to be the instantaneous phase of the input. We then quantify the randomness in phase as the sum of $e^(i * \phi)$ (where ϕ is the stimulus phase) for all spikes. Normalizing this sum to the $[0, 1]$ range gives us the PLV.

3.3 RESULTS

3.3.1 FSI network results: low DA

In the low DA condition, the model FSI network sparsely locks to gamma frequencies in a manner that does not impact population firing rate. In general, sufficiently powerful square wave input at a given frequency causes a peak at that frequency in the power spectrum of FSI network level spiking (Figure 1A). However, this peak is not driven by individual cells spiking at the input frequency. Rather, the network as a whole displays sparse entrainment without any increase in firing rate at any particular input frequency or input strength (Figure 1B, C). This lack of variation in firing rate, even in response to high amplitude input, may be a result of strong lateral inhibition in the FSI network in the low DA state; see discussion.

Note however that the overall network firing rate in the low DA condition has a wide variance due to noise (between 2 and 14 Hz in the set of simulations shown here), making it difficult to draw conclusions without performing statistical analysis.

Despite the lack of impact of input on firing rate, average network PLV is high in response to inputs at the 'baseline' gamma frequency of the network, i.e. the frequency at which there would be a peak in the power spectrum were the network given input that contains no frequency content, as in Chapter 2. Maximum PLV is centered at this value, but the stronger the input, the broader the range of values the low dopamine network phase locks to. At an input strength of 0.2 mV, PLV is maximized at 58 Hz with a value around 0.6 and tapers off quickly above and below that frequency, while square wave inputs of 1 mV strength generate PLVs above 0.8 for all frequencies between 45 and 70 Hz, and above 0 for all frequencies 1-100 Hz (Figure 1D). There does not appear to be a relationship between network firing rate and PLV.

Sufficiently strong inputs in the 50-60 Hz range can generate a small amount of power in the network at 1 Hz. Figure 1E depicts the frequency below 10 Hz which has the highest power in the spectral density of the surrogate LFP of the network; this frequency is usually apparently random, but specific gamma input frequencies seem to cause it to tend towards 1 Hz. Figure 1F depicts the phase locking value of the network as a whole to the network frequencies (not the input frequency) identified in 2D. When given 50-60 Hz input, network phase locking to 1 Hz can be as high as 0.4. This is notable for several reasons. First, PLVs to input frequencies below 10 Hz are low (Figure 1D). Second, in the low DA condition, the FSI network does not have a delta or theta peak present in the power spectrum

when given noise input or input frequencies other than 50-60 Hz. This suggests that, despite the fact that in chapter 2 the low DA FSI network produces network frequencies only in the gamma range, there is a potential mechanism by which cortical input can generate a striatal delta rhythm in the low DA state.

3.3.2 FSI network results: high DA

By contrast, in the high DA condition, firing rate is increased by entrainment to sufficiently strong input at the baseline gamma frequency of the network (Figure 2A, B). (The 'baseline frequency' of the network is, as before, defined as the frequency the network produces when given only noise as input.) Average firing rate is maximized at 40 Hz when square wave input between 70 and 75 Hz is applied. Note that despite this increase in firing rate, cells in the network do not appear to ever attain the one-to-one entrainment to input pulses that characterize the response of individual cells to square wave input; this is because they are quiescent during half of the delta/theta cycle, so they can entrain only during the bursting phase of theta (Figure 2C). Firing rates are also slightly higher at subharmonics of the preferred network gamma, with small, broad peaks in firing rate centered at 35 and 17 Hz (Figure 2B).

Entrainment range is narrower in the high dopamine condition than in the low DA condition; in the high DA condition, PLVs are nonzero only between 55 and 95 Hz, as well as a narrow band of high PLV at 3 Hz (Figure 2D). However, in both high and low dopamine conditions, PLV is highest in response to inputs at the baseline gamma frequency of the network, and the high PLV range is wider with stronger input. The input generating maximal PLV overlaps with the input generating maximal firing rate, although maximal PLV (around 0.9) is attained at

a slightly wider range of frequencies and input strengths than maximal firing rate. Unlike firing rate, PLV is not higher at subharmonics of the network gamma.

The high DA network produces some amount of delta/theta power to any of the input strengths and frequencies tested, but unlike in Chapter 2, this frequency is not always 3 Hz. The frequency of the theta output is responsive to gamma input. Despite the high PLV at 3 Hz, presumably due to the high DA network also having a baseline 3 Hz frequency, there is no increase in firing rate when input is given at 3 Hz (Figure 2B, E). However, inputs between 60-70 Hz, just under the frequencies that maximize firing rate and PLV, cause low frequency activity to speed up from 3 Hz to upwards of 10 Hz (Figure 2A, F, G, I). This is notable in that, given noise as input, neither input strength nor network structure change this frequency; it is determined solely by the inactivation time constant of the D-current (as shown in Chapter 2). The frequencies that cause this behavior are below the baseline gamma frequency, which is locked at around 75 Hz for these parameters, and is still expressed in the networks spiking in addition to the input frequency and the elevated-frequency theta (Figure 2I). Other input frequencies at sufficient strengths, particularly the subharmonic at 30-35 Hz but including most of the gamma range, can cause the network frequency to speed up to 4 or 5 Hz (Figure 2 G; color indicates peak frequency).

The increased frequency of the theta is accompanied by a reduction in theta power (Figure 2A). The FSI network as a whole in the high DA condition displays some degree of phase locking to the baseline low frequency of the network over a large range of parameter space, with PLVs around 0.8 (Figure 2H; color indicates PLV). However, the same input frequencies (60-70 Hz) that cause this low frequency to become faster also cause network level PLV to the low frequency to

drop to around 0.4, indicating that these faster frequencies do not have as consistent a degree of participation as the typical low network frequencies. Sufficiently strong inputs between 60-70 Hz actually causes the FSI network to fire continuously at gamma, abolishing the low frequency content entirely (Figure 2J); this is discussed in the final section of the results.

3.3.3 SPN network results (without FSIs)

The SPN-only network entrains to a range of frequencies, centered at the beta band, that is determined by excitation level; above this, the network goes quiet if insufficiently excited, or produces a beta oscillation if sufficiently excited (Figure 3A). Figure 3 shows the differences in behavior between an isolated network of SPNs at a baseline state of excitation (the 'low dopamine' state of my model), and the behaviors of the D1 and D2 subnetworks in simulated high DAergic tone. Note that the 'low DA' state does not differentiate between D1 SPNs and D2 SPNs as they have equal levels of excitation in this condition and are therefore functionally identical. The extent of the range of frequencies the SPN network produces as output is determined both by input strength and by background excitation; the upper bound on this entrainment is in the low gamma range (30-40 Hz) for the parameter range tested (see Figure 3A). What happens at stimulation frequencies higher than this range depends on background excitation.

If background excitation is lower than 1.2 μA (which is true for D2 SPNs in the high dopamine condition; see Methods), for input strengths below 0.4 μA, the network entrains to input below a certain frequency and becomes silent above that frequency (Figure 3A iii; Table 1A). Note that in order to better show this difference, Figure 3A shows the output frequencies of the network at input strengths of

0.2 μA. If excitation is high (as is the case for D1 SPNs in the high DA condition and all SPNs in the network in the low dopamine condition; see Methods), the network generates its baseline beta frequency (i.e. its oscillatory response to noise) in response to inputs higher than it can entrain to (Figure 3A i, ii; Table 1Biii, Ciii). (See Sherfey et al. (2018) for examples of a similar phenomenon.) Input strength contributes to this excitation level; at input strengths above 0.4 μA, the D2 SPNs produce a beta in response to high gamma input as well (Table 2 B iii, iv). The baseline beta frequency of the network is affected by input strength, but not by input frequency (Figure 3A). For each input strength and background excitation level, there is an input frequency that maximizes SPN firing rate. Firing rate is dependent on input frequency; the frequency at which maximal firing rate occurs is in the 20-40 Hz range, dependent on background excitation and input strength (Figure 3B). The network entrains well to the frequency maximizing firing rate (compare high firing rate areas marked in yellow in Figure 3B to the same region of Figure 3C). However, the frequency maximizing firing rate is a distinct, higher frequency than the baseline beta frequency of the network (which can be identified as the response to high gamma input in Figure 3A i and ii). Providing input at the baseline beta induces phase locking, but does not increase firing rate, as the cells are already firing at that frequency.

The SPN network has high PLVs in response to most inputs, including harmonics of beta ; low PLVs can occur in response to low frequencies in a highly excited network, or to very high gamma frequencies that are not a multiple of the intrinsic beta (Figure 3C). Phase locking values in the SPN network are close to 1 for a broad range of frequencies. The stronger the input, the broader the range of frequencies generating high PLVs. However, frequencies above a certain value (generally in

the high gamma range) produce PLVs near zero, with the exception of frequencies that are harmonics of the baseline beta oscillation, which show up as small regions of high PLVs in Figure 3C. The precise location of these regions varies by input strength because input strength changes the baseline beta oscillation of the network. Columns ii, iii, and iv of Table 1 show responses of the SPN subnetwork to 15, 43, and 45 Hz input respectively. 15 Hz is at or close to the baseline beta frequency of the network, so the network entrains well to this frequency. Because 43 Hz is outside of the range of beta/low gamma frequencies with high PLV for these parameters, the network shows poor entrainment to this frequency and produces a beta oscillation that is not locked to the input. However, because 45 Hz is a harmonic of 15 Hz, the network will produce a beta oscillation entrained specifically to 45 Hz input.

If background excitation is high, PLV at low frequencies is substantially lower than it would be if background excitation were low, but still well above zero (Figure 3C iii); this may be due to the fact that the baseline beta is being expressed in the network, limiting the ability to lock to frequencies below it. (Table 1, C i) Stronger input causes better phase locking at the lowest frequencies, but also raises the network beta and therefore increases the threshold at which PLV near 1 can be achieved (Figure 3C iii). PLV is also slightly lower at input frequencies immediately above the input frequency maximizing firing rate, presumably because cells are unable to fire fast enough to maintain strong entrainment.

3.3.4 Combined FSI-SPN network results

There are two obvious impacts of adding FSI input to the SPN network in either the low or high dopamine condition. First, the beta output of the SPN network

in response to receiving input in the gamma range is greatly reduced in power (Figure 4A). Second, the SPN network response to inputs outside the beta range is regularized; the small regions of entrainment to resonance observed in the previous section are abolished, and the ability of SPNs to lock to frequencies below the beta range is diminished. In the low DA condition, the beta produced by SPNs in response to frequencies above their entrainment range is completely abolished. In the high DA condition, both D1s and D2s produce a beta when the input frequency is above their entrainment range, but this beta is lower in power and frequency, and more broadband, than it would be without FSIs. In the high DA condition, FSIs also cut down on SPN firing rate in general compared to the low DA condition.

Aside from the D2 SPNs having marginally lower network firing rates than the D1 SPNs, the D1s and D2s behave almost identically in both conditions when given inputs of varying strengths or frequencies; they fire more in response to stronger input and input at their baseline beta frequency, which is still determined by overall excitation (including input strength). The increase in firing rate in response to input at the baseline beta is larger for both SPN subtypes in the low DA condition than in the high DA condition, especially for strong inputs. This is because FSI activity in the high DA condition substantially decreases maximum SPN firing rate, from 30 Hz to 22 Hz (Figure 4 B ii; note the difference in scale of the color bars). Because of this broad inhibition from FSIs, in the high DA condition, the maximum SPN firing rate is achieved by a substantially lower frequency of beta input than in the low DA condition, as the SPN network is much less excitable.

The most notable impact the FSIs have on SPN phase locking is on inputs in the high gamma range that are harmonics of the network beta: without FSIs, the SPN

network achieves PLVs near 1 for inputs at these frequencies, whereas when FSIs are present, these high-frequency peaks in PLV are suppressed (compare Figure 4C with Figure 3C). In response to input above the low gamma range, the SPN subnetwork produces no rhythm in the low DA condition and a weak beta in the high DA condition (Figure 4 A). In the combined SPN-FSI network, phase locking values for SPNs are maximal at the baseline beta. The range of input frequencies that produce high PLVs is broader in the low DA condition (Figure 4 C i) than in the high DA condition (Figure 4 C ii and iii) and broader for stronger input. In the low DA condition, the SPN subnetwork entrains to all input up to some frequency in the low gamma range, the highest frequency of which is determined by input strength (Figure 4 A i; Table 2 A). This can cause the SPNs and FSIs to fire in sync with each other in frequency ranges where they both entrain well to the same low gamma (Table 3 A i).

In the high DA condition, the SPNs have lower PLVs in response to low frequency input than they would if the FSIs were not present (Figure 4 C ii). The FSI subnetwork has poor phase locking to almost all frequencies below the gamma range, with the exception of 3 Hz in the high DA network; by contrast, the isolated SPN subnetwork has high PLVs in response to most of these frequencies. The inhibition generated by the FSIs, which is not locked to low input frequencies, therefore cuts down on the degree to which SPNs can entrain to low frequency inputs. The entrainment of the SPNs to input at low frequencies is slightly worse in the high DA condition than in the low DA condition; in the low DA condition, SPNs can produce as many beta cycles as the duty cycle of the input permits (Table 2 A i and ii), whereas in the high DA condition, SPN behavior in response to low frequency inputs is irregular (Table 2 B, C i and ii). The SPNs have slightly better

phase locking to 3 Hz than to surrounding frequencies in the high DA condition due to the FSIs imposing a 3 Hz rhythm on the network, but it does not actually exceed the phase locking to 3 Hz in the low DA condition.

The frequency and strength of the input in the high DA condition determines whether FSIs and SPNs alternate (and if so at what timescale), spike at the same time as each other, or act independently. Given noise as input, the high dopamine network is entrained to a 3 Hz theta, with FSIs spiking at a gamma frequency at the peaks and SPNs spiking at a beta frequency in the troughs (Chapter 2). In the present study, the response of the SPN subnetwork to square wave input in the high DA condition is similar to that of the isolated SPN-only network in that it produces only frequencies in the beta range as output. The difference in the full network is that rather than producing an uninterrupted beta in the high DA condition, SPN beta occurs only in a subset of theta phases (Table 2B, 3B, C).

There are two exceptions in which the switching between gamma and beta described in Chapter 2 does not occur in the high DA condition. The first exception is that strong input in low to beta range frequencies (1-25 Hz) causes the SPN subnetwork to entrain exactly or nearly exactly to the input, overriding the theta-coupled gamma from the FSIs. The SPNs will spike even when the FSIs are most active, including in response to input at the baseline 3 Hz theta (Table 2 C). The second exception is that 55-70 Hz input at sufficient strengths causes the FSI theta to speed up to over 10 Hz, as shown above (see 'FSI network results: high DA', Figure 2F, Table 3 C ii). Input above 2 μA in strength causes FSIs to break free of the theta cycle entirely and spike continuously at the input gamma frequency; this causes the SPNs to entrain to this same gamma (Table 3 D ii). At input frequencies above the 60-70 Hz range, the behavior of the high DA network goes back to being very

similar to its behavior when given noise as input.

3.4 DISCUSSION

In general, the resonance properties of the model striatal network mirror the oscillations produced by the noise-driven network in Chapter 2. As expected, we found that in both the low and high dopamine conditions, FSI network PLV is high in response to inputs at the baseline gamma frequency of the network. Similarly, the SPNs will phase lock to inputs in the beta band or slightly above or below it.

However, the simulations described above provide valuable insight into properties of network behavior in response to oscillations that could not be predicted from the behavior of the network given noise alone. For instance, in the low DA state, the model FSI network will not change firing rate in response to input strength and frequency, but in the high DA state, the FSIs fire much more in response to high gamma input, to a degree that is proportionate to input strength. This suggests that dopamine may alter not only the frequency of the gamma in the FSI network but also its response properties to gamma input, and provides evidence that the gamma oscillations generated in low and high dopamine conditions are meaningfully mechanistically different. There is also evidence for a weak 1 Hz rhythm present in the low DA condition, which was not evident in the noiseless condition or from examining the rasters; this suggests that there may be a mechanism for delta generation independent of the theta generation mechanism identified in Chapter 2, and warrants further investigation. It is also worth noting that the theta oscillation in the high DA condition does not change its frequency to entrain to low frequency input, suggesting that frequencies other than 3 Hz generated in response to low frequency input may have a distinct origin; however, the

theta will change frequency in response to gamma band input, an effect discussed below.

Additionally, the FSI subnetwork in the model performs several surprising signal transformation functions on the SPN subnetwork, discussed below. Specifically, the FSI network prevents the SPN networks generation of phase-locked beta oscillations in response to betas harmonic frequencies, ensuring fidelity of transmission of cortical beta rhythms, and limits or entrains SPN activity in response to certain gamma frequency inputs. These effects of the striatal network architecture could potentially illuminate the role of striatum in processing cortical input that is transmitted to the basal ganglia.

3.4.1 Role of SPNs and FSIs in patterning striatal resonance response

Modeling work has already shown that the SPN network in isolation is conducive to beta oscillations, and the frequency of the SPN network beta is dependent on excitation (McCarthy et al. (2011)). Therefore, it is no surprise that the SPN network entrains to a range of frequencies (centered at beta) that is determined by excitation level, and produces a beta oscillation in response to input frequencies both below the beta range (Figure 4C, Table 1 C i) and above it (Figure 4A, Table 1 B, C iii and iv), if sufficiently excited. The M-current inhibitory rebound mechanism described in (McCarthy et al. (2011)) promotes SPN network activity at beta; it appears that input outside the beta frequency range can engage this mechanism. This beta response to non-beta input could pose a problem for faithful transduction of the beta oscillations present in the cortico-basal ganglia-thalamic loop. Beta oscillations are important for function in the corticostriatal circuit in health (Ardid et al. (2019)), but are also pathologically amplified in disease (Stein & Bar-Gad (2013)).

A functioning network needs to both be able to transmit beta oscillations when necessary and prevent beta oscillations from occurring when unnecessary. The SPN subnetwork works well for conduction of beta oscillations from cortex, but producing beta oscillations in response to non-beta inputs could result in Parkinsonian pathologies.

Suppression of beta resonance to input outside of the beta range could be an essential function of the striatal FSI network. Striatal projection neurons have a broad range of entrainment to input frequencies in vitro (Beatty et al. (2015)), and the model striatal neurons in the present study share this property. However, this general responsiveness to excitatory input of many frequencies can also lead to inputs outside the beta range being transformed into beta oscillations. Without FSIs, the beta response of the SPN subnetwork in response to frequencies outside the beta range is much more powerful (compare Figure 3A and C to Figure 4A and C). Therefore, one important combined role of striatal FSIs and SPNs may be to act as a band pass filter on cortical input such that only beta oscillations can reliably produce a beta in response. Within the beta range, however, the specific frequency preferences of the SPN network output are highly tunable by background excitation, allowing the striatum to control which frequency of cortical beta input comes through the strongest. Both in vitro and modeling studies suggest that SPNs have a broad range of frequencies to which they can entrain (Beatty et al. (2015); Belić et al. (2017)), but in vivo studies have found that SPNs seem to entrain to beta and theta but not gamma frequency input (Zhang et al. (2016); Berke (2009); Sharott et al. (2009, 2012)). The inhibitory filtering effect of the FSIs could be the reason for this frequency specificity.

Despite the fact that FSIs prevent SPNs from producing a beta oscillation in re-

sponse to gamma input, they also appear to provide a means for the entire striatal network to entrain to specific gamma oscillations. In response to input frequencies between 60-70 Hz, FSIs speed up their theta oscillations to such an extent that sufficiently strong inputs cause them to produce a continuous gamma, which generates gamma entrainment in the SPN subnetwork (Table 3 D ii). This is notable in that the SPN subnetwork will not otherwise produce a high gamma as output; without FSIs, the SPN subnetwork produces a beta in response to high gamma input (Figure 3A). Since SPNs are the only output neurons of the striatum, this action of the FSI subnetwork is the only mechanism in this model that allows for the striatum to produce a gamma oscillation as output. This FSI-mediated response to gamma input has implications for the role of fast-spiking interneurons in the striatal microcircuit in vivo. Several studies have noted that striatal FSIs are more capable of entraining to gamma input than are striatal projection neurons (Berke (2009); Sharott et al. (2009, 2012); Naze et al. (2018)); in addition, striatal FSIs receive much stronger cortical input than SPNs (Owen et al. (2018)). These properties, combined with the continuous spiking behavior demonstrated by the FSIs in response to a narrow band of input frequencies, suggest that gamma oscillations from cortex, when combined with dopaminergic input, could be a specific signal for FSIs to start spiking continuously and override the other frequencies (i.e. delta/theta or beta) that can be produced by the striatal network.

This 'gamma override' hypothesis has important implications for the hypothesis presented in Chapter 2 that the role of FSI gamma is to disrupt the ongoing SPN network beta in order to encourage motor program switching. Ordinarily, this gamma is limited to half a theta cycle, but with specific cortical input, it seems that FSI gamma could be induced during a different phase of theta and could last

for an indefinitely long or short amount of time. The fact that this can occur only in the high dopamine condition suggests that perhaps this override signal is sent during times of highly motivated behavior when rapid changes in strategy are needed. In this case, cortical input could induce a gamma in an FSI population in order to direct specific FSIs to interrupt specific beta-producing SPNs with their coordinated gamma bursts. This may be a mechanism by which the cortex, working in concert with the local striatal response to dopamine, interrupts habitual motor programs to allow for goal-directed behavior to occur. The FSIs could pause SPN beta while the cortex provides input essential to decision making, and then release the SPN network to resume producing beta once this information has been integrated. Of note, Belic et al. (Belić et al. (2016)) found that during levodopa-induced dyskinesia, i.e. a pathologically high dopamine state, gamma oscillations in striatum that are usually coupled to theta lose this low-frequency coupling and increase in power. This could be a direct result of the continuous FSI spiking at gamma modeled in the present study.

3.4.2 Caveats and limitations

The input used in the present study was entirely composed of square waves of injected current, which lack biological realism; real input from striatum to cortex likely has complex waveforms and is shaped by synaptic currents. The behavior of the FSI network in response to non-square currents is likely to be different in some aspects. A single model FSI responds differently to Gaussian or sinusoidal input than to square waves. Inputs with slower rise times are more likely to cause FSIs to burst, which can cause differences in firing rates and phase locking values to different shaped waveforms of the same frequency (unpublished work). The response

of a single model FSI to input of various properties is worth further study, as this behavior may translate to a different likelihood of bursting in the FSI network in response to different input shapes. The mechanism of theta oscillations in the network is dependent on bursting, and therefore the network theta may be stronger in response to inputs with slower rise times; however, this hypothesis would need to be tested in a full network model.

Additionally, within the present study, the properties of the FSI D current (and the SPN M current) were never varied. The frequencies of the gamma and theta oscillations in FSIs and the beta oscillations in SPNs are respectively determined by the time constants of these currents. In order to truly understand the properties of the input response of single cell models used in these situations, the parameters of these currents would need to be systematically tested in order to examine their impact on the trajectory of the state variables of the model through phase space. It is possible that the resonant frequencies of the network are determined solely by the time constants of the D and M currents, but it could also be the case that other properties of these currents have an impact on the frequency response properties of the network.

Another avenue for future inquiry utilizing this model is to examine how the correlations between disparate streams of input impact network behavior. Hjorth, Blackwell, and Kotaleski (Hjorth et al. (2009)) found that correlations in cortical input streams can increase firing rate in striatal FSIs. Gap junctions between striatal FSIs act as correlation detectors: when input is heterogeneous, gap junctions allow electrical shunting from depolarized neurons into hyperpolarized ones, inhibiting spiking, while shunting does not occur with homogeneous inputs. However, Hjorth et al. did not explore whether correlated input induces oscillations in the

FSI network, nor what might be the downstream impact of correlated input on the SPN network.

Unfortunately, due to the preliminary nature of the present study, the simulations described above have several shortcomings that may limit their applicability to generating hypotheses about in vivo activity. The most critical drawback of these simulations is that each point in parameter space has only been simulated once rather than being averaged over multiple runs as in Chapter 2. Because many of the phenomena described here are highly sensitive to specificity in frequency and input strength, this means that characterizations of these phenomena are both imprecise and possibly vulnerable to fluctuations in noise and initial conditions. For instance, the resonance of the SPN network at specific gamma frequencies is attributed here to beta harmonics, but it is possible that the gamma frequencies at which this resonance occurs are to some degree influenced by noise. A preliminary analysis suggests that these gamma frequencies are in fact stable per parameter regime (see Supplementary Figure 1), but statistical analysis would still be preferable. Another issue of the present data is the limitations on parameter space. Input strengths above and below those presented here can produce varied behaviors in the striatal network that are not described by the above analysis. Additionally, the ratio between input strength to FSIs and input strengths to SPNs has been arbitrarily set to 2:1 here; this choice of ratio may have important impacts on the network behavior as a whole. Overall, there are a wealth of possible manipulations possible with the present model and the scope of this chapter is only able to scratch the surface. However, even limited to the region of parameter space explored here, we are able to model network behavior with significant possible functional implications.

3.5 FIGURES AND TABLES

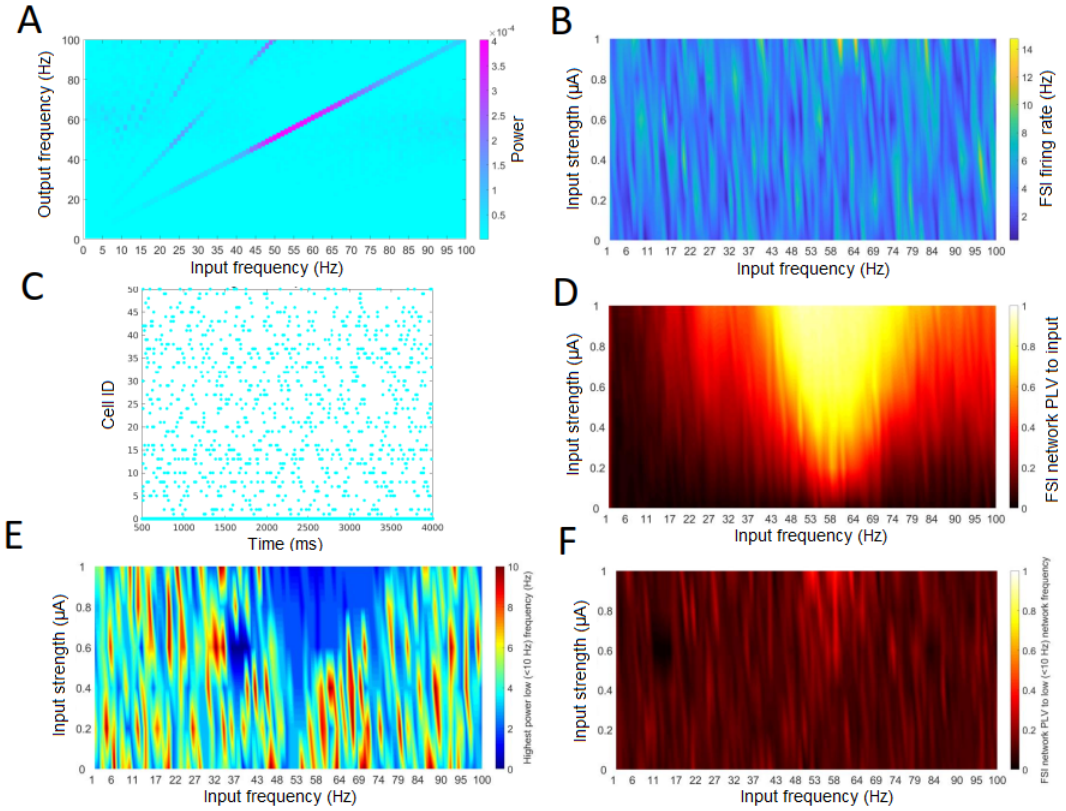

Figure 3.1: FSI network responses to square wave inputs of frequencies between 1 and 100 Hz in the low dopamine condition.

A. Power spectrum of surrogate LFP of FSI network in response to square wave inputs with an intensity of 1 μA (color indicates power in arbitrary units). B. Average firing rate of the FSI network in response to inputs of varying strength (color indicates network mean firing rate in Hz). C. Example raster plot showing the response of the FSI network to input at 65 Hz of 1 μA over 3500 milliseconds. D. Phase locking value of FSI network spiking to the input frequency (color indicates PLV). E. Strongest frequency in the network power spectral density below 10 Hz (color indicates frequency). F. Phase locking value of FSI network spiking to the network output frequency identified in E, given inputs from 1-100 Hz.

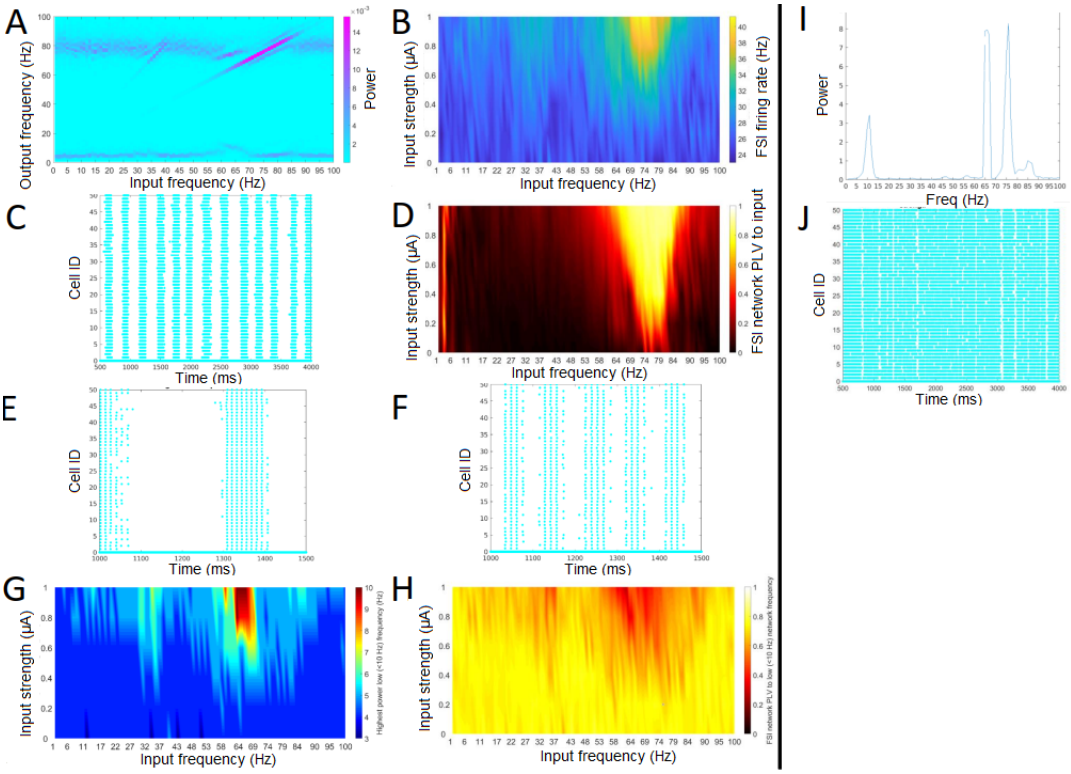

Figure 3.2: FSI network responses to square wave inputs of frequencies between 1 and 100 Hz in the high dopamine condition.

A. Power spectrum of surrogate LFP of FSI network in response to square wave inputs with an intensity of 1 μA. B. Average firing rate of the FSI network in response to inputs of varying strength. C. Example raster plot showing the response of the FSI network to input at 65 Hz of 0.2 μA over 3500 milliseconds. D. Phase locking value of FSI network spiking to the input frequency. E. Example raster plot showing the response of the FSI network to input at 3 Hz of 1 μA over 500 milliseconds. F. Example raster plot showing the response of the FSI network to input at 65 Hz of 1 μA over 500 miliseconds. G. Strongest frequency in the network power spectral density below 10 Hz. H. Phase locking value of FSI network spiking to the network output frequency identified in D, given inputs from 1-100 Hz. I. Power spectrum (arbitrary units) of the network activity shown in F, showing peaks at 10 Hz, 65 Hz (the input frequency), and 75 Hz. J. Example raster plot showing the response of the FSI network to input at 65 Hz of 2 μA over 3500 milliseconds.

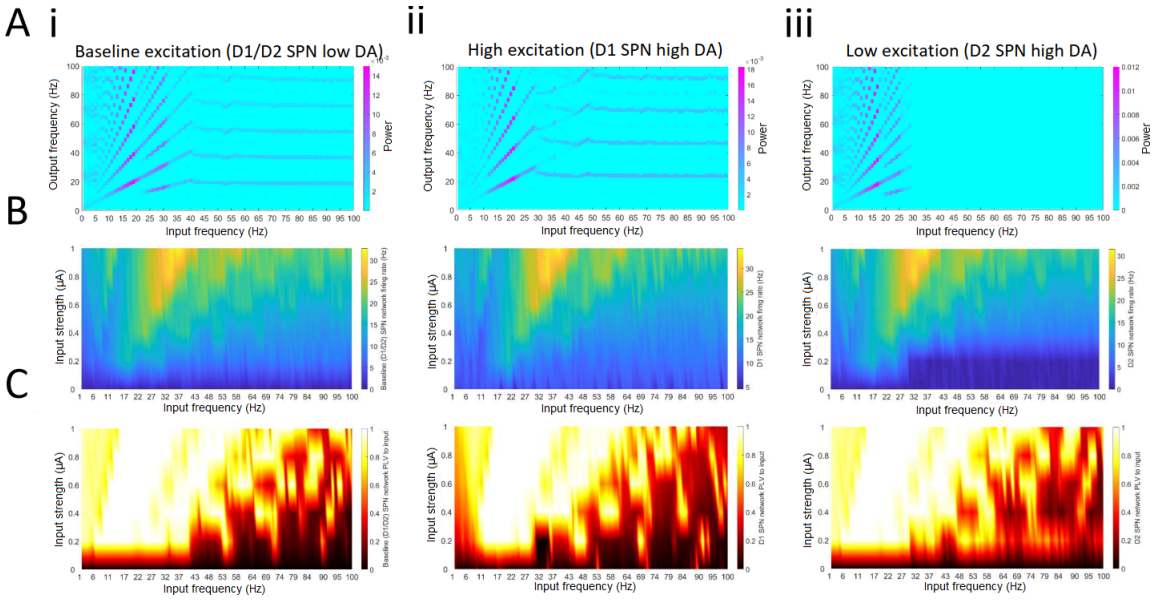

Figure 3.3: Isolated SPN network responses to square wave inputs of frequencies between 1 and 100 Hz, without FSI input.

Left (i): baseline/ low DA excitation level (equivalent for D1s and D2s), center (ii): high dopamine D1 SPN excitation level, right (iii): high dopamine D2 SPN excitation level. A. Power spectrum of surrogate LFP of SPN network in response to square wave inputs with an intensity of 0.2 μA. B. Average firing rate of the SPN network in response to inputs of varying strength. C. Phase locking value of SPN network spiking to the input frequency.

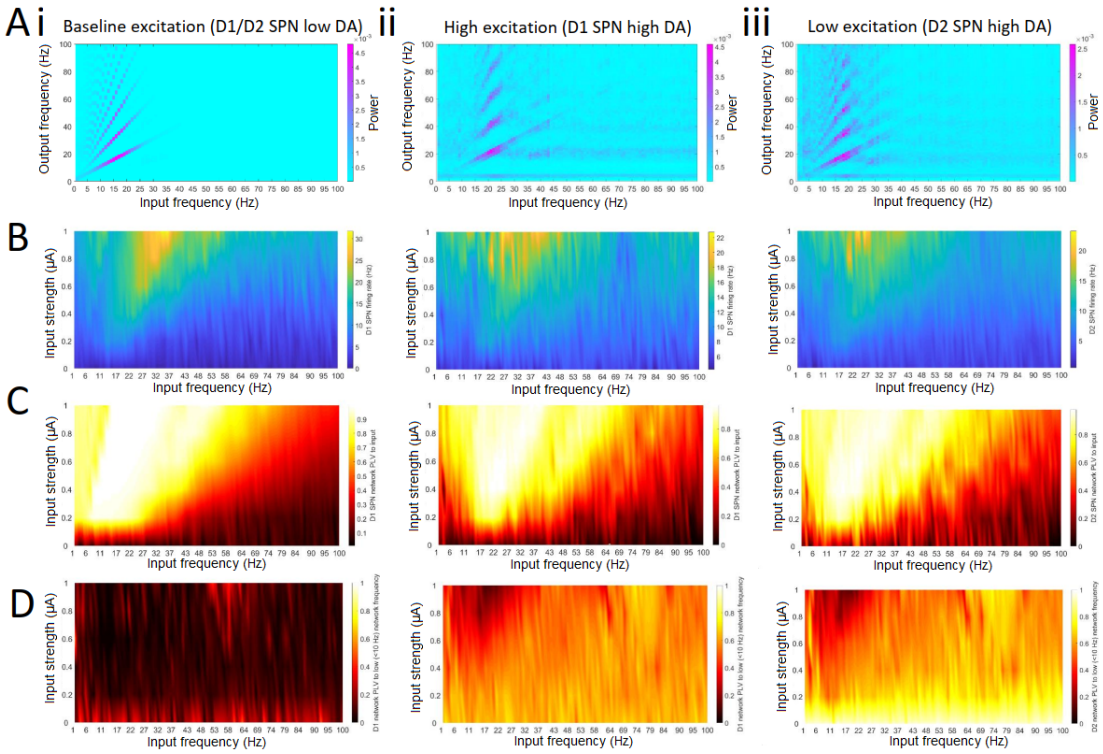

Figure 3.4: SPN network responses to square wave inputs of frequencies between 1 and 100 Hz in the full network, with FSIs present.

Left: baseline/ low DA excitation level (equivalent for D1s and D2s), center (ii): high dopamine D1 SPN excitation level, right (iii): high dopamine D2 SPN excitation level. A. Power spectrum of surrogate LFP of SPN network in response to square wave inputs with an intensity of 0.2 μA. B. Average firing rate of the SPN network in response to inputs of varying strength. C. Phase locking value of SPN network spiking to the input frequency. D. Phase locking value of FSI network spiking to the network output frequency identified in Figures 2D (for i) and 3D (for ii and iii), given inputs from 1-100 Hz.

Table 1. Rasters showing examples of the SPN network at different levels of background excitation responding to inputs of varying strengths and frequencies.

At all input strengths and levels of excitation, the SPN network will respond to 1 Hz input with output at 1 Hz (column i). However, if background excitation is high, the SPN network will also produce a beta oscillation that is not coupled to the low frequency input (row C i). The network entrains well to 15 Hz input in all conditions (column ii). If background excitation is low and input is weak, the SPN network will go silent in response to input frequencies above the beta range (row A, columns iii and iv). Otherwise, if either excitation or input strength is sufficiently high, the network will respond to all inputs by producing a beta oscillation (rows B and C, columns iii and iv). Phase locking values are higher when the input is a multiple of the natural beta frequency of the network (rows B and C, column iv).

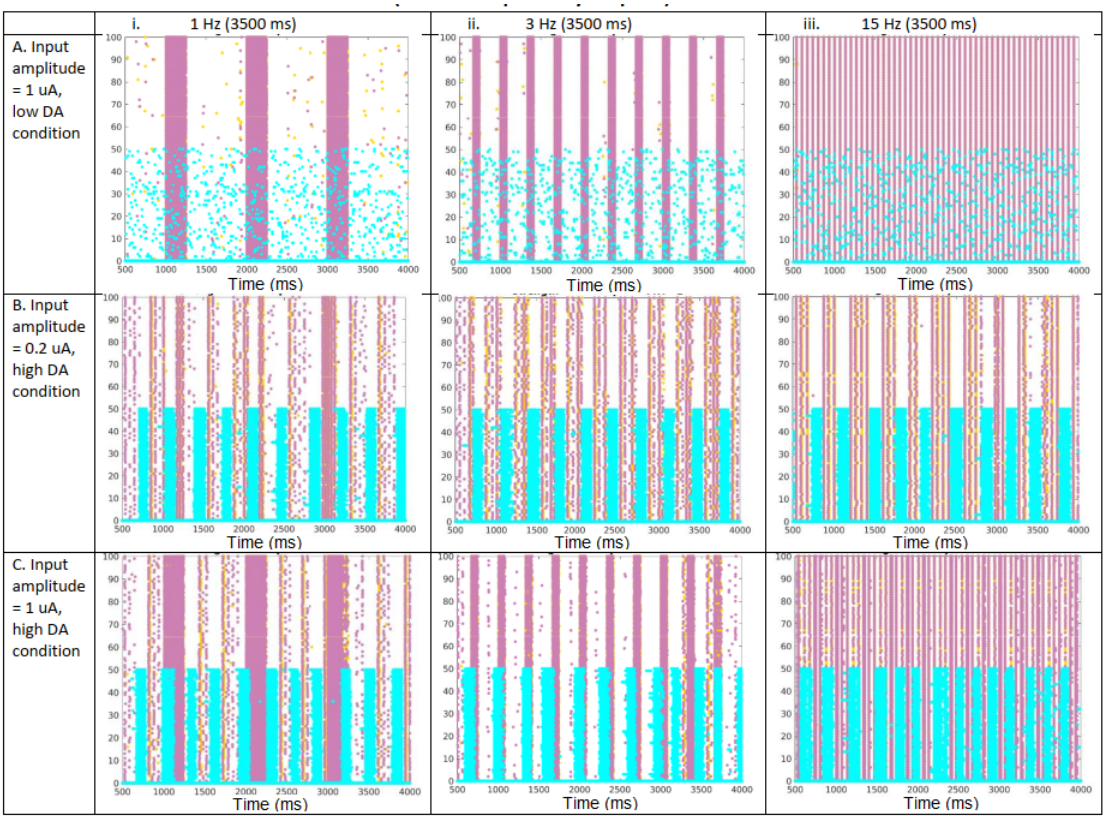

Table 2. Rasters showing examples of the full network in the low and high dopamine conditions responding to inputs of varying strengths and frequencies between 1 and 15 Hz.

Cyan indicates FSIs, magenta indicates D1 SPNs, and yellow indicates D2 SPNs. In the low dopamine condition (row A), the SPNs entrain well to inputs at these frequencies, and the FSIs do not. In the high DA condition, the FSI subnetwork produces a theta-coupled gamma in response to any input below 15 Hz (rows B and C). When input strength is low (row B), the SPN subnetwork is also patterned by theta, and spikes antiphase to the FSI subnetwork. However, when input strength is high (row C), the SPN subnetwork entrains to the input instead of to theta and SPNs will fire at the same time as the FSIs.

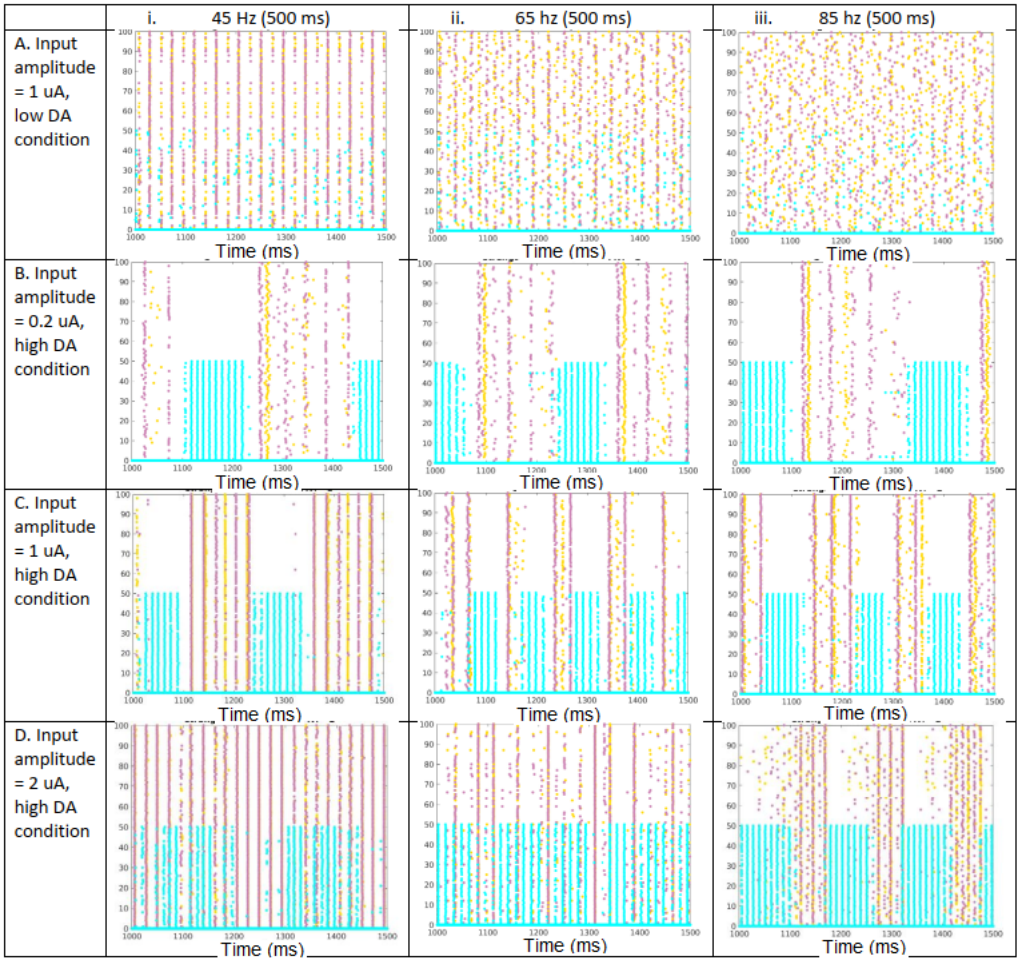

Table 3. Rasters showing examples of the full network in the low and high dopaminergic condition responding to inputs of varying strengths and frequencies between 45 and 85 Hz.

Cyan indicates FSIs, magenta indicates D1 SPNs, and yellow indicates D2 SPNs. In the low dopamine condition, there is a band of low gamma frequencies which both FSIs and SPNs will entrain to (row A, column i). Above a low gamma, the SPNs entrain poorly to input and produce little oscillatory power (row A, columns ii and iii). In the high dopamine condition, as in the low dopamine condition, weak inputs result in the SPN and FSI networks alternating spiking at theta (row B). When input is strong and between 55 and 70 Hz (column iii), the frequency of the FSI theta increases. For inputs over 2 μA, this increased theta frequency gives way to continuous FSI spiking at gamma, to which the SPNs also entrain (row D, column iii). Above 70 Hz, FSI theta returns to a lower frequency (rows C and D, column iv).

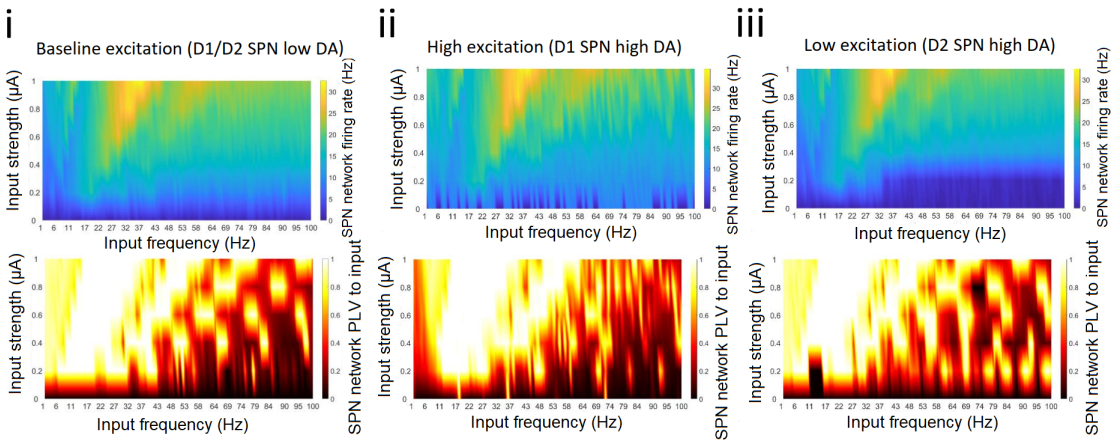

Supplementary Figure 1. Noiseless SPN network

CHAPTER 4

Reward learning generates theta-coupled beta rhythms in human EEG that are sensitive to feedback valence

4.1 INTRODUCTION

The present data analysis is motivated by predictions made by the striatal model developed in Chapter 2. Specifically, this model predicts that during periods of high dopaminergic tone, the striatum should be producing a high beta around 20 Hz and a high gamma around 80 Hz, nested within alternating phases of a low frequency around 3 Hz (either high delta or low theta). The high gamma is expressed only by local fast-spiking interneurons and is not conducted downstream to the striatal projection neurons, making it hard to observe. However, the beta is expressed in projection neurons and is expected to travel through the basal ganglia (BG)-thalamus loop and into cortex (Brittain & Brown (2014)).Therefore, if this model is correct, periods of high striatal dopamine should be associated with a 3 Hz-nested beta. Models of the trajectory of striatal dopamine during reward learning suggest that peak dopaminergic tone should occur when an unexpected reward is given (Keiflin & Janak (2015)). Thus, one way to test whether my model holds true in humans would be to look for this signature 3 Hz-nested beta activity in human electrophysiological recordings (from striatum, thalamus, and/or cortex) during a probabilistic (i.e. chance-based) reward learning task, immediately after feedback is given.

Recording electrical activity directly from human striatum is possible via invasively implanted electrodes, making acquiring large quantities of data to test these model predictions difficult. Instead, I explored whether the network behavior pre-

dicted by my model would be detectable in noninvasive electroencephalogram (EEG) recordings. There is evidence that striatal activity can be detected via EEG during reward learning, a task in which striatum is heavily involved due to its integral role in the dopaminergic reward processing system (Keiflin & Janak (2015)). Reward learning tasks in humans produce several characteristic responses in the EEG, both as event-related potentials and as induced oscillatory activity (Cohen et al. (2007); Cavanagh (2015); HajiHosseini et al. (2012)); several studies have suggested striatal involvement in producing these EEG signatures (Foti et al. (2015); Mas-Herrero et al. (2015); Andreou et al. (2017)). Immediately after feedback presentation in a reward-learning task, recordings at frontal electrodes show power increases in several frequency bands relative to baseline, with the identity of these frequencies depending on feedback. Positive feedback is associated with increases in power in the delta (1-3 Hz) and beta (20-30 Hz) bands (Cavanagh (2015); HajiHosseini et al. (2012)), while negative feedback is associated with increased power in the theta (4-8 Hz) band (Cohen et al. (2007)). Source localization studies suggest that the delta and beta oscillations can be related to activity in the striatum, specifically nucleus accumbens, whereas the theta oscillation appears to arise from anterior cingulate (Foti et al. (2015); Mas-Herrero et al. (2015); Andreou et al. (2017)).

Delta and beta oscillations arising in striatum in response to positive feedback (when striatal dopamine should be high) could be the same rhythms predicted by my model. If so, the beta should be tightly coupled to the delta; my model predicts that in high dopaminergic tone conditions, beta can only be produced during the permissive phase of the delta in which striatal fast-spiking interneurons are silent. In order to determine whether my striatal models predictions are applicable to cortical signals, I measured phase amplitude coupling (PAC) between delta (3 Hz)

and beta frequencies detected in human reward learning data. Phase amplitude coupling is defined as the modulation of the amplitude envelope of a faster oscillation by the phase of a slower oscillation. In order to assess PAC between any two oscillations, one must find the instantaneous phase of the lower frequency oscillation and the instantaneous amplitude of the higher frequency oscillation and then compute one of several available PAC metrics. In this analysis, I used the measure proposed by Tort et al. (2010), as it fares well in tests of sensitivity to the degree of dependence of amplitude on phase (Seymour et al. (2017)). I was successfully able to detect theta-beta PAC in the data presented here, suggesting that the alternating striatal rhythms predicted by my model can be detected noninvasively at cortical electrodes.

4.2 DATA DESCRIPTION

EEG and behavioral data were recorded during a probabilistic learning task in which participants had to learn which of two computer generated images of fractals was more likely to result in a positive outcome. The task used here is based on the task design of (Frank (2004)). Feedback given after choosing one of these options was probabilistic; one image resulted in a 60 percent probability of correct (positive) feedback, whereas the other resulted in a 40 percent probability of positive feedback. The task consisted of 360 trials. Each trial began with a fixation cross for 800-1200 milliseconds, followed by a black and white image displayed for a maximum of 4000 milliseconds. Subjects were instructed to choose a target by pressing a gamepad button using the thumb of their right hand. Immediately after their decision, feedback indicating whether their decision was correct or incorrect was displayed for 200 milliseconds. Visual feedback is provided following each

choice (the word 'Correct!' printed in blue or 'Incorrect' printed in red). If no response is made within four seconds, the words 'no response detected' are printed in red.

The task duration for each experiment was approximately 30 minutes. EEG was collected from 96 electrodes sampling at 1000 Hz and was online referenced to the right mastoid electrode. Eye position (horizontal and vertical) and blinks were also monitored with electrodes for the purpose of artifact detection. EEG processing and analyses were conducted in MATLAB using the Fieldtrip toolbox. The recorded EEG data were initially high-pass filtered at 0.1 Hz and low- pass filtered at 170 Hz. In order to avoid edge artifacts, data segments from 4 seconds before until 5 seconds after feedback onset were extracted for analysis on a shorter timescale. Trials containing muscle artifacts were removed by visual inspection. Once these had been removed, an independent component analysis of the data was used to identify components that appeared to be blink or noise artifacts, which were then removed. For exploratory and total power analysis prior to assessment of phase-amplitude coupling, time frequency analysis was performed using complex Morlet wavelets.

4.3 METHODS

PAC analyses search for fluctuations in amplitude that are coupled to fluctuations in phase; both types of fluctuations are only possible in broadband oscillatory components. Thus, the filtering that precedes PAC analyses must use broadband filters. Complex Morlet wavelets are preferable to other filtering methods because they are intrinsically broadband, and do not exhibit steep rolloff in frequency space. They also output instantaneous phase and amplitude data for every frequency of

interest, eliminating the need to Hilbert transform the data before finding these values (Pittman-Polletta et al. (2014)). For each trial and channel, the EEG time series was convolved with complex Morlet wavelets corresponding to phase-giving (i.e., low) frequencies from 2 to 7.5 Hz, spaced at 0.5 Hz, and amplitude-giving (i.e., high) frequencies from 12 to 100 Hz, spaced at 1 Hz. The low frequency wavelets had a width of 3 cycles and the high frequency wavelets had a width of 7.5 cycles. The latter number was chosen such that the bandwidth of frequencies considered for the amplitude-giving oscillation is at least as large as the frequency of the fastest phase-giving oscillation. This way, changes in amplitude at the timescale of this fastest phase-giving oscillation could be assessed (Pittman-Polletta et al. (2014)). After convolution, the instantaneous phase of the low frequency oscillations is then given by the angle of the resulting complex time series, while the instantaneous amplitude of the high frequency oscillation is the magnitude of the resulting complex time series.

Next, for each frequency pair of interest, I calculated an empirical marginal distribution of instantaneous amplitude by instantaneous phase. First, I binned the phase domain (the interval from 0 to 360 degrees) into 20 18-degree intervals, and identified the sets of times at which the phase of the low frequency oscillation fell into each of these bins. Then I averaged the instantaneous amplitudes of the high frequency oscillation at these sets of times, to obtain the mean high-frequency amplitude observed in each (low-frequency) phase bin. This distribution of amplitude by phase was then normalized by the sum of all of these mean amplitudes to generate a probability density function. From this, I calculated the mutual information (MI) PAC metric (Tort et al. (2010)) by finding the Kullback-Liebler (KL) distance between this distribution and the uniform distribution. This distance is

also known as inverse entropy and is given by the difference between the Shannon entropy of the empirical amplitude distribution and the entropy of the uniform distribution. The entropy H of a distribution P is given by

$$H(P) = -\sum_{j=1}^{N} P(j)log[P(j)] \tag{4.1}$$

The KL distance between this distribution and the uniform distribution U is then defined as

$$D_{KL}(P, U) = log(N) - H(P) \tag{4.2}$$

The entropy of the uniform distribution is always $log(N)$, where N is the number of phase bins, because this is the maximum possible entropy value. The MI is simply the KL distance normalized to $log(N)$ so that it only takes values between 0 and 1. In this case, 0 would represent an empirical distribution identical to the uniform distribution (no phase-amplitude dependence) and 1 would represent the high frequency oscillation only having nonzero amplitude during one phase bin of the low frequency oscillation.

In practice, due to finite data length, the MI is always nonzero, even for non-simultaneous phase- and amplitude-giving time series (for which there can be no phase-amplitude coupling). The size of the MI for a given pair of nonsimultaneous time series depends on many factors, including the frequency of fluctuations in amplitude and phase. Furthermore, as it can only be between 0 and 1, the MI cannot be normally distributed. All these factors make it difficult to tell from the value of the MI whether it represents a difference from the 'baseline' coupling value we expect due to finite size effects even for nonsimultaneous time series. Rather than identifying a distribution function, the most straightforward way to

assess whether the MI is significantly different from this baseline distribution is to use nonparametric testing based on surrogate data. We generated a surrogate 'baseline' MI distribution by randomly (without replacement) selecting phase giving oscillations from one trial and pairing them with amplitude giving oscillations from another, then calculating the resulting MI. Pairs for which the phase and amplitude giving oscillations came from the same trial are excluded from this distribution in order to exclude the actual observed PAC in the background estimate. The time vector for the surrogate data remains aligned by the time point of feedback, allowing us to account for the fact that background PAC may change over the course of the experiment. This analysis is done on a per-subject basis such that each subject has an individual mean surrogate MI value, and both that subjects real data and their surrogate data are normalized to this value. We can then assign a p-value to each subjects real normalized mean MI value by identifying where it lies in the ensemble (normalized) surrogate distribution over all subjects. When comparing between two conditions (in this case, comparing trials where the choice was rewarded versus trials where the choice was unrewarded), the surrogate distribution was calculated by selecting nonsimultaneous phase- and amplitude-giving time series randomly from trials in both conditions.

Because the precise identity of the frequencies at which we expect to see phase-amplitude coupling was not known in advance, exploratory analyses were performed using 'comodulograms' that covered broad ranges of frequencies. Given the number of possible phase-amplitude pairs within the frequency ranges used, some amount of correction for multiple comparisons is necessary. To address this issue, I utilized the cluster-based algorithm described in (Maris & Oostenveld (2007)). This algorithm is a means of solving the multiple comparisons problem

by incorporating biophysically motivated constraints. Namely, we expect that the underlying structure of biological data will cause adjacent data points to have similar values, and therefore that real effects of experimental manipulations are likely to appear as a cluster of adjacent data points that are all improbable under the null hypothesis as opposed to isolated outlier values. Therefore, this algorithm utilizes a test statistic that is calculated based on a set of adjacent points that all exhibit a similar difference from the baseline distribution of values.

This test statistic is calculated by first comparing two data sets. In the present study, one data set consisted of PAC values at each possible pair of frequencies, calculated from real data from trials of one condition (correct or incorrect), and the other data set consisted of PAC values for the same frequency pairs, calculated from shuffled surrogate data comprised of trials from all conditions. These two data sets are combined into one set, and then randomly partitioned into two sets, which are each the same size as the original two, but which contain a randomly chosen subset of the combined data. For these two randomly partitioned sets, we calculate a t-value for the sets of observed MI at each frequency pair, using a dependent samples t-test. We do this partitioning 1000 times in order to generate 1000 'permutation' comodulograms with t-values for each frequency pair. We can now assign a p- value to both observed and permutation t-values (at each frequency pair), by calculating the proportion of random partitions that resulted in a larger t-value than the given t-value. Once we have done this, for each comodulogram we select all frequency pairs with a p-value less than an alpha level of 0.05 as cluster candidates. All of the candidate frequency pairs that are adjacent to each other are considered to be in the same cluster (Maris & Oostenveld (2007)). Each cluster is then assigned a cluster-level test statistic, the sum of the t-values within the

cluster, which depends on both the size of the cluster and the size of the t-values of individual frequency pairs in the cluster.

Next, we used the same permutation comodulograms to test the significance of each cluster. For each of the 1000 permutation comodulograms, we select the largest cluster-level test statistic in order to form a permutation distribution of cluster-level test statistics. This permutation distribution can now be used to assign p-values to the test statistics arising from the clusters in the observed comodulogram. If any of these p-values are below the alpha level of 0.05, we consider that cluster significant. In the figures below, the significant clusters are outlined in black.

4.4 RESULTS

Our analysis of total power at electrode Fz immediately after feedback was in good agreement with previous findings in the literature (Cavanagh (2015); HajiHosseini et al. (2012); Cohen et al. (2007)) regarding the role of the low frequency bands in reward learning. In my analysis, I found that delta oscillations were stronger after correct feedback (Figure 1A, C), and theta and beta oscillations were stronger after incorrect feedback (Figure 1B, C). This finding about beta is at odds with previous results in the literature (HajiHosseini et al. (2012); Mas-Herrero et al. (2015); Andreou et al. (2017)).

Significant phase-amplitude coupling was present between several of the frequency bands studied, and was sensitive to feedback valence. Within the first 500 milliseconds after subjects were told their answer was correct, amplitude at all beta and gamma frequencies showed increased modulation by the phase of a 3-5 Hz rhythm, ($p < 0.001$, cluster statistic $= 723.77$) accompanied by a drop in cou-

pling of high gamma (70-100 Hz) to a 7-8 Hz rhythm ($p = 0.018$, cluster statistic $= -161.79$; Figure 2A). Expanding the analysis window to include the first second after feedback suggests that this coupling to 3-5 Hz phase is strongest specifically in the high beta to low gamma band (20-60 Hz) ($p < 0.001$, cluster statistic $= 347.22$; Figure 2B).

An exploratory data analysis with a significance level of 0.1 revealed additional structure in the data that could prompt further investigation; the remainder of the results in this section were analyzed at this significance level. (Note that the p-values here to have been adjusted to correct for testing at multiple frequency pairs, but have not been corrected by the number of tests run.) In order to assess whether coupling was affected at even lower frequencies that may not have had a sufficient number of cycles in this 1 second time window to allow PAC detection, I further expanded the analysis to a 2 second long period starting 500 milliseconds before feedback was given. Doing so revealed that there appears to be a near-significant reduction in coupling between 2 Hz and high gamma (65-95 Hz) associated with positive feedback ($p = 0.071$, clustering statistic $= -55.45$; Figure 2C).

The reward learning task used in this experiment is simple enough that by the end of the experiment, subjects had reached near ceiling in terms of performance; 46.1 percent ($SEM = 3.0$ percent) of trial 1 responses were rewarded, while 58 percent ($SEM = 1.8$ percent) of trial 360 responses were rewarded, with 60 percent being the maximum optimal performance. In order to assess whether the observed results differed early in learning before mastery had been achieved, I examined PAC restricted solely to the first 30 correct and incorrect trials each. Doing so revealed that correct feedback was associated with an increase in coupling between 4-8 Hz and 60 Hz ($p = 0.068$, cluster statistic $= 64.91$), whereas incorrect feedback

was associated with increased coupling between 4-8 Hz and 70-90 Hz ($p = 0.025$, cluster statistic $= -100.07$; Figure 3A). Interestingly, these effects are present in the 500 millisecond window prior to the actual feedback onset, suggesting a role in reward anticipation ($p = 0.076$, cluster statistic $= -58.48$; Figure 3B).

4.5 DISCUSSION

To a first approximation, the results in Figure 2 are novel and appear to be in agreement with my model of striatal dynamics, suggesting striatum may be the source of these EEG oscillations. Specifically, my model predicts higher coherence between a 3 Hz low theta/high delta and a high beta around 20 Hz during conditions of higher dopaminergic tone, and coherence is indeed higher between these frequencies in the rewarded condition. This suggests that the beta generated during reward learning is in fact modulated by the delta generated by reward, in agreement with both of these rhythms being generated within the striatum as predicted by my model. While previous studies have established that both beta and delta are associated with positive feedback, this is the first demonstration that the reward-associated beta is modulated by a lower frequency.

However, several aspects of the results shown in figure 2 do not necessarily support my model and may be at odds with the literature as well. Most notably, the frequency that is coupled with the beta in the current data is between 3 and 5 Hz, consistent with my model. However, there are several candidate definitions of delta or theta bands that this frequency actually represents, which could include frequencies ranging from 1 to 8 Hz. While my model makes specific predictions about a 3 Hz low-theta frequency, it is based on data that includes a much higher 8 Hz theta (Berke (2009)), and the specific identity of the low frequency generated by

my model depends on properties of the input; given specific gamma frequencies as input, an 8 Hz theta is achievable by my model (see Chapter 3). However, if the present data are to be considered evidence for my model, it relies on the assumption that the low frequency detected at electrode Fz after positive feedback is the striatally-generated delta, which other studies have described as between 1 and 3 Hz (Cavanagh (2015); Foti et al. (2015)). It is possible that the 3-5 Hz band in these data does not correspond to the striatal delta at all, and may represent the 4-8 Hz theta frequency that has been reported in frontal EEG (Foti et al. (2015); Mas-Herrero et al. (2015); Andreou et al. (2017)). Furthermore, Figure 2C shows that there is some degree of decoupling between a 2 Hz frequency and a high gamma in the correct feedback condition; this 2 Hz frequency may be the delta described in the literature, providing further evidence that the 3-5 Hz band may not be representative of the positive feedback associated delta. My model also predicts relatively specific coupling between theta and beta, and the coupling to 3-5 Hz in these data is not specific to beta, but rather is centered around a low gamma. Gamma is typically thought to represent local activity (Whittington et al. (2011)), so this gamma may arise from frontal cortical network activity that is patterned by the striatal delta.

It is notable that the data analyzed here did not seem to provide evidence for the beta associated with positive feedback that has been detected in previous studies (HajiHosseini et al. (2012); Mas-Herrero et al. (2015); Andreou et al. (2017)); in fact, there appears to be an association between beta and negative feedback. However, there is a large amount of beta power present in both conditions, and the immediate post-feedback beta (around 20 Hz) may not be the same as the beta present later in the trial, which is closer to 13 Hz. The reward- associated beta

reported in previous studies is typically a high beta, verging on low gamma (HajiHosseini & Holroyd (2015)). The later, lower beta in these data may be related to pre-cue preparatory processing for the next trial (Kilavik et al. (2013)). The pre-cue beta is thought to be related to attention; perhaps the reason beta is more elevated after negative feedback is because participants are paying more attention to the task. The PAC shown in Figure 2B appears to be more strongly associated with high beta, suggesting that the low-frequency modulation of beta is more associated with the earlier, feedback-related response than with the later, possibly preparatory response.

If the PAC detected here is indeed evidence for the striatal delta/beta coupling predicted by my model, this has implications for the role of the striatal beta in corticostriatal communication. Several people have hypothesized that the striatal beta represents a 'status quo' signal that encourages maintenance of the current state (Brittain & Brown (2014)). This has been proposed to refer not just literally to staying still (though beta is higher during static hold; (Kilavik et al. (2013)); it may also be the case that beta oscillations are useful as a reinforcing learning signal, encouraging the continuing activity of cell assemblies relevant to the current task so that they can be tagged for potentiation (van de Vijver et al. (2011)). This fits well with my models prediction that high-dopamine states are associated with packets of high beta originating in striatal projection neurons, as dopamine is also thought of as a reinforcement learning signal (Keiflin & Janak (2015)). Beta is also thought of as a long-range synchrony signal; whereas gamma reflects activity of local cortical circuits (Whittington et al. (2011)), beta oscillations travel through the basal ganglia-thalamocortical loop (Brittain & Brown (2014)). The role of the striatally generated delta/theta-modulated beta in this task may be to propagate learning-

associated signals through the BG and thalamus so that they can reach cortex and pattern local cortical gamma. This would explain why oscillatory signals originating from striatum would be detectable on EEG, as well as why gamma activity during reward learning seems to be locally generated in frontal cortex (HajiHosseini & Holroyd (2015)).

While this is the first report of low-frequency coupling to the reward-associated beta, it is not the first report of theta-beta coupling during a rewarded task. A 2013 paper by Kawasaki and Yamaguchi (Kawasaki & Yamaguchi (2013)) also finds coupling between a low frequency (6 Hz) and a high beta (24 Hz) at electrode Fz during reward anticipation, but did not examine response to feedback; this PAC occurred during the period between the task cue and the response. The authors of that study suggest that this theta-coupled beta may represent reward anticipation, and point out that it has similar properties to the trajectory of striatal dopamine; it is stronger for larger rewards, and is more sustained when reward is uncertain. Examining cue-associated activity in the present data set, especially in later trials, could confirm whether we see the same patterns in beta PAC in these data. Another informative analysis would be to assess whether positive feedback resulting from the stimulus that was correct only 40 percent of the time produced stronger PAC than positive feedback resulting from the stimulus that was correct 60 percent of the time. If this is the case, it would bear out the prediction that this PAC is a result of phasic increases in striatal dopamine, as dopamine release is predicted to be higher for unexpected than expected rewards (Keiflin & Janak (2015)).

There are several avenues of inquiry that could be addressed by further analysis of the present dataset. For instance, one could test whether coherence exists between beta and gamma frequencies if this were present, it would suggest ei-

ther that the striatal gamma generated in my model represents a signal that can be detected even at the level of EEG, or that the reward-associated beta could be patterning local gamma activity. There is also the possibility of looking at activity associated with task points besides feedback for instance, measuring PAC around the time of cue onset or the time of the subjects response. According to models of reward prediction error, striatal dopamine levels should be higher when the reward is given earlier in learning, but after learning has occurred, striatal dopamine levels should be highest at the time of the cue that a reward will be given (Keiflin & Janak (2015)). Examining the time period between response and reward delivery could also be useful; reward anticipation early in learning is associated with a slow increase in dopamine (Keiflin & Janak (2015)). Analyzing this time period would also help elucidate what might be occurring in Figure 3; the two gamma bands are not predicted by my model, and may be a novel finding.

4.6 FIGURES AND TABLES

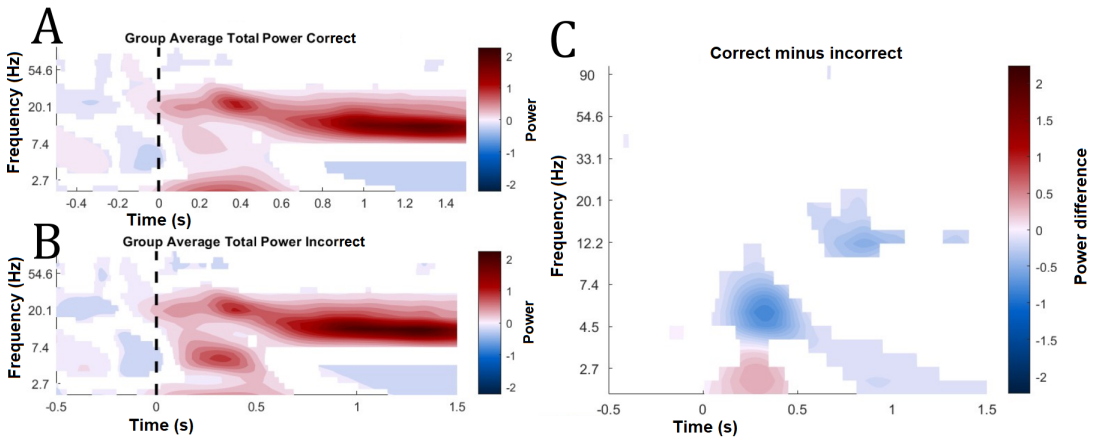

Figure 4.1: Total power results

A. Instantaneous power (arbitrary units) in all measured frequencies averaged over all correct trials. 0 indicates the time at which feedback was given. Color indicates magnitude; white indicates no significant power difference from surrogate data at alpha = 0.05. B. Instantaneous power in all measured frequencies averaged over all incorrect trials. C. Difference between correct and incorrect trials in terms of power (A-B). Red indicates where power was stronger after correct trials; blue indicates where power was stronger after incorrect trials. White indicates no significant difference between correct and incorrect trials at alpha = 0.05.

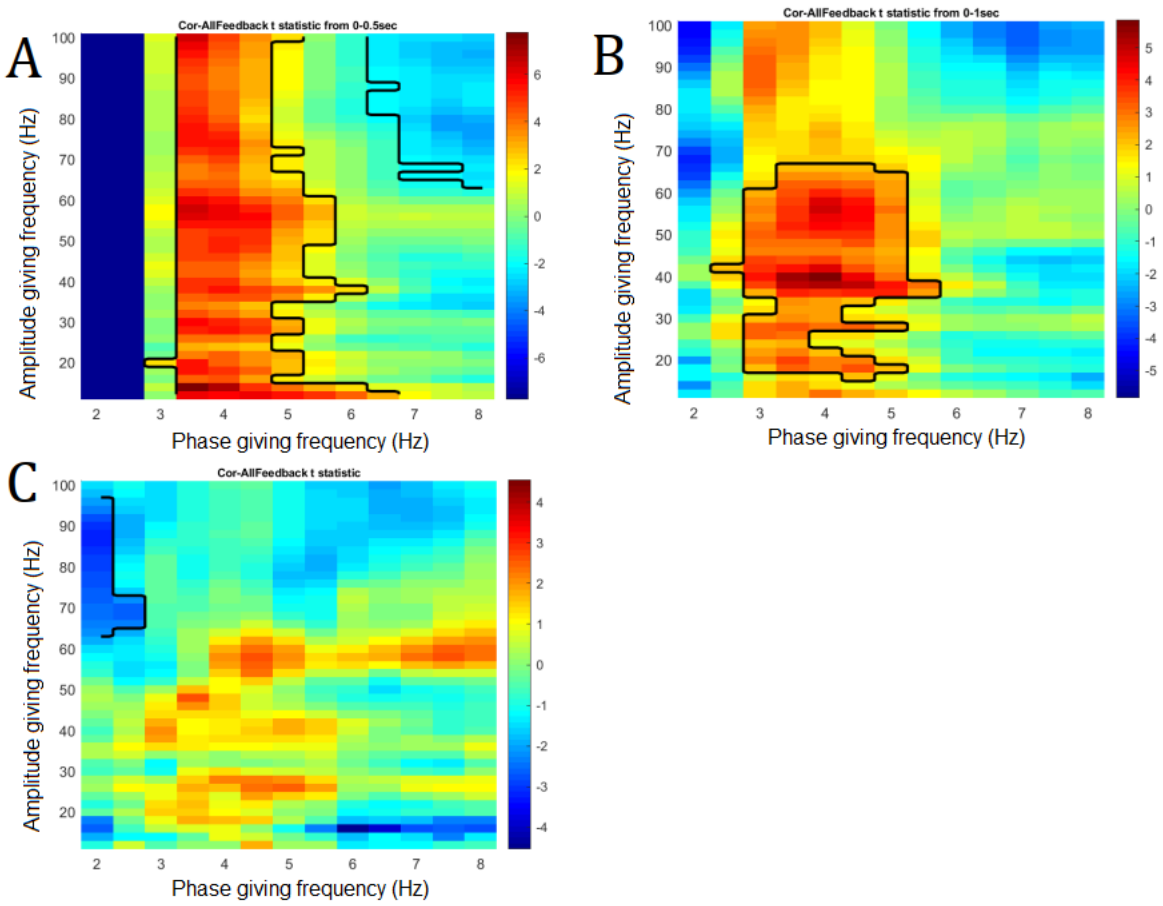

Figure 4.2: Phase amplitude coupling results

A. Phase amplitude coupling in correct trials versus a joint surrogate distribution of shuffled data from correct and incorrect trials, over the first 0.5 seconds following feedback. Black line indicates significant clusters. Data below 2 Hz is unavailable due to the short analysis time window. B. Phase amplitude coupling in correct trials versus a joint surrogate distribution of shuffled data from correct and incorrect trials, over the first 1 second following feedback. C. Phase amplitude coupling in correct trials versus a joint surrogate distribution of shuffled data from correct and incorrect trials, over a time window encompassing 0.5 seconds before feedback was given until 1.5 seconds after feedback was given.

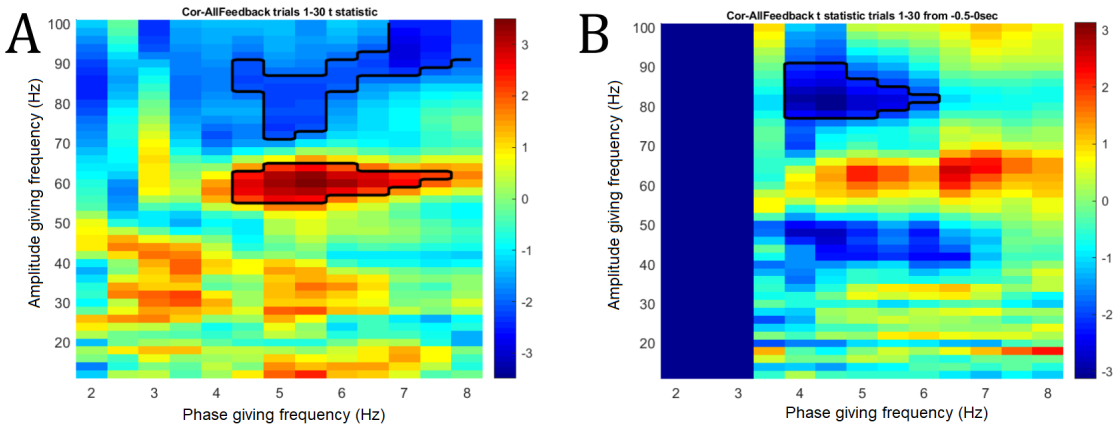

Figure 4.3: Phase amplitude coupling in the first 30 trials

A. Phase amplitude coupling in the first 30 correct trials versus a joint surrogate distribution of shuffled data from the first 30 correct and the first 30 incorrect trials, over a time window encompassing 0.5 seconds before feedback was given until 1.5 seconds after feedback was given. Black line indicates significant clusters. B. Phase amplitude coupling in the first 30 correct trials versus a joint surrogate distribution of shuffled data from the first 30 correct and the first 30 incorrect trials, over the 0.5 seconds immediately prior to feedback. Data below 2 Hz is unavailable due to the short analysis time window.

BIBLIOGRAPHY

Alam, M., Capelle, H., Schwabe, K., & Krauss, J. K. (2014). Effect of deep brain stimulation on Levodopa-induced dyskinesias and striatal oscillatory local field potentials in a rat model of Parkinson ' s disease. *Brain Stimulation*, *7*(1), 13–20.

Alberico, S. L., Kim, Y.-C., Lence, T., & Narayanan, N. S. (2017). Axial levodopa-induced dyskinesias and neuronal activity in the dorsal striatum. *Neuroscience*, *343*.

Andreou, C., Frielinghaus, H., Rauh, J., Mußmann, M., Vauth, S., Braun, P., Leicht, G., & Mulert, C. (2017). Theta and high-beta networks for feedback processing: a simultaneous EEGfMRI study in healthy male subjects. *Translational Psychiatry*, *7*(1), e1016–e1016.

Ardid, S., Sherfey, J. S., McCarthy, M. M., Hass, J., Pittman-Polletta, B. R., & Kopell, N. (2019). Biased competition in the absence of input bias revealed through corticostriatal computation. *Proceedings of the National Academy of Sciences*, *116*(17), 8564–8569.

Beatty, J. A., Song, S. C., & Wilson, C. J. (2015). Cell-type-specific resonances shape the responses of striatal neurons to synaptic input. *Journal of Neurophysiology*, *113*(3), 688–700.

Belić, J. J., Halje, P., Richter, U., Petersson, P., & Hellgren Kotaleski, J. (2016). Untangling cortico-striatal connectivity and cross-frequency coupling in L-DOPA-induced dyskinesia. *Frontiers in Systems Neuroscience*, *10*, 26.

Belić, J. J., Kumar, A., Kotaleski, J. H., & Hellgren Kotaleski, J. (2017). Interplay between periodic stimulation and GABAergic inhibition in striatal network oscillations. *PLoS ONE*, *12*(4), e0175135.

Bem, T., & Rinzel, J. (2004). Short duty cycle destabilizes a half-center oscillator, but gap junctions can restabilize the anti-phase pattern. *Journal of Neurophysiology*, *91*(2), 693–703.

Berke, J. D. (2008). Uncoordinated firing rate changes of striatal fast-spiking interneurons during behavioral task performance. *Journal of Neuroscience*, *28*(40), 10075–10080.

Berke, J. D. (2009). Fast oscillations in cortical-striatal networks switch frequency following rewarding events and stimulant drugs. *European Journal of Neuroscience*, *30*(5), 848–859.

Berke, J. D. (2011). Functional properties of striatal fast-spiking interneurons. *Frontiers in Systems Neuroscience*, *5*(6), 45.

Berke, J. D., Breck, J. T., & Eichenbaum, H. (2009). Striatal Versus Hippocampal Representations During Win-Stay Maze Performance. *Journal of Neurophysiology*, *101*(3), 1575–1587.

Berke, J. D., Okatan, M., Skurski, J., & Eichenbaum, H. B. (2004). Oscillatory entrainment of striatal neurons in freely moving rats. *Neuron*, *43*(6), 883–896.

Bernat, E. M., Nelson, L. D., & Baskin-Sommers, A. R. (2015). Time-frequency theta and delta measures index separable components of feedback processing in a gambling task. *Psychophysiology*, *52*(5), 626–637.

Bokil, H., Purpura, K., Schoffelen, J.-M., Thomson, D., & Mitra, P. (2007). Comparing spectra and coherences for groups of unequal size. *Journal of Neuroscience Methods*, *159*(2), 337–345.

Börgers, C., Talei Franzesi, G., LeBeau, F. E. N., Boyden, E. S., Kopell, N. J., Franzesi, G., LeBeau, F. E. N., Boyden, E. S., & Kopell, N. J. (2012). Minimal size of cell assemblies coordinated by gamma oscillations. *PLoS Computational Biology*, *8*(2), e1002362.

Bracci, E., Centonze, D., Bernardi, G., & Calabresi, P. (2003). Voltage-dependent membrane potential oscillations of rat striatal fast-spiking interneurons. *Journal of Physiology*, *549*(1), 121–130.

Bracci, E., Centonze, D., Bernardi, G., Calabresi, P., Neurologica, C., Neuroscienze, D., Vergata, T., Lucia, F. S., Centonze, D., & Bernardi, G. (2002). Dopamine excites fast-spiking interneurons in the striatum. *Journal of Neurophysiology*, *87*(4), 2190–2194.

Brittain, J. S., & Brown, P. (2014). Oscillations and the basal ganglia: motor control and beyond. *NeuroImage*, *85*.

Brown, P. (2007). Abnormal oscillatory synchronisation in the motor system leads to impaired movement. *Current Opinion in Neurobiology*, *17*(6), 656–664.

Brown, P., & Williams, D. (2005). Basal ganglia local field potential activity: Character and functional significance in the human. *Clinical Neurophysiology*, *116*(11), 2510–2519.

Buxton, D., Bracci, E., Overton, P. G., & Gurney, K. (2017). Striatal neuropeptides enhance selection and rejection of sequential actions. *Frontiers in Computational Neuroscience*, *11*, 62.

Catanese, J., Carmichael, J. E., & van der Meer, M. A. A. (2016). Low- and high-gamma oscillations deviate in opposite directions from zero-phase synchrony in the limbic corticostriatal loop. *Journal of Neurophysiology*, *116*(1), 5–17.

Cavanagh, J. F. (2015). Cortical delta activity reflects reward prediction error and related behavioral adjustments, but at different times. *NeuroImage*, *110*, 205–216.

Cepeda, C., Galvan, L., Holley, S. M., Rao, S. P., André, V. M., Botelho, E. P., Chen, J. Y., Watson, J. B., Deisseroth, K., & Levine, M. S. (2013). Multiple sources of striatal inhibition are differentially affected in Huntington's disease mouse models. *Journal of Neuroscience*, *33*(17), 7393–406.

Chartove, J. A. K., McCarthy, M. M., Pittman-Polletta, B. R., & Kopell, N. J. (2020). A biophysical model of striatal microcircuits suggests gamma and beta oscillations interleaved at delta/theta frequencies mediate periodicity in motor control. *PLOS Computational Biology*, *16*(2), e1007300.

Chow, C. C., White, J. A., Ritt, J., & Kopell, N. (1998). Frequency control in synchronized networks of inhibitory neurons. *Journal of Computational Neuroscience*, *5*(4), 407–420.

Cohen, M. X., Axmacher, N., Lenartz, D., Elger, C. E., Sturm, V., & Schlaepfer, T. E. (2009). Good vibrations: cross-frequency coupling in the human nucleus accumbens during reward processing. *Journal of Cognitive Neuroscience*, *21*(5), 875–889.

Cohen, M. X., Elger, C. E., & Ranganath, C. (2007). Reward expectation modulates feedback-related negativity and EEG spectra. *NeuroImage*, *35*(2), 968–978.

Corbit, V. L., Whalen, T. C., Zitelli, K. T., Crilly, S. Y., Rubin, J. E., & Gittis, A. H. (2016). Pallidostriatal projections promote oscillations in a dopamine-depleted biophysical network model. *Journal of Neuroscience*, *36*(20), 5556–5571.

DeCoteau, W. E. W., Thorn, C., Gibson, D. J., Courtemanche, R., Mitra, P., Kubota, Y., & Graybiel, A. M. (2007). Oscillations of local field potentials in the rat dorsal striatum during spontaneous and instructed behaviors. *Journal of Neurophysiology*, *97*(5), 3800–3805.

Dejean, C., Arbuthnott, G., Wickens, J. R., Le Moine, C., Boraud, T., & Hyland, B. I. (2011). Power fluctuations in beta and gamma frequencies in rat globus pallidus: association with specific phases of slow oscillations and differential modulation by dopamine D1 and D2 receptors. *Journal of Neuroscience*, *31*(16), 6098–6107.

Doñamayor, N., Schoenfeld, M. A., & Münte, T. F. (2012). Magneto- and electroencephalographic manifestations of reward anticipation and delivery. *NeuroImage*, *62*(1), 17–29.

Dzirasa, K., Coque, L., Sidor, M. M., Kumar, S., Dancy, E. A., Takahashi, J. S., McClung, C. A., & Nicolelis, M. A. L. (2010). Lithium ameliorates nucleus accumbens phase-signaling dysfunction in a genetic mouse model of mania. *Journal of Neuroscience*, *30*(48), 16314–16323.

Emmons, E. B., Ruggiero, R. N., Kelley, R. M., Parker, K. L., & Narayanan, N. S. (2016). Corticostriatal field potentials are modulated at delta and theta frequencies during interval-timing task in rodents. *Frontiers in Psychology*, *7*(4).

Engel, A. K., & Fries, P. (2010). Beta-band oscillations—signalling the status quo? *Current Opinion in Neurobiology*, *20*(2), 156–165.

Feingold, J., Gibson, D. J., DePasquale, B., & Graybiel, A. M. (2015). Bursts of beta oscillation differentiate postperformance activity in the striatum and motor cortex of monkeys performing movement tasks. *Proceedings of the National Academy of Sciences*, *112*(44), 13687–13692.

Foti, D., Weinberg, A., Bernat, E. M., & Proudfit, G. H. (2015). Anterior cingulate activity to monetary loss and basal ganglia activity to monetary gain uniquely contribute to the feedback negativity. *Clinical Neurophysiology*, *126*(7), 1338–1347.

Frank, M. J. (2004). By Carrot or by Stick: Cognitive Reinforcement Learning in Parkinsonism. *Science*, *306*(5703), 1940–1943.

Fukuda, T. (2009). Network Architecture of Gap Junction-Coupled Neuronal Linkage in the Striatum. *Journal of Neuroscience*, *29*(4), 1235–1243.

Galarreta, M., & Hestrin, S. (2002). Electrical and chemical synapses among parvalbumin fast-spiking GABAergic interneurons in adult mouse neocortex. *Proceedings of the National Academy of Sciences of the United States of America*, *99*(19), 12438–12443.

Garas, F. N., Shah, R. S., Kormann, E., Doig, N. M., Vinciati, F., Nakamura, K. C., Dorst, M. C., Smith, Y., Magill, P. J., & Sharott, A. (2016). Secretagogin expression delineates functionally-specialized populations of striatal parvalbumin-containing interneurons. *eLife*, *5*(9), e16088.

Ghiglieri, V., Bagetta, V., Calabresi, P., & Picconi, B. (2012). Functional interactions within striatal microcircuit in animal models of Huntington's disease. *Neuroscience*, *211*, 165–184.

Gittis, A. H., & Kreitzer, A. C. (2013). Striatal microcircuitry and movement disorders. *Trends in Neurosciences*, *31*(9), 1713–1723.

Gittis, A. H., Leventhal, D. K., Fensterheim, B. A., Pettibone, J. R., Berke, J. D., & Kreitzer, A. C. (2011). Selective inhibition of striatal fast-spiking interneurons causes dyskinesias. *Journal of Neuroscience*, *31*(44), 15727–31.

Gittis, A. H., Nelson, A. B., Thwin, M. T., Palop, J. J., & Kreitzer, A. C. (2010). Distinct roles of GABAergic interneurons in the regulation of striatal output pathways. *Journal of Neuroscience*, *30*(6), 2223–2234.

Golomb, D., Donner, K., Shacham, L., Shlosberg, D., Amitai, Y., & Hansel, D. (2007). Mechanisms of firing patterns in fast-spiking cortical interneurons. *PLoS Computational Biology*, *3*(8), 1498–1512.

Gorelova, N., Seamans, J. K., & Yang, C. R. (2002). Mechanisms of dopamine activation of fast-spiking interneurons that exert inhibition in rat prefrontal cortex. *Journal of Neurophysiology*, *88*(6), 3150–3166.

Graveland, G. A., Williams, R. S., & DiFiglia, M. (1985). Evidence for degenerative and regenerative changes in neostriatal spiny neurons in Huntington's disease. *Science (New York, N.Y.)*, *227*(4688), 770–3.

Gross, J., Timmermann, L., Kujala, J., Dirks, M., Schmitz, F., Salmelin, R., & Schnitzler, A. (2002). The neural basis of intermittent motor control in humans. *Proceedings of the National Academy of Sciences*, *99*(4), 2299–302.

Gruber, A. J., Hussain, R. J., & O'Donnell, P. (2009). The nucleus accumbens: a switchboard for goal-directed behaviors. *PLoS ONE*, *4*(4), e5062.

HajiHosseini, A., & Holroyd, C. B. (2015). Sensitivity of frontal beta oscillations to reward valence but not probability. *Neuroscience Letters*, *602*, 99–103.

HajiHosseini, A., Rodríguez-Fornells, A., & Marco-Pallarés, J. (2012). The role of beta-gamma oscillations in unexpected rewards processing. *NeuroImage*, *60*(3), 1678–1685.

Hernandez, L. F. (2014). Firing dynamics and LFP oscillatory patterns in the dopamine-depleted striatum during maze learning. *Basal Ganglia*, *3*(4), 213–219.

Hjorth, J., Blackwell, K. T., & Kotaleski, J. H. (2009). Gap junctions between striatal fast-spiking interneurons regulate spiking activity and synchronization as a function of cortical activity. *Journal of Neuroscience*, *29*(16), 5276–5286.

Hohlefeld, F. U., Huchzermeyer, C., Huebl, J., Schneider, G. H., Brücke, C., Schönecker, T., Kühn, A. A., Curio, G., & Nikulin, V. V. (2014). Interhemispheric functional interactions between the subthalamic nuclei of patients with Parkinson's disease. *European Journal of Neuroscience*, *40*(8), 3273–3283.

Howe, M. W., Atallah, H. E., McCool, A., Gibson, D. J., & Graybiel, A. M. (2011). Habit learning is associated with major shifts in frequencies of oscillatory activity and synchronized spike firing in striatum. *Proceedings of the National Academy of Sciences*, *108*(40), 16801–16806.

Humphries, M. D., Wood, R., & Gurney, K. (2009). Dopamine-modulated dynamic cell assemblies generated by the GABAergic striatal microcircuit. *Neural Networks*, *22*(8), 1174–1188.

Ikarashi, Y., Takahashi, A., Ishimaru, H., Arai, T., & Maruyama, Y. (1997). Regulation of dopamine D1 and D2 receptors on striatal acetylcholine release in rats. *Brain Research Bulletin*, *43*(1), 107–115.

Jenkinson, N., & Brown, P. (2011). New insights into the relationship between dopamine, beta oscillations and motor function. *Trends in Neurosciences*, *34*(12), 611–618.

Jenkinson, N., Kühn, A. a., & Brown, P. (2013). Gamma oscillations in the human basal ganglia. *Experimental Neurology*, *245*, 72–76.

Kalanithi, P. S. A., Zheng, W., Kataoka, Y., DiFiglia, M., Grantz, H., Saper, C. B., Schwartz, M. L., Leckman, J. F., & Vaccarino, F. M. (2005). Altered parvalbumin-positive neuron distribution in basal ganglia of individuals with Tourette syndrome. *Proceedings of the National Academy of Sciences*, *102*(37), 13307–13312.

Kalenscher, T., Lansink, C. S., Lankelma, J. V., & Pennartz, C. M. A. (2010). Reward-associated gamma oscillations in ventral striatum are regionally differentiated and modulate local firing activity. *Journal of Neurophysiology*, *103*(3), 1658–1672.

Kawasaki, M., & Yamaguchi, Y. (2013). Frontal theta and beta synchronizations for monetary reward increase visual working memory capacity. *Social Cognitive and Affective Neuroscience*, *8*(5), 523–530.

Keiflin, R., & Janak, P. H. (2015). Dopamine Prediction Errors in Reward Learning and Addiction: From Theory to Neural Circuitry. *Neuron*, *88*(2), 247–263.

Khanna, P., & Carmena, J. M. (2017). Beta band oscillations in motor cortex reflect neural population signals that delay movement onset. *eLife*, *6*, 1–31.

Kilavik, B. E., Zaepffel, M., Brovelli, A., MacKay, W. A., & Riehle, A. (2013). The ups and downs of beta oscillations in sensorimotor cortex. *Experimental Neurology*, *245*, 15–26.

Kimchi, E. Y., Torregrossa, M. M., Taylor, J. R., & Laubach, M. (2009). Neuronal correlates of instrumental learning in the dorsal striatum. *Journal of Neurophysiology*, *102*(1), 475–489.

Kondabolu, K., Roberts, E. A., Bucklin, M., McCarthy, M. M., Kopell, N., & Han, X. (2016). Striatal cholinergic interneurons generate beta and gamma oscillations in the corticostriatal circuit and produce motor deficits. *Proceedings of the National Academy of Sciences*, *113*(22), E3159–E3168.

Koós, T., & Tepper, J. M. (1999). Inhibitory control of neostriatal projection neurons by GABAergic interneurons. *Nature neuroscience*, *2*(5), 467–72.

Koós, T., & Tepper, J. M. (2002). Dual cholinergic control of fast-spiking interneurons in the neostriatum. *Journal of Neuroscience*, *22*(2), 529–35.

Koos, T., Tepper, J. M., & Wilson, C. J. (2004). Comparison of IPSCs evoked by spiny and fast-spiking neurons in the neostriatum. *Journal of Neuroscience*, *24*(36), 7916–7922.

Kopell, N., & Ermentrout, B. (2004). Chemical and electrical synapses perform complementary roles in the synchronization of interneuronal networks. *Proceedings of the National Academy of Sciences*, *101*, 15482–15487.

Kulik, J. M., Pawlak, A. P., Kalkat, M., Coffey, K. R., West, M. O., Mark, O., Brunswick, N., & West, M. O. (2018). Representation of the body in the lateral striatum of the freely moving rat: Fast spiking interneurons respond to stimulation of individual body parts. *Brain Research*, *1657*, 101–108.

Lachaux, J., Rodriguez, E., Martinerie, J., & Varela, F. J. (1999). Measuring phase synchrony in brain signals. *Human Brain Mapping*, *8*(4), 194–208.

Lalla, L., Rueda Orozco, P. E., Jurado-Parras, M.-T., Brovelli, A., Robbe, D., Rueda-Orozco, P., Jurado-Parras, M.-T., Brovelli, A., Robbe, D., Rueda Orozco, P. E., Jurado-Parras, M.-T., Brovelli, A., & Robbe, D. (2017). Local or not local: investigating the nature of striatal theta oscillations in behaving rats. *eNeuro*, *4*(10), ENEURO.0128–17.2017.

Lau, T., Gage, G. J., Berke, J. D., & Zochowski, M. (2010). Local dynamics of gap-junction-coupled interneuron networks. *Physical Biology*, *7*(1), 016015.

Leckman, J. F., Bloch, M. H., Smith, M. E., Larabi, D., & Hampson, M. (2010). Neurobiological substrates of Tourette's disorder. *Journal of Child and Adolescent Psychopharmacology*, *20*(4), 237–47.

Lemos, J. C., Friend, D. M., Kaplan, A. R., Shin, J. H., Rubinstein, M., Kravitz, A. V., & Alvarez, V. A. (2016). Enhanced GABA transmission drives bradykinesia following loss of dopamine D2 receptor signaling. *Neuron*, *90*(4), 824–838.

Lepski, G., Arévalo, A., do Valle, A., Ballester, G., & Gharabaghi, A. (2012). Increased coherence among striatal regions in the theta range during attentive wakefulness. *Brazilian Journal of Medical and Biological Research*, *45*(8), 763–770.

Leung, L. S., & Yim, C. Y. C. (1993). Rhythmic delta-frequency activities in the nucleus accumbens of anesthetized and freely moving rats. *Canadian Journal of Physiology and Pharmacology*, *71*(5-6), 311–320.

Lewis, T. J., & Rinzel, J. (2000). Self-organized synchronous oscillations in a network of excitable cells coupled by gap junctions. *Network: Computation in Neural Systems*, *11*(4), 299–320.

Lewis, T. J., & Rinzel, J. (2004). Dendritic effects in networks of electrically coupled fast-spiking interneurons. *Neurocomputing*, *58-60*, 145 – 150. Computational Neuroscience: Trends in Research 2004.

Little, S., & Brown, P. (2014). The functional role of beta oscillations in Parkinson's disease. *Parkinsonism and Related Disorders*, *20*(SUPPL.1), S44–S48.

López-Azcárate, J., Nicolás, M. J., Cordon, I., Alegre, M., Valencia, M., & Artieda, J. (2013). Delta-mediated cross-frequency coupling organizes oscillatory activity across the rat cortico-basal ganglia network. *Frontiers in Neural Circuits*, *7*(10), 1–16.

Mahon, S., Vautrelle, N., Pezard, L., Slaght, S. J., Deniau, J.-M., Chouvet, G., & Charpier, S. (2006). Distinct patterns of striatal medium spiny neuron activity during the natural sleep-wake cycle. *Journal of Neuroscience*, *26*(48), 12587–95.

Mainen, Z. F., & Sejnowski, T. J. (1996). Influence of dendritic structure on firing pattern in model neocortical neurons. *Nature*, *382*(6589), 363–366.

Mancilla, J. G., Lewis, T. J., Pinto, D. J., Rinzel, J., & Connors, B. W. (2007). Synchronization of electrically coupled pairs of inhibitory interneurons in neocortex. *Journal of Neuroscience*, *27*(8), 2058–2073.

Maris, E., & Oostenveld, R. (2007). Nonparametric statistical testing of EEG- and MEG-data. *Journal of Neuroscience Methods*, *164*(1), 177–190.

Markowitz, J. E., Gillis, W. F., Beron, C. C., Neufeld, S. Q., Robertson, K., Bhagat, N. D., Peterson, R. E., Peterson, E., Hyun, M., Linderman, S. W., Sabatini, B. L., & Datta, S. R. (2018). The striatum organizes 3D behavior via moment-to-moment action selection. *Cell*, *174*(1), 44–58.e17.

Mas-Herrero, E., Ripollés, P., HajiHosseini, A., Rodríguez-Fornells, A., & Marco-Pallarés, J. (2015). Beta oscillations and reward processing: Coupling oscillatory activity and hemodynamic responses. *NeuroImage*, *119*, 13–19.

Masimore, B., Schmitzer-Torbert, N. C., Kakalios, J., & Redish, A. D. (2005). Transient striatal gamma local field potentials signal movement initiation in rats. *Neuroreport*, *16*(18), 2021–2024.

McCarthy, M. M., Moore-Kochlacs, C., Gu, X., Boyden, E. S., Han, X., & Kopell, N. (2011). Striatal origin of the pathologic beta oscillations in Parkinson's disease. *Proceedings of the National Academy of Sciences*, *108*(28), 11620–11625.

Miller, B. R., Walker, A. G., Barton, S. J., & Rebec, G. V. (2011). Dysregulated neuronal activity patterns implicate corticostriatal circuit dysfunction in multiple rodent models of Huntington's Disease. *Frontiers in Systems Neuroscience*, *5*(5), 26.

Munro, E., & Börgers, C. (2010). Mechanisms of very fast oscillations in networks of axons coupled by gap junctions. *Journal of Computational Neuroscience*, *28*(3), 539–555.

Naze, S., Humble, J., Zheng, P., Barton, S., Rangel-Barajas, C., Rebec, G. V., & Kozloski, J. R. (2018). Cortico-striatal cross-frequency coupling and gamma genesis disruptions in Huntington's disease mouse and computational models. *eNeuro*, *5*(6).

Onn, S., & Grace, A. A. (1999). Alterations in electrophysiological activity and dye coupling of striatal spiny and aspiny neurons in dopamine-denervated rat striatum recorded in vivo. *Synapse*, *33*(1), 1–15.

Onn, S. P., & Grace, A. A. (1994). Dye coupling between rat striatal neurons recorded in vivo: compartmental organization and modulation by dopamine. *Journal of Neurophysiology*, *71*(5), 1917–1934.

Oswal, A., Beudel, M., Zrinzo, L., Limousin, P., Hariz, M., Foltynie, T., Litvak, V., & Brown, P. (2016). Deep brain stimulation modulates synchrony within spatially and spectrally distinct resting state networks in Parkinson's disease. *Brain*, *139*(5), 1482–1496.

Owen, S. F., Berke, J. D., & Kreitzer, A. C. (2018). Fast-Spiking Interneurons Supply Feedforward Control of Bursting, Calcium, and Plasticity for Efficient Learning. *Cell*, *172*(4), 683–695.e15.

Pittman-Polletta, B., Hsieh, W.-H., Kaur, S., Lo, M.-T., & Hu, K. (2014). Detecting phase-amplitude coupling with high frequency resolution using adaptive decompositions. *Journal of Neuroscience Methods*, *226*, 15–32.

Pittman-Polletta, B. R., Quach, A., Mohammed, A. I., Romano, M., Kondabolu, K., Kopell, N. J., Han, X., & McCarthy, M. M. (2018). Striatal cholinergic receptor

activation causes a rapid, selective, & state-dependent rise in corticostriatal β activity. *European Journal of Neuroscience*, (pp. 1–13).

Popescu, A. T., Popa, D., & Paré, D. (2009). Coherent gamma oscillations couple the amygdala and striatum during learning. *Nature Neuroscience*, *12*(6), 801–807.

Reiner, A., Shelby, E., Wang, H., DeMarch, Z., Deng, Y., Guley, N. H., Hogg, V., Roxburgh, R., Tippett, L. J., Waldvogel, H. J., & Faull, R. L. (2013). Striatal parvalbuminergic neurons are lost in Huntington's disease: implications for dystonia. *Movement Disorders*, *28*(12), 1691–1699.

Rinzel, J. (2003). Dendritic effects in networks of fast-spiking interneurons connected by inhibition and electrical coupling. *Computer Science Preprint Archive*, *2003*(2), 144–152.

Rothe, T., Deliano, M., Wójtowicz, A., Dvorzhak, A., Harnack, D., Paul, S., Vagner, T., Melnick, I., Stark, H., & Grantyn, R. (2015). Pathological gamma oscillations, impaired dopamine release, synapse loss and reduced dynamic range of unitary glutamatergic synaptic transmission in the striatum of hypokinetic Q175 Huntington mice. *Neuroscience*, *311*, 519–538.

Russo, G., Nieus, T. R., Maggi, S., & Taverna, S. (2013). Dynamics of action potential firing in electrically connected striatal fast-spiking interneurons. *Frontiers in Cellular Neuroscience*, *7*(11), 209.

Schiffmann, S. N., Fisone, G., Moresco, R., Cunha, R. A., & Ferré, S. (2007). Adenosine a2a receptors and basal ganglia physiology. *Progress in Neurobiology*, *83*(5), 277–292.

Schultz, W., Dayan, P., & Montague, P. R. (1997). A neural substrate of prediction and reward. *Science*, *275*(5306), 1593–9.

Schulz, J. M., Pitcher, T. L., Savanthrapadian, S., Wickens, J. R., Oswald, M. J., & Reynolds, J. N. J. (2011). Enhanced high-frequency membrane potential fluctuations control spike output in striatal fast-spiking interneurones in vivo. *Journal of Physiology*, *589*(17), 4365–4381.

Schwemmer, M. A., & Lewis, T. J. (2014). The robustness of phase-locking in neurons with dendro-dendritic electrical coupling. *Journal of Mathematical Biology*, *68*(1-2), 303–340.

Sciamanna, G., Bonsi, P., Tassone, A., Cuomo, D., Tscherter, A., Viscomi, M. T., Martella, G., Sharma, N., Bernardi, G., Standaert, D. G., Pisani, A., Giuseppe Sciamanna a, B., Bonsib, P., Tassoneb, A., Dario Cuomoa, B., Anne Tschertera, B., Viscomib, M. T., Giuseppina Martellaa, B., Sharmac, N., Giorgio Bernardia, B.,

David G. Standaertd, & Antonio Pisania, B. (2009). Impaired striatal D2 receptor function leads to enhanced GABA transmission in a mouse model of DYT1 dystonia. *Neurobiology of Disease*, *34*(1), 133–145.

Sciamanna, G., & Wilson, C. J. (2011). The ionic mechanism of gamma resonance in rat striatal fast-spiking neurons. *Journal of Neurophysiology*, *106*(6), 2936–2949.

Seymour, R. A., Rippon, G., & Kessler, K. (2017). The Detection of Phase Amplitude Coupling during Sensory Processing. *Frontiers in Neuroscience*, *11*(SEP), 487.

Sharott, A., Doig, N. M., Mallet, N., & Magill, P. J. (2012). Relationships between the firing of identified striatal interneurons and spontaneous and driven cortical activities in vivo. *Journal of Neuroscience*, *32*(38), 13221–13236.

Sharott, A., Moll, C. K. E., Engler, G., Denker, M., Grun, S., Engel, A. K., Grün, S., & Engel, A. K. (2009). Different subtypes of striatal neurons are selectively modulated by cortical oscillations. *Journal of Neuroscience*, *29*(14), 4571–4585.

Shen, W. (2005). Cholinergic Suppression of KCNQ Channel Currents Enhances Excitability of Striatal Medium Spiny Neurons. *Journal of Neuroscience*, *25*(32), 7449–7458.

Sherfey, J. S., Soplata, A. E., Ardid, S., Roberts, E. A., Stanley, D. A., Pittman-Polletta, B. R., & Kopell, N. J. (2018). DynaSim: A MATLAB Toolbox for Neural Modeling and Simulation. *Frontiers in Neuroinformatics*, *12*, 10.

Sherman, A., & Rinzel, J. (1992). Rhythmogenic effects of weak electrotonic coupling in neuronal models. *Proceedings of the National Academy of Sciences*, *89*(6), 2471–2474.

Sherman, A., Rinzel, J., & Keizer, J. (1988). Emergence of organized bursting in clusters of pancreatic beta-cells by channel sharing. *Biophysical Journal*, *54*(3), 411–425.

Skinner, F. K., Zhang, L., Velazquez, J. L. P., & Carlen, P. L. (1999). Bursting in Inhibitory Interneuronal Networks : A Role for Gap-Junctional Coupling. *Journal of Neurophysiology*, *81*(3), 1274–1283.

Stein, E., & Bar-Gad, I. (2013). Beta oscillations in the cortico-basal ganglia loop during parkinsonism. *Experimental Neurology*, *245*, 52–59.

Stenner, M.-P., Dürschmid, S., Rutledge, R. B., Zaehle, T., Schmitt, F. C., Kaufmann, J., Voges, J., Heinze, H.-J., Dolan, R. J., Schoenfeld, M. A., Mp, S., Dürschmid, S., Rb, R., Zaehle, T., & Fc, S. (2016). Perimovement decrease of alpha/beta oscillations in the human nucleus accumbens. *Journal of Neurophysiology*, *116*(4), 1663–1672.

Stenner, M. P., Litvak, V., Rutledge, R. B., Zaehle, T., Schmitt, F. C., Voges, J., Heinze, H. J., & Dolan, R. J. (2015). Cortical drive of low-frequency oscillations in the human nucleus accumbens during action selection. *Journal of Neurophysiology*, *114*(1), 29–39.

Surmeier, D. J., Carrillo-Reid, L., & Bargas, J. (2011). Dopaminergic modulation of striatal neurons, circuits, and assemblies. *Neuroscience*, *198*, 3–18.

Tan, H., Wade, C., & Brown, P. (2016). Post-movement beta activity in sensorimotor cortex indexes confidence in the estimations from internal models. *Journal of Neuroscience*, *36*(5).

Taverna, S., Ilijic, E., & Surmeier, D. J. (2008). Recurrent collateral connections of striatal medium spiny neurons are disrupted in models of Parkinson's disease. *Journal of Neuroscience*, *28*(21), 5504–5512.

Tepper, J. M. (2008). GABAergic interneurons of the striatum. *Handbook of Basal Ganglia Structure and Function*, *20*, 151–166.

Tepper, J. M., Koós, T., & Wilson, C. J. (2004). GABAergic microcircuits in the neostriatum. *Trends in Neurosciences*, *27*(11), 662–669.

Tepper, J. M., Tecuapetla, F., Koós, T., Ibáñez-sandoval, O., & Kreitzer, A. (2010). Heterogeneity and diversity of striatal GABAergic interneurons. *Frontiers in Neuroanatomy*, *4*(12), 1–18.

Tepper, J. M., Wilson, C. J., & Koós, T. (2008). Feedforward and feedback inhibition in neostriatal GABAergic spiny neurons. *Brain Research Reviews*, *58*(2), 272–281.

Thorn, C. A., & Graybiel, A. M. (2014). Differential entrainment and learning-related dynamics of spike and local field potential activity in the sensorimotor and associative striatum. *Journal of Neuroscience*, *34*(8), 2845–2859.

Tinkhauser, G., Pogosyan, A., Tan, H., Herz, D. M., Kühn, A. A., & Brown, P. (2017). Beta burst dynamics in Parkinson's disease off and on dopaminergic medication. *Brain*, *140*(11), 2968–2981.

Tort, A. B. L., Komorowski, R., Eichenbaum, H., & Kopell, N. (2010). Measuring Phase-Amplitude Coupling Between Neuronal Oscillations of Different Frequencies. *Journal of Neurophysiology*, *104*(2), 1195–1210.

Tort, A. B. L., Kramer, M. A., Thorn, C., Gibson, D. J., Kubota, Y., Graybiel, A. M., & Kopell, N. J. (2008). Dynamic cross-frequency couplings of local field potential oscillations in rat striatum and hippocampus during performance of a T-maze task. *Proceedings of the National Academy of Sciences*, *105*(51), 20517–20522.

Traub, R. D., Kopell, N., Bibbig, a., Buhl, E. H., LeBeau, F. E., & Whittington, M. a. (2001). Gap junctions between interneuron dendrites can enhance synchrony of gamma oscillations in distributed networks. *Journal of Neuroscience*, *21*(23), 9478–9486.

van de Vijver, I., Ridderinkhof, K. R., & Cohen, M. X. (2011). Frontal Oscillatory Dynamics Predict Feedback Learning and Action Adjustment. *Journal of Cognitive Neuroscience*, *23*(12), 4106–4121.

van der Meer, M. a. a., Kalenscher, T., Lansink, C. S., Pennartz, C. M. A., Berke, J. D., & Redish, a. D. (2010). Integrating early results on ventral striatal gamma oscillations in the rat. *Frontiers in Neuroscience*, *4*(9), 1–12.

van der Meer, M. A. A., & Redish, A. D. (2009). Low and high gamma oscillations in rat ventral striatum have distinct relationships to behavior, reward, and spiking activity on a learned spatial secision task. *Frontiers in Integrative Neuroscience*, *3*(6), 9.

van der Meer, M. A. A., Redish, A. D., Meer, M. A. A. V. D., & Redish, A. D. (2011). Theta phase precession in rat ventral striatum links place and reward information. *Journal of Neuroscience*, *31*(8), 2843–2854.

Van Vreeswijk, C., Abbott, L., & Ermentrout, G. B. (1994). When inhibition not excitation synchronizes neural firing. *Journal of Computational Neuroscience*, *1*(4), 313–321.

Vinner, E., Israelashvili, M., & Bar-Gad, I. (2017). Prolonged striatal disinhibition as a chronic animal model of tic disorders. *Journal of Neuroscience Methods*, *292*, 20–29.

von Nicolai, C., Engler, G., Sharott, A., Engel, A. K., Moll, C. K., Siegel, M., Nicolai, C. V., Engler, G., Sharott, A., Engel, A. K., Moll, C. K., Siegel, M., von Nicolai, C., Engler, G., Sharott, A., Engel, A. K., Moll, C. K., & Siegel, M. (2014). Corticostriatal coordination through coherent phase-amplitude coupling. *Journal of Neuroscience*, *34*(17), 5938–48.

Wall, N. R., De La Parra, M., Callaway, E. M., & Kreitzer, A. C. (2013). Differential Innervation of Direct- and Indirect-Pathway Striatal Projection Neurons. *Neuron*, *79*(2), 347–360.

Wang, X.-J., & Buzsáki, G. (1996). Gamma oscillation by synaptic inhibition in a hippocampal interneuronal network model. *Journal of Neuroscience*, *16*(20), 6402–6413.

Wang, X.-J., & Rinzel, J. (1992). Alternating and synchronous rhythms in reciprocally inhibitory model neurons. *Neural Computation*, *4*(1), 84–97.

West, T., Farmer, S., Berthouze, L., Jha, A., Beudel, M., Foltynie, T., Limousin, P., Zrinzo, L., Brown, P., & Litvak, V. (2016). The Parkinsonian subthalamic network: Measures of power, linear, and non-linear synchronization and their relationship to L-DOPA treatment and OFF state motor severity. *Frontiers in Human Neuroscience*, *10*(10).

West, T. O., Berthouze, L., Halliday, D. M., Litvak, V., Sharott, A., Magill, P. J., & Farmer, S. F. (2018). Propagation of beta/gamma rhythms in the cortico-basal ganglia circuits of the Parkinsonian Rat. *Journal of Neurophysiology*, (p. jn.00629.2017).

White, J. A., Chow, C. C., Rit, J., Soto-Treviño, C., & Kopell, N. (1998). Synchronization and oscillatory dynamics in heterogeneous, mutually inhibited neurons. *Journal of Computational Neuroscience*, *5*(1), 5–16.

Whittington, M. A., Cunningham, M. O., LeBeau, F. E., Racca, C., & Traub, R. D. (2011). Multiple origins of the cortical gamma rhythm. *Developmental Neurobiology*, *71*(1), 92–106.

Whittington, M. A., Traub, R. D., & Jefferys, J. G. (1995). Synchronized oscillations in interneuron networks driven by metabotropic glutamate receptor activation. *Nature*, *373*(6515), 612.

Whittington, M. a., Traub, R. D., Kopell, N., Ermentrout, B., & Buhl, E. H. (2000). Inhibition-based rhythms: experimental and mathematical observations on network dynamics. *International Journal of Psychophysiology*, *38*, 315–336.

Womelsdorf, T., Vinck, M., Leung, L. S., & Everling, S. (2010). Selective Theta-Synchronization of Choice-Relevant Information Subserves Goal-Directed Behavior. *Frontiers in Human Neuroscience*, *4*(1), 210.

Xu, M., Li, L., & Pittenger, C. (2016). Ablation of fast-spiking interneurons in the dorsal striatum, recapitulating abnormalities seen post-mortem in Tourette syndrome, produces anxiety and elevated grooming. *Neuroscience*, *324*(2), 321–329.

Zahid, T., & Skinner, F. K. (2009). Predicting synchronous and asynchronous network groupings of hippocampal interneurons coupled with dendritic gap junctions. *Brain Research*, *1262*, 115–129.

Zhang, Y., Pan, X., Wang, R., & Sakagami, M. (2016). Functional connectivity between prefrontal cortex and striatum estimated by phase locking value. *Cognitive Neurodynamics*, *10*(3), 245–254.

CURRICULUM VITAE